HUNGARIAN JOURNAL OF
INDUSTRY AND CHEMISTRY
HJIC

Contents

HUNGARIAN JOURNAL OF
INDUSTRY AND CHEMISTRY
HJIC

Separation of Fumaric and Maleic Acid Crystals from the Industrial Wastewater of Maleic Anhydride Production

Edisa Papraćanin[1*], Abdel Đozić[2], Ermin Mujkić[3], Maida Hodžić[3], Irma Hodžić[1], Belmin Poljić[1] and Ajla Ramić[1]

[1]Department of Chemical Engineering, Faculty of Technology, University of Tuzla, Urfeta Vejzagića br. 8, 75000 Tuzla, Bosnia and Herzegovina
[2]Department of Environmental Engineering, Faculty of Technology, University of Tuzla, Urfeta Vejzagića br. 8, 75000 Tuzla, Bosnia and Herzegovina
[3]Global Ispat Coke Industry, Željeznička 1, 75300 Lukavac, Bosnia and Herzegovina

In this research, a physicochemical analysis of the industrial wastewater from a factory that produces maleic anhydride was performed. Based on the conducted analysis (pH, electrical conductivity, density of the liquid phase, boiling point of the waste suspension, chemical as well as biological oxygen demand, and dry matter), it can be concluded that the waste stream obtained at the outlet pipe from the plant resulting from the production of maleic anhydride requires appropriate treatments. Some of the parameters measured, e.g. pH (0.97±0.06), boiling point (106.8±1.3°C) and acidity, indicate the presence of organic acids such as fumaric and maleic acids, which are formed during the production of maleic anhydride. The possibility of extracting crystals by adding urea and thiourea followed by forced cooling in a heat exchanger was investigated. The most effective method was the addition of thiourea when the most significant amount of crystals was obtained, namely 17.29 wt%. The addition of thiourea in combination with forced cooling greatly facilitates the process of separating the solid and liquid phases of the waste suspension, which could later be adequately treated by physical, chemical or biological methods.

Keywords: MAN production, separation, thiourea, cooling, wastewater

1. Introduction

Since the chemical industry and the waste streams generated during chemical production have a harmful effect on the environment, it is necessary to minimize their harmful impact before releasing them into the environment and comply with legal regulations, both locally and globally. Moreover, it is important to conduct environmental impact assessments and environmental management with regard to the practical implementation of environmental regulations [1], e.g. determining the Informative Environment Qualifying Index.

The production process of maleic anhydride (MAN) is based on two different technological processes in the gas phase, namely the oxidation of benzene and the oxidation of n-butane [2]. In 2015, the global capacity of MAN production amounted to 2800 million metric tons [3]. Scientific and technological developments in the manufacture and use of maleic anhydride as well as maleic and fumaric acids have been reviewed over the past 20 years [4]. During MAN production, a certain amount of wastewater is generated, which must be

processed and treated in order to minimize environmental pollution. The increasing need to mitigate environmental impacts has led industries to develop more sustainable processes, which may be an arduous task since economic, safety, social and environmental factors must be considered [5]-[6]. The impact assessment of the chemical industry on the environment is becoming more and more important with regard to projecting and designing processes. A special problem is represented by facilities involved in exploitation, which are in the process of complying with EU regulations on environmental protection. Given that Bosnia and Herzegovina, a country in transition, is increasingly adopting the laws of the European Union, it is necessary to take measures that will reduce the harmful effects of the chemical industry both locally and globally. Furthermore, the Federation of Bosnia and Herzegovina has introduced legislation [7] which is in accordance with EU legislation.

Due to the fact that MAN production facilities have a detrimental impact on the environment, various methods have recently been applied for the treatment of wastewater streams. The wastewater flow from the MAN

production plant consists of a mixture of organic omponents, containing mainly fumaric and maleic acids, which can be treated by following different physical, chemical and biological methods [8]-[14]. Considering the physical characteristics of fumaric and maleic acids [15], especially their solubility in water (fumaric acid is poorly soluble in water), a waste stream consisting of a crystal suspension as well as a mother liquor of fumaric and maleic acids is obtained at the outlet of the plant. Before any treatment, such a suspension must be separated into the crystal flow and the mother liquor flow, which, if necessary, could be treated later or possibly reused to obtain products that do not require highly pure fumaric or maleic acid.

This research was carried out in order to examine the possibility of separating the wastewater suspension from the industrial MAN production plant and the crystal stream, which consists of a mixture of fumaric and maleic acids along with other organic impurities, from the mother liquor stream. Considering the physical, chemical and biological properties of the waste stream as well as its components, the goals of this research are to choose the most efficient method to separate the crystalline product from the waste stream in addition to making recommendations concerning its processing and further use in the industrial production of unsaturated polyester resins. Another aim is to make recommendations for possible biological treatments by analyzing the liquid component of the waste stream.

2. Experimental

2.1 Treatment of the waste stream

The waste stream of the suspension at the outlet of the MAN production facility owned by the company Global Ispat Koksna Industrija Lukavac (GIKIL) (Bosnia and Herzegovina) was used in this research. The above-mentioned waste stream is generated discontinuously by the process of washing the distillation column and cooler with water at a temperature of 100°C. In the aforementioned industrial plant, the distillation system is washed every 4 days when approximately 70 m³ of water is consumed in an hour, resulting in water with a low pH due to the presence of maleic and fumaric acids. The aftercooler is washed twice a month, consuming 10 m³ of water. Given that wastewater contains fumaric acid, which is the basic raw material for the production of unsaturated polyester resins, it is necessary to investigate the possibility of using this waste stream in terms of extracting (crystallizing) fumaric acid. The total amount of waste suspension generated under industrial conditions on a monthly basis is approximately 300 m³, which has a significant impact on the environment if it is not processed adequately.

Experimental research and analyses were carried out in the Chemical Engineering laboratory of the Faculty of Technology at the University of Tuzla. Samples were taken twice a month directly at the outlet of the tank used to collect the waste stream. Most samples

(a)

(b)

Figure 1. The samples: (a) immediately after being taken from the plant; (b) after being delivered to the laboratory.

were taken after the first wash when the concentration of organic matter is the highest. The samples immediately after being taken from the plant and after being delivered to the laboratory are shown in *Fig.1*. They were collected and delivered to the laboratory in plastic containers with a volume of 5L. Certain aliquots were extracted to perform physicochemical and other analyses.

Based on the research objectives, the following tasks were conducted:
- Laboratory modelling of the washing of the distillation column and the discharge of the waste stream was performed;
- Physical and chemical analyses of the waste stream were performed under laboratory conditions;
- The quantity of the resulting crystalline product was determined in relation to the volume of the waste stream under laboratory conditions;
- Examination of the possibility of extracting crystals from the waste stream was carried out in several ways:
   a) by cooling the flow under laboratory conditions,
   b) by adding urea and thiourea,
   c) by cooling the waste stream with water in a system of tubular heat exchangers.

Among the physicochemical analyses, the pH, electrical conductivity, boiling point as well as the chemical and biological oxygen demand were measured. All measurements refer to a homogenized sample, moreover, after separating the liquid and solid phases, the dry matter and acidic properties of the liquid phase were determined.

The density of the liquid phase was determined using a pycnometer and the bulk density of the dried crystalline product was measured according to the ISO 1183-1:2004 standard.

2.2 Materials and Methods

For the purpose of experimental modelling, washing of the distillation column and the discharge of the waste stream, a special system was designed, consisting of a glass container with a volume of 25 liters with openings at the top and bottom. The vessel includes a distillation column and a glass vessel of the same volume was used as a receiving vessel. The amount of sample used was 5 liters and was preheated to 100°C.

To obtain a real picture of the industrial plant, the process of crystal formation was tested by cooling down the waste stream to ambient temperature (laboratory conditions). 250 ml samples that were observed were taken from a 5-liter sample after mixing and heating to a temperature of 100°C. The resulting crystals were filtered and air-dried under laboratory conditions.

Following the addition of urea and thiourea, the 400 ml samples preheated to 100°C, the temperature of the rinsing water, were taken from a 5-liter sample. The test was performed by adding urea and thiourea in different percentages concerning the volume of the sample. After the addition of urea and thiourea, the samples were allowed to settle before the crystals were separated by filtration on filter paper and air-dried.

For the purposes of testing whether the waste suspension stream crystallizes, a cooling system consisting of three laboratory-scale tubular heat exchangers was designed. The cooling conditions and crystal formation were investigated for different flow rates of cooling water. The cooling system is shown in *Fig.2*.

The total area for heat exchange of the laboratory-scale cooling system was about 0.43 m^2. Once the waste suspension had passed through the tubular cooling system, the resulting crystals were collected on a metal grid and placed on a glass container before being dried and weighed on an analytical scale.

All measurements were performed three times and statistical data processing was conducted in Microsoft Excel, namely the mean and standard deviation were calculated.

Electrometric measurements of the pH and electrical conductivity were carried out by direct measurements using a METTLER TOLEDO FE 20-30/EL 20-30 pH meter/conductometer. The pH was measured using the standard method BAS EN ISO 10523, while the electrical conductivity was determined using the standard method BAS EN 27888.

The Chemical Oxygen Demand (COD) is the oxygen equivalent of the amount of potassium dichromate consumed during the complete oxidation of the organic matter in the measured volume of the sample. The COD and Biological Oxygen Demand (BOD) are determined by the BAS ISO 6060 and BAS EN 1899-1 methods, respectively.
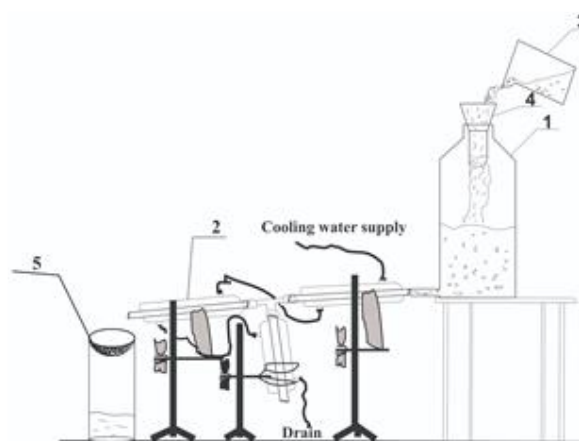

Figure 2. Schematic diagram of the waste-stream cooling system: 1) glass container for rinsing, 2) system consisting of three tubular heat exchangers, 3) cup containing the sample, 4) glass funnel, 5) metal grid for collecting crystals

After separating the liquid and solid phases, the liquid sample was filtered, evaporated at 100°C and dried overnight in an oven before the mass of the dry matter was measured on an analytical scale. The content of the dry matter was determined according to Method 2540-Solid B [16]. Furthermore, the solid phase in the solid sample was analysed gravimetrically by drying it at 105°C for 24 h.

3. Results and evaluation

3.1 Characterization of the waste stream

Considering that the waste stream represents a heterogeneous mixture (suspension) under laboratory conditions, for the purpose of the analysis, the samples were homogenized and heated to a temperature of 100°C because the waste stream was obtained by washing the distillation column in the MAN plant with water at a temperature of 100°C. On the walls of the distillation column, organic substances, predominantly fumaric and maleic acids, are deposited that may occur during the production of MAN. Due to its physical and chemical properties, fumaric acid is insoluble in water, while the solubility of maleic acid in water is 478.8 g/L at 20.0°C, i.e. 3926 g/L at 97.5°C [17]. Therefore, by washing the distillation column, a suspension is formed in which crystals of fumaric acid as well as a solution of maleic and fumaric acids are present. Considering the aforementioned fact and the boiling points of the pure acids, fumaric acid at 287°C and maleic acid at 135°C [15], the boiling point of the suspension was measured to be 106.8±1.3°C under laboratory conditions. This data indicate the presence of other substances that have significantly lower boiling points compared to the components that are primarily present.

As expected, the measured pH is very low, namely 0.97±0.06, due to the presence of organic acids, while the measured electrical conductivity is 33.62±4.03 mS. In view of the pH prescribed in [6], the measured value does

Table 1 Mass of the crystalline product obtained following the addition of urea and thiourea

Mass added (g)	Volume of filtrate collected (ml)		Mass of crystals (g)	
	Thiourea	Urea	Thiourea	Urea
1	100	200	69.0	44.9
3	60	210	71.4	46.7
5	150	200	71.8	46.9

not comply with the legal framework, which indicates that this waste stream of industrial wastewater should be treated in an appropriate way. The relatively low electrical conductivity, for which no legally prescribed limits are found, indicates a low concentration of free ions in the waste stream. A pycnometer measured the density of the liquid phase after separation to be 1038.84 ± 4.31 kg/m^3, while the bulk density of the solid phase was 394.0 ± 1.4 kg/m^3.

To further examine the characteristics of the waste stream, the COD and BOD of the homogenized sample were determined to be 233600 and 87280 mg O_2/L, respectively. The permitted limits for the discharge of a waste stream into the environment for COD and BOD are 25-250 and 135-700 mg O_2/L, respectively, which indicates the need for pretreatment of the waste stream before being discharged into the environment.

By separating the solid and liquid phases by filtering and decanting under laboratory conditions, a homogenized 2.5 L sample contains 5.09 ± 0.05 wt% of dry crystalline products. As a result, the total amount of solid matter discharged every month (300 m^3) is about 15.27 kg. Therefore, a huge amount of solid waste can be treated or possibly used for other purposes. The amount of dry matter in the liquid phase is 16.3 ± 0.2 wt%, which also exceeds the permitted limits.

By titration of the liquid phase with NaOH and phenolphthalein as an indicator, it was determined that 1 g of the liquid solution is titrated with 3.95 mmol of NaOH. In simple terms, if the acidity is due to the presence of maleic acid, this would correspond to a maleic acid concentration of 0.247 mg/ml.

3.2 Separation efficiency

Considering the results of the physicochemical analysis of the industrial waste stream resulting from MAN production, it was observed that this waste stream must be adequately treated before being discharged into the environment. Due to the composition and characteristics of the waste stream, it is necessary to separate it into the solid and liquid phases. In this research, several experiments based on different methods were conducted to obtain an efficient method for separation.

As described earlier in the Experimental section, before testing the aforementioned methods, laboratory modelling of the process by which the distillation column is washed was carried out. The reason for performing the

Figure 3. Crystals obtained by forced cooling

experimental simulation is to experimentally and visually determine how the crystals are formed during the discharge of the waste-stream suspension into the collector. During the simulation, it was observed that immediately after the waste stream comes out of the outlet pipe, a larger amount of crystals were formed, meaning that other organic substances, predominantly maleic acid, also crystallized.

Simply by highlighting the flow, a sudden drop in the temperature of the flow from 100°C to ambient temperature is observed, during which more intense crystallization occurs. Following this observation, a system of three heat exchangers (*Fig.2*) was designed under laboratory conditions to cool down the waste stream more quickly and test such an efficient way of separating the solid and liquid phases. At the outlet from the cooling system, a container collected the waste flow, on top of which a metal grid to separate the crystals was placed. After the cooling and separation processes, the crystalline product obtained was dried and measured. The mass of crystals obtained by forced cooling (sample volume of 5 L) was 638.37 ± 2.34 g, that is, 12.3 wt% of the dry crystalline product.

Compared with the amount of crystals obtained by natural cooling to ambient temperature, it can be seen that this method (forced cooling and separation by filtration) is significantly more efficient. This technique of collecting crystals on a metal grid is very simple to perform due to the very structure and size of the resulting crystals. The appearance of the crystals obtained is shown in *Fig.3*.

After experiments were performed using forced cooling, the influence of the addition of urea and thiourea on the formation and separation of crystals of organic substances in the industrial waste stream was examined. These components were added to better isolate the crystalline product from the mixture of fumaric and maleic acids, that is, thiourea acts as a catalyst in the isomerization of maleic acid to fumaric acid [18].

The masses of the resulting crystalline product following the addition of urea and thiourea are presented in Table 1. Analyses were performed using a sample that

Table 2 Mass of the obtained crystalline product following the addition of smaller quantities of thiourea

Mass added (g)	Volume of filtrate collected (ml)	Mass of crystals (g)
0.25	180	45.2
0.50	160	52.7
0.75	170	60.3

was heated to 100°C and homogenized in a volume of 400 ml.

The masses of urea and thiourea added were 1, 3 and 5 g. Samples where different amounts of urea and thiourea were added (U1 and T1 1g, U2 and T2 3g, U3 and T3 5g) are shown in *Fig.4*.

As can be seen in *Table 1*, the largest amount of crystalline product was obtained following the addition of 5 g of thiourea. As a percentage of the 400 mL sample, this value is 17.29 wt% of dry crystalline product, which is significantly more compared to forced and natural cooling of the waste stream.

The addition of urea also enhances separation of the solid phase from the suspension of the waste stream, however, considering the results obtained, the effect of adding thiourea on the separation process is significantly greater.

As can be seen in the table, given that the amounts of the crystalline product obtained following the addition of all three amounts of thiourea are very similar, an additional experimental optimization of the mass of thiourea to be added to the waste stream was performed. Amounts of less than 1 g were added to see if a larger difference in the amount of crystalline product formed was observed. Amounts of thiourea added of less than 1 g are presented in *Table 2*. As can be seen, even small amounts of thiourea significantly enhance the separation of crystals from the waste stream.

If 1 g of thiourea is added to a suspension sample of 400 ml as an optimal cost price and to achieve separation of the crystals when treating the waste stream generated from an industrial plant, it would be necessary to add 750 kg to 300 m³ of waste suspensions per month, which is a huge amount. However, if 0.25 g of thiourea is added to a suspension sample of 400 mL, which equates to approximately 0.06%, about 1250 kg of thiourea would need to be added annually at a cost of approximately $98,550 [19]. In this case, this price is reasonable if the separated fumaric acid crystals were to be used for the production of resins.

In light of the research conducted, in the future, some other methods for extracting the mixture of fumaric and maleic acid crystals should be examined, which would be economically profitable and technologically feasible in an already existing plant. Furthermore, the composition of the crystalline product following the addition of thiourea should be tested using appropriate methods and analyses.

Figure 4. Separation of crystals by cooling at room temperature following the addition of urea and thiourea: U1, U2, U3 – samples to which urea was added; T1, T2, T3 – samples to which thiourea was added

4. Conclusions

In this research, a physicochemical analysis of the wastewater flow from an industrial plant resulting from the production of maleic anhydride was conducted. Based on the obtained results, it is evident that a very low pH as well as electrical conductivity indicate the presence of organic acids left over from distilling MAN. Given that the resulting flow is a suspension flow at the temperature of water used to wash the distillation column as well as the physical and chemical properties of fumaric and maleic acids, it can be stated that both are the two dominant components in the waste flow. This was also confirmed by determining the acidity by titration with NaOH. The research determined the density of the liquid phase as well as the bulk density of the separated crystalline product. By carrying out different experimental methods, the crystals were separated from the waste suspension by a combination of cooling and the addition of thiourea, a technique which can be applied in an industrial plant, facilitating the isomerization reaction of maleic to fumaric acid. Furthermore, the installation of a metal grid at the inlet to the receiving court is a simple structural solution whereby the resulting crystalline product, with appropriate analyses, could be used in processes that do not require highly pure fumaric acid, e.g. resin production. The liquid component, that is, the mother solution obtained by separating the waste suspension, due to the high COD and BOD, following the adjustment of other parameters like pH, could be successfully treated by the process of anaerobic digestion or co-digestion. Therefore, the liquid stream could serve as a good co-digestate for adjusting the characteristics of waste sludge that is normally applied in anaerobic digestive processes.

Following a literature review, since it was observed that very few studies have been conducted in this regard or require significant financial resources, this research opens up new possibilities and perspectives for the implementation of simple as well as inexpensive industrial and implementable solutions.

REFERENCES

[1] Utasi, A.; Sebestyén, V.; Rédey, Á.: Informative environment qualifying index, *Hung. J. Ind. Chem.*, 2000 **48**(2), 23–36, DOI: 10.33927/hjic-2020-24

[2] Abbas, S.K.: Production of maleic anhydride from oxidation of n-butane, *A design project submitted to the Faculty of Engineering and Built Environment in partial fulfilment of the requirements for Design of Chemical Processes computer aided Class KKKK6014*, 2015 p. 4, DOI: 10.13140/RG.2.1.4096.8569

[3] Mestl, G.; Lesser, D.; Turek, T.: Optimum performance of vanadyl pyrophosphate catalysts, *Top Catal*, 2016 **59**, 1533–1544, DOI: 10.1007/s11244-016-0673-0

[4] Felthouse, T.R.; Burnett, J.C.; Horrell, B.; Mummey, M.J.; Kuo, Y.J.: Maleic anhydride, maleic acid, and fumaric acid. In: Kirk-Othmer Encyclopedia of chemical technology (John Wiley & Sons, New York, NY.) 2001, DOI: 10.1002/0471238961.1301120506051220.a01.pub2

[5] Mangili, P.V.; dos Santos, R.O.; Caxiano, I.N.; de Sousa Santos, L.; Prata, D.M.: Environmental analysis of the maleic anhydride production process, *XXI National Meeting on Computer Modelling & IX Meeting on Materials Science and Technology*, 2018, https://www.researchgate.net/publication/330422302-ENVIRONMENTAL_ANALYSIS_OF_THE_MALEIC_ANHYDRIDE_PRODUCTION_PROCESS

[6] Mangili, P. V.; Prata, D. M.: Preliminary design of sustainable industrial process alternatives based on eco-efficiency approaches: The maleic anhydride case study, *Chem. Eng. Sci.*, 2020 **212**, 115313, DOI: 10.1016/j.ces.2019.115313

[7] Government of the Federation of Bosnia and Herzegovina: Regulation on the conditions of Wastewater discharge into natural recipients and the public sewage system, 2012, https://fbihvlada.gov.ba/bosanski/zakoni/2012/uredbe/2hrv.html

[8] Brackin, M.J.; McKenzie, D.E.; Hughes, B.M.; Heitkamp, M.A.: Laboratory-scale evaluation of fluidized bed reactor technology for biotreatment of maleic anhydride process wastewater, *J. Ind. Microbiol.*, 1996 **16**(4), 216–223, DOI: 10.1007/BF01570024

[9] Safronova, I.Y.; Semenova, E.V.: Optimum conditions for transformation of maleic acid by immobilized cells of *Alcaligenes xylosoxidanssubsp. xylosoxidans260*, *Appl. Biochem. Microbiol.*, 2001 **37**(4), 374–375, DOI: 10.1023/A:1010245903543

[10] Li, S.J.; Chen, H.L.; Xu, J.Y.; Zhang, L.: Recovery of fumaric acid from industrial wastewater by chemical extraction and stripping, *Sep. Sci. Technol.*, 2007 **42**(10), 2347–2360, DOI: 10.1080/01496390701446498

[11] Li, S.; Zhuang, J.; Zhi, T.; Chen, H.; Zhang, L.: Combination of complex extraction with reverse osmosis for the treatment of fumaric acid industrial wastewater, *Desalination*, 2008 **234**(1-3), 362–369, DOI: 10.1016/j.desal.2007.09.105

[12] Lameloise, M.L.; Lewandowski, R.: Recovering L-malic acid from a beverage industry waste water: Experimental study of the conversion stage using bipolar membrane electrodialysis, *J. Membr. Sci.*, 2012 **403–404**, 196–202, DOI: 10.1016/j.memsci.2012.02.053

[13] Fontanals, N.; Zohar, J.; Borrull, F.; Ronka, S.; Marcé, R.M.: Development of a maleic acid-based material to selectively solid-phase extract basic compounds from environmental samples, *J. Chromatogr. A*, 2021 **1647**, 462165, DOI: 10.1016/j.chroma.2021.462165

[14] Huang, J.; Long, Q.; Xiong, S.; Shen, L.; Wang, Y.: Application of poly (4-styrenesulfonic acid-co-maleic acid) sodium salt as novel draw solute in forward osmosis for dye-containing wastewater treatment, *Desalination*, 2017 **421**, 40–46, DOI: 10.1016/j.desal.2017.01.039

[15] ILO International Chemical Safety Cards (ICSC) https://www.ilo.org/dyn/icsc/showcard.home

[16] Eaton, A.D.; Clesceri, L.S.; Rice, E.W.; Greenberg, A.E.; Franson, M.A.H. (eds.): Standard methods of water and wastewater (Amer Public Health Assn, Washington, D.C.) 2005 21st ed., pp. 2–61, ISBN: 0875530478

[17] Verschueren, K.: Handbook of Environmental Data on Organic Chemicals (John Wiley & Sons, New York, NY.) 2001 **12** 4th ed., p. 1396

[18] Lobo, V.T.; Pacheco Ortiz, R.W.; Gonçalves, V.O.O.; Cajaiba, J.; Kartnaller, V.: Kinetic modeling of maleic acid isomerization to fumaric acid catalyzed by thiourea determined by attenuated total reflectance Fourier-transform infrared spectroscopy, *Org. Process Res. Dev.*, 2020 **24**(6), 988–996, DOI: 10.1021/acs.oprd.9b00487

[19] https://www.chemicalbook.com/Price/Thiocarbamide.htm

Optimization of Erythritol Fermentation by High-Throughput Screening Assays

Edina Eszterbauer[1] and Áron Németh[1]*

1 Department of Applied Biotechnology and Food Science, Budapest University of Technology and Economics, Műegyetem rkp. 3, Budapest, 1111, HUNGARY

In this research, the erythritol-producing ability of three *Yarrowia lipolytica* strains was investigated. The focus of our research was to achieve the highest possible erythritol concentration by examining and optimizing the cultivation conditions of erythritol fermentation. The complex utilization of the produced fermentation broth was also sought, e.g. the ergosterol extraction of yeast cells and isolation of a biodetergent from the foam formed during erythritol fermentation. Erythritol is a naturally occurring, widespread sugar alcohol that is gaining popularity, moreover, due to increases in usage, its demand among consumers is rising, which is why the importance of its biological production is becoming all the more critical in the food industry. Erythritol is 60-70% as sweet as sucrose and a low-calorie sweetener. Some microorganisms are capable of producing erythritol from glucose, meanwhile *Yarrowia lipolytica* strains have been reported as glycerol-consuming erythritol producers. These two sources of carbon were compared despite being subjected to further conditions like the initial pH, nitrogen sources and some additives. The largest production of erythritol was achieved by *Y. divulgata* resulting in 44g/L on glycerol compared to only 2g/L on glucose. The best supplementation was found to include ammonium nitrate and sodium citrate resulting in a product yield of 33%.

Keywords: erythritol, fermentation, *Yarrowia,* glycerol, glucose

1. Introduction

Due to the current lifestyle of society, the number of people suffering from diabetes mellitus and obesity is increasing. The desire of consumers to become healthier has created a whole market for sugar-free and zero-calorie foods, an important part of which is the production of sugar alcohols called polyols. Erythritol ($C_4H_{10}O_4$) is a naturally occurring sugar alcohol. Since the synthesis of erythritol is more difficult than those of other polyols, intensive research has been conducted to optimize its production in terms of the erythritol concentration, production rate (productivity) and/or yield [1].

Although erythritol is 60-70% as sweet as table sucrose, it is almost calorie-free (0.2 kcal/g), does not affect the blood sugar level nor cause tooth decay [2], has antioxidant effects, binds free radicals, possesses a glycemic index of 0 and increases the ability to absorb fructose [3]. Many methods are available to produce erythritol, both chemically and biotechnologically. Even though one of the most well-known chemical methods is high-temperature chemical synthesis from dialdehyde starch in the presence of a metal catalyst, namely nickel, which yields equimolar amounts of erythritol and ethylene glycol, this chemical process involves several steps [2,4-5]. However, it is not used in industry due to its very low yield and relatively high costs. Currently, biotechnological methods are far superior to chemical methods. The large-scale production of erythritol uses microbial fermentation processes with pure glucose, sucrose and glucose syrup from chemically and enzymatically hydrolyzed wheat and corn starches [2]. The main microbiological strains in the synthesis of erythritol are osmophilic yeasts, e.g. *Moniliella pollinis*, *Trichosporonoides megachiliensis* and *Y. lipolytica*, as well as many strains of lactic acid bacteria, e.g. *Oenococcus oeni*, *Leuconostoc mesenteroides* and *Lactobacillus sanfranciscensis* [5]. Within the food industry, erythritol is mainly used as a sweetener in finished goods. Sugar-free, reduced sugar and calorie- or sugar-free alternative foodstuffs can be produced. As a sugar substitute, erythritol can be found as a tabletop sweetener as well as a sweetener in drinks, chewing gum, chocolate, candy and baked goods. Polyols are also commonly used in products from the personal care industry such as cosmetics or toiletries. As an additive, it is increasingly included in care products such as toothpastes, mouthwashes, creams, make-up, perfumes or deodorants. Due to its properties, erythritol offers good fluidity and stability as an excipient, making it an ideal candidate for active ingredients in sachets and capsules [6]. *Yarrowia lipolytica* is one of the most

widely studied species of yeast [7]. *Y. lipolytica* exhibits strong proteolytic and lipolytic activity [8-9]. One of its most important products is lipase, an enzyme widely used in various areas of industry. *Y. lipolytica* can produce succinic acid [15] as well as erythritol and mannitol using glycerol as a substrate both in the presence and absence of sodium chloride [10]. Erythritol (170 g/l) was produced at pH 3.0 with the acetate-negative strain *Y. lipolytica* Wratislavia K1 by fed-batch fermentation [11]. In terms of its industrial use, it is most widespread in the food industry, moreover, is known for both its positive and negative effects [8]. To increase erythritol production, the effects of various additives, including sodium citrate and mannitol, were investigated in order to down-regulate the formation of by-products during erythritol fermentation. Furthermore, the supplementation of metal ions provides cofactors for key enzymes [10], various nitrates [13] and polyethylene glycol (PEG) as an osmoticum [12].

2. Experimental

The planned experiment in terms of erythritol production was performed by three *Yarrowia lipolytica* strains from the National Collection of Agricultural and Industrial Microorganisms (NCAIM, Hungary), namely NCAIM *Yarrowia lipolytica* 00597, NCAIM *Yarrowia lipolytica* 00594 and NCAIM *Yarrowia divulgata* 1485. During the fermentations, a 24-well deep-well microtiter plate (*Fig.1*) was applied with a sandwich cover by enzyscreen.com (The Netherlands) for each strain separately since many small-scale experiments can be conducted at the same time. Due to the high osmotic pressure and low pH during erythritol production, cells grow slowly, so a thorough study of many parallel fermentations needs to be performed. Using the microtiter plate, 24 experiments in different or even the same media in parallel fermentations were performed simultaneously to provide a comparison.

The ability of the strains to produce erythritol and the conditions required for erythritol fermentation were examined in order to increase the efficiency of production and achieve the highest possible erythritol concentration. The effects of the initial pH and C:N ratio were investigated during the fermentation. Given that previous studies [12,14] have shown that proper osmolarity has a significant effect on erythritol production, the effect of changing it was also investigated to determine the most appropriate range of osmolarity for erythritol production with these strains. The main consideration was the comparison of two substrates, that is, glycerol and glucose, in terms of erythritol production. After determining the most efficient fermentation conditions, our intention was to scale up the process. In the case of significant erythritol production, extraction of the product from the fermentation medium was sought. Our aim was to use the residual cells, e.g. *Yarrowia lipolytica* lysates, to further investigate cosmetic purposes after ultrasonic treatment.

Figure 1. Deep-well microplate

All the inoculum medium was contained, that is, glycerol (50 g/l), yeast extract (3 g/l), malt extract (3 g/l) and peptone (5 g/l). The erythritol fermentation medium was also contained, namely glycerol (150 g/l), NH_4Cl (3 g/l), $MgSO_4*7H_2O$ (1 g/l), KH_2PO_4 (0.2 g/l) and yeast extract (1 g/l) [11]. In order to increase erythritol production, the effects of the following additives was also tested. 20 g/l of both mannitol and sodium citrate were added during the fermentation. Metal ion supplementation resulted in the following concentrations of salts in the medium: $CuSO_4*5H_2O$ (2.5 mg/l), $FeSO_4*7H_2O$ (10 mg/l), $MnSO_4*7H_2O$ (25 mg/l) and $ZnSO_4*7H_2O$ (20 mg/l). 100 g/l of the supplement PEG (Polyethylene Glycol) was added, moreover, 4.6 g/l of nitrate supplementation was applied. Furthermore, co-fermentation was investigated in combination with the two carbon sources, namely glucose and glycerol.

The strains were inoculated in 100 ml of inoculum medium in 250 ml flasks and incubated on a rotary shaker (New Brunswick Innova 40) at 250 rpm for 3 days at 25°C. All wells of the microplate contained 5 ml of fermentation medium and were incubated on a rotary shaker at 250 rpm for at least 20 days at 25°C. The pH was measured by a Mettler Toledo FiveEasy pH meter and controlled at 3.0 with NaOH (6N).

The cell density was measured optically at 600 nm by a Camspec M501 Single Beam UV/Vis spectrophotometer every other day. Fermentation products were determined by a Waters Breeze isocratic HPLC system equipped with a Bio-Rad Aminex HPX-87H column at 65°C. An RI detector was applied at 40°C and the eluent was 5mM H_2SO_4 in ultrapure water (Simplicity, Millipore). To determine the osmotic pressure of the fermentation, 60 µl of fermentation medium was analyzed by measuring the freezing-point depression using an osmometer (Gonotec Osmomat 3000).

3. Results and Discussion

3.1. Yarrowia lipolytica strain 594

Y. lipolytica strain 594 was produced using the least amount of erythritol compared to the other two tested strains. The highest concentration (10.95 g/l) was achieved on the 14th day of the fermentation in the basic fermentation media containing 100 g/l glycerol with 50 g/l glucose supplementation, i.e. co-fermentation. The highest product yield of 14.81% was also recorded using the same experimental setup, where glycerol in the media was completely consumed but not the glucose. In the case of *Y. lipolytica* strain 594, it can be stated that erythritol was not produced when only glucose was used as a substrate together with any of the other supplements. The highest erythritol concentration of 8.65 g/l was achieved when glycerol was used as the substrate supplemented with PEG, which is also rather low in comparison to other reports. Glucose as a substrate was not useful with regard to erythritol production using *Y. lipolytica* strain 594.

3.2. Yarrowia lipolytica strain 597

Y. lipolytica strain 597 was able to produce more erythritol than *Y. lipolytica* strain 594. The highest concentration (14.04 g/l) was produced in glycerol containing a medium supplemented with $NaNO_3$, which was achieved on the 20th day of fermentation and corresponded to a yield of 30.31%. The average osmolarity with a slight decrement was 2243 mOsmol/kg, which is twice that of glucose. The maximum osmolarity of the medium containing glucose was approximately 1200 mOsmol/kg, which decreased in correlation with the reduction in glucose concentration. This may explain why erythritol was produced in larger quantities in the medium containing glycerol. Glycerol was only completely consumed by the end of the fermentation when the media were combined, containing 100 g/l of glucose and 50 g/l of glycerol. On the 14th day, erythritol production had reached its maximum (11.13 g/l), after which its amount began to decrease. Although the osmolarity was 1043 mOsmol/kg on the 14th day, it was initially 1346 mOsmol/kg. In the case of glucose, the highest concentration of erythritol was 2.04 g/l, which was achieved in a medium supplemented with ammonium sulfate and corresponded to a yield of 4.54%. Using this setup, even though the average osmolarity was 1165 mOsmol/kg, which is very low for erythritol production, 4.24 g/l of mannitol was produced. Therefore, when glucose was used as the substrate supplemented with ammonium sulfate, mannitol was produced by *Y. lipolytica* strain 597 instead of erythritol.

3.3 Yarrowia divulgata strain 1485

Once again, two different substrates, namely glycerol and glucose, were compared. Among the tested additives (*Fig.2A*), the largest increase in erythritol concentration was experienced in the case of sodium citrate compared to the control samples. The highest concentration of
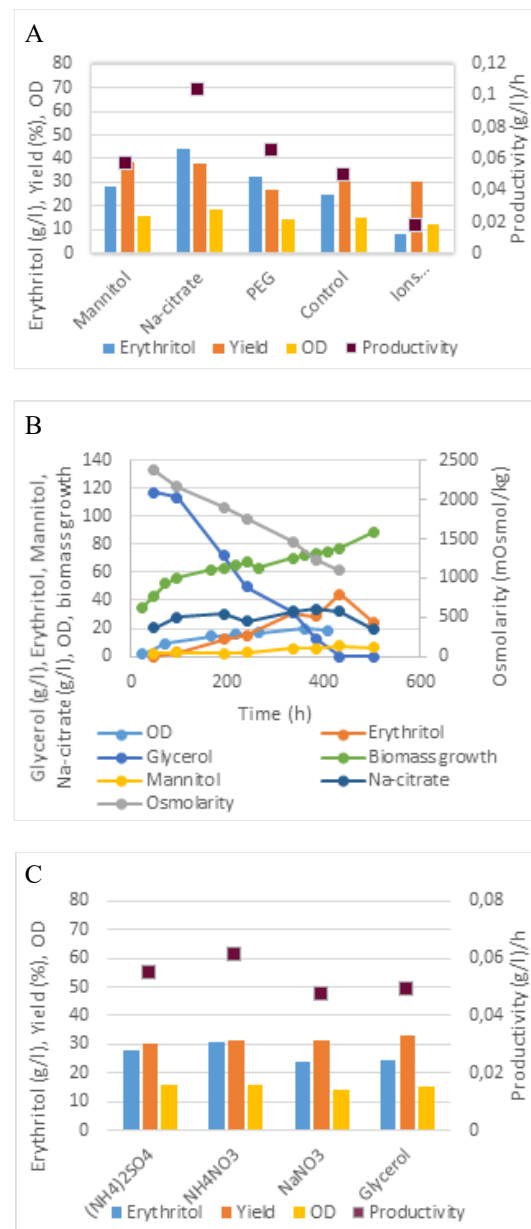

Figure 2. Results of *Y. divulgata* strain 1485 - A) effect of supplements, B) time course of best run, C) effect of N-sources

erythritol (44.38 g/l) was produced by *Y. divulgata* on the 18th day of the fermentation using glycerol as a substrate supplemented with sodium citrate (*Fig.2B*). The glycerol was completely used up in the medium. The highest productivity of 0.1 (g/l)/h and highest yield of 37.86% were achieved with this supplementation. The osmolarity of the medium decreased in correlation with the exhaustion of glycerol from 2371 mOsmol/kg initially to 1099 mOsmol/kg by the end of the fermentation.

In the case of PEG and metal supplementation, 32.44 and 8.31g/L of erythritol had been produced by the end of the fermentation, respectively. Among the tested nitrogen sources (*Fig.2C*), ammonium nitrate yielded the highest erythritol concentration of 30.75 g/l, corresponding to a yield of 31.11% based on glycerol. Compared to the control media, neither of the nitrogen

sources could significantly increase the erythritol production. By the end of the fermentation supplemented with ammonium nitrate, 5.13 g/l of mannitol had been produced. Regarding the fermentations supplemented with ammonium sulfate and sodium nitrate, 27.60 and 23.87 g/l of erythritol had been produced by the end of the fermentation, respectively. In the case of the substrate glucose, the highest production of erythritol (12.95 g/l) was achieved in the medium supplemented with sodium citrate.

4. Discussion

In the present work, 3 strains of *Yarrowia* species were examined on two carbon sources, namely glycerol and glucose, in terms of erythritol fermentation. Glycerol proved to be more usable. Among the 3 *Yarrowia* strains tested, *Y. divulgata* was the most productive, achieving 44.38 g/l of erythritol in the media supplemented with sodium citrate during the microplate fermentation. In the case of *Y. lipolytica* strain 594, the highest erythritol concentration of 10.95 g/l was achieved without supplementation but in a medium containing 100 g/l of glycerol supplemented with 50 g/l of glucose on the 14th day of the fermentation. Finally, in the case of *Y. lipolytica* strain 597, the highest concentration of erythritol was 14.04 g/l in the medium supplemented with sodium nitrate. The tested supplementations could increase the erythritol concentration from 24.70 to 44.38 g/L, yield from 33.15 to 37.86% and productivity from 0.049 to 0.102.

Among the reported *Yarrowia* results, although the aforementioned erythritol concentrations achieved are not particularly high, *Y. divulgata* may reach the recently used strains after optimization. In addition to the use of erythritol alone, the complex utilization of the broth for the application of ergosterol and cosmetics may be of greater interest and feasibility.

In the future, given the high number of variables influencing erythritol productivity, a neural network will be used to optimize erythritol fermentation for *Y. divulgata* strain 1485, which proved to be the best. Additionally, isolation and determination of the ergosterol content of the cells as well as the produced biodetergent will also be investigated

REFERENCES

[1] de Cock, P.: Sweeteners and sugar alternatives in food technology, (Wiley-Blackwell, Chichester, West Sussex, UK) 2012, pp. 215–241, ISBN: 9781118373941

[2] Godswill, A.C.: Sugar alcohols: chemistry, production, health concerns and nutritional importance of mannitol, sorbitol, xylitol, and erythritol, *Int. J. Adv. Acad. Res.*, 2017, **3**(2), 31–66, ISSN: 2488-9849

[3] Martău, G.A.; Coman, V.; Vodnar, D.C.: Recent advances in the biotechnological production of erythritol and mannitol, *Crit. Rev. in Biotechnol.*, 2020, **40**(5), 608–622, DOI: 10.1080/07388551.2020.1751057

[4] Janek, T.; Dobrowolski, A.; Biegalska, A.; Mirończuk, A.M.: Characterization of erythrose reductase from Yarrowia lipolytica and its influence on erythritol synthesis, *Microb. Cell Factories*, 2017, **16**(1), 1–13, DOI: 10.1186/s12934-017-0733-6

[5] Rakicka-Pustułka, M.; Mirończuk, A. M.; Celińska, E.; Białas, W.; Rymowicz, W.: Scale-up of the erythritol production technology – Process simulation and techno-economic analysis, *J. Cleaner Prod.*, 2020, **257**, 120533, DOI: 10.1016/j.jclepro.2020.120533

[6] Regnat, K.; Mach, R.L.; Mach-Aigner, A.R.: Erythritol as sweetener — wherefrom and whereto? *Appl. Microbiol. Biotechnol.*, 2018, **102**(2), 587–595, DOI: 10.1007/s00253-017-8654-1

[7] Gonçalves, F.A.G.; Colen, G.; Takahashi, J.A.: *Yarrowia lipolytica* and its multiple applications in the biotechnological industry, *Sci. World J.*, 2014, 476207, DOI: 10.1155/2014/476207

[8] Nagy, E.S.: Biodiversity of food spoilage Yarrowia group in different kinds of food. PhD theses (in Hungarian), (Corvinus University, Budapest, Hungary) 2015, DOI: 10.14267/phd.2015033

[9] Groenewald, M.; Boekhout, T.; Neuvéglise, C.; Gaillardin, C.; Van Dijck, P.W.; Wyss, M.: *Yarrowia lipolytica*: safety assessment of an oleaginous yeast with a great industrial potential, *Crit. Rev. Microbiol.*, 2014, **40**(3), 187–206, DOI: 10.3109/1040841X.2013.770386

[10] Tomaszewska, L.; Rywińska, A.; Gładkowski, W.: Production of erythritol and mannitol by Yarrowia lipolytica yeast in media containing glycerol, *J. Ind. Microbiol. Biotechnol.*, 2012, **39**(9), 1333–1343, DOI: 10.1007/s10295-012-1145-6

[11] Rymowicz, W.; Rywińska, A.; Marcinkiewicz, M.: High-yield production of erythritol from raw glycerol in fed-batch cultures of *Yarrowia lipolytica*, *Biotechnol. Lett.*, 2009, **31**(3), 377–380, DOI: 10.1007/s10529-008-9884-1

[12] da Silva, L.V.; Coelho, M.A.Z.; Amaral, P.F.F.; Fickers, P.: A novel osmotic pressure strategy to improve erythritol production by Yarrowia lipolytica from glycerol, *Bioproc. Biosyst Eng*, 2018, **41**(12), 1883–1886, DOI: 10.1007/s00449-018-2001-5

[13] Rakicka, M.; Rukowicz, B.; Rywińska, A.; Lazar, Z.; Rymowicz, W.: Technology of efficient continuous erythritol production from glycerol, *J. Cleaner Prod.*, 2016, **139**, 905–913, DOI: 10.1016/j.jclepro.2016.08.126

[14] Ibrahim, O.: Erythritol chemical structure, biosynthesis pathways, properties, applications, and production, *Int. J. Microbiol. Biotechnol.*, 2021, **6**(3), 59–63 DOI: 10.11648/j.ijmb.20210603.11

[15] Németh, Á.: Investigations Into Succinic Acid Fermentation, *Hung. J. Ind. Chem.*, 2019, **47**(2), 1–4, DOI: 10.33927/hjic-2019-13

The Rhizosphere of *Petrosimonia Triandra* may Possess Growth-Inducing and Salinity-Tolerance Potential

Gyöngyi Székely[1,2,3]*, Norbert Zsolt Szígyártó[1,2], András Tóth[1,2] and Csengele Barta[4]

1 Hungarian Department of Biology and Ecology, Faculty of Biology and Geology, Babeș-Bolyai University, 5-7 Clinicilor St., Cluj-Napoca, 400006, Romania
2 Institute for Research-Development-Innovation in Applied Natural Sciences, Babeș-Bolyai University, 30 Fântânele St., Cluj-Napoca, 400294, Romania
3 Centre for Systems Biology, Biodiversity and Bioresources (3B), Babeș-Bolyai University, 5-7 Clinicilor St., Cluj-Napoca, 400006, Romania
4 Department of Biology, Missouri Western State University, 4525 Downs Drive, Agenstein-Remington Halls, St. Joseph, MO 64507, USA

The root microbiome of halotolerant plants can represent a great source of salt-tolerant plant growth-promoting rhizobacteria (ST-PGPR) with a wide range of beneficial effects on plants growth, development and productivity. The better understanding of the variety of complex salt tolerance and adaptive mechanisms of halophytes can contribute to improve salt tolerance in crops, and as a result, a better and increased use of saline areas worldwide. In addition, reclaiming saline areas for agricultural use may be able to alleviate the global threat of progressive soil salinization.

Keywords: ST-PGPR, molecular analysis, saline soil

1. Introduction

Although the threat of the continuous expansion of areas of saline soil exhibiting enhanced levels of salinity has a negative effect on soil structure, fertility and plant health, by progressively constraining plants in narrower habitats, they can grow and develop optimally without experiencing the negative, stressful impacts of saline conditions. Habitat narrowing is expected to decrease biodiversity and have negative impacts on the usability of land for agricultural practices. One of the most damaging abiotic stress factors for plants is the excessive accumulation of salt in their natural habitats caused by soil salinization. Soil salinity is most often defined by its electrical conductivity (EC) with values above 4 dSm^{-1} indicative of saline soils [1]. Soil salinity can be determined by the occurrence of a variety of salts such as NaCl, Na$_2$SO$_4$, Na$_2$CO$_3$, MgSO$_4$, MgCl$_2$, KCl and CaSO$_4$. All of these salts have the potential to induce salinity stress in plants. From among the aforementioned salts, the accumulation of NaCl is the most frequent in soils. The adverse effects of NaCl stress on plants has been extensively documented [2-4]. Saline soils represent a substantial limiting factor for the development and propagation of the majority of plant species belonging to the group of non-halophytes (also referred to as glycophytes). Only halophytes, that is,

plants adapted to and capable of achieving optimal development in saline environments, can persist in saline soils. To counteract salinity stress, salt-tolerant species have developed a wide range of tolerance traits such as osmotic adjustment, ion sequestration, ion exclusion, adaptations of the membrane transport system and protection enhanced by the synthesis of a variety of macromolecules with osmolytic properties, e.g. glycine betaine, proline, etc. [5].

Petrosimonia triandra is a halophyte able to complete its life cycle under moderate saline conditions (EC: 4.45 dSm^{-1}) native to the saline area of Cojocna in Cluj County, Romania (*Fig.1*) [6]. While the salt tolerance mechanisms of *P. triandra* are currently poorly understood, Podar et al. (2019) documented several adaptive mechanisms in this species that can withstand soil salinity such as morphological, physiological and biochemical adaptations, e.g. the development of efficient photosynthetic and antioxidative systems as well as the accumulation of the protective osmolyte proline. Similar salt tolerance mechanisms have also been documented in other halophyte species [7-8].

Another strategy of halophyte plant species to improve their range of salt tolerance is co-habitation with groups of rhizosphere-specific bacteria called plant growth-promoting rhizobacteria (PGPR), which live in the immediate vicinity of plants' root systems (also referred to as the rhizosphere) as well as exert a positive

effect on plant growth and development. These effects are underpinned by diverse mechanisms such as the addition of essential nutrients (N, K, Zn, Fe, PO_4); production of 1-aminocyclopropane-1-carboxylate (ACC) deaminase, volatile organic compounds and phytohormones; as well as the facilitation of favorable plant-microbe interactions, antifungal effects, etc. [9-10]. Some PGPR species have been found to be salt tolerant, namely ST-PGPR, and successfully used over recent decades to enhance crop yield and improve soil fertility. Most recently, Ayub et al. (2020) clearly emphasized the role of PGPRs in the salt tolerance of halophytes. In addition, nowadays, ST-PGPRs are also used as bioinoculants to improve crop productivity and provide protection from phytopathogens [11-12]. Therefore, ST-PGPRs are promising tools to enhance the salinity tolerance of plants.

The goal of the current study was to identify ST-PGPR species from the rhizosphere of P. triandra. A better understanding of the rhizobial community - contributing to the enhancement of salt tolerance in species adapted to and native to saline areas - is expected to lead to valuable applications, thereby enhancing the tolerance of high-value crops and other species of horticultural use as well as provide technologies to expand land-use practices for agricultural purposes to underutilized, highly saline areas [13].

2. Experimental

2.1. Soil sampling site

Soil samples were collected from the rhizosphere of the halophyte *P. triandra*, native to the saline zone of Cojocna in Cluj County, Romania (GPS coordinates N46.74328 E23.84295, *Fig.1*). The salinity of this site is characterized by EC = 4.45 dSm^{-1}, which corresponds to moderate saline soil [1]. The specific physicochemical characteristics of the soil at the sampling site have been described in our former study [6].

2.2. Isolation of bacterial species from the rhizosphere of P. triandra

P. triandra plants were carefully dug up and removed from the soil before gently shaking their roots to remove the excess soil. The soil that was directly adhered to the roots was collected and transported back to the laboratory for analysis where it was transferred into a flask containing 99 ml of sterilized distilled water. After shaking the flask for 15 minutes, the soil samples were subjected to a 10-fold serial dilution and 100 µl of the solution was spread on plates containing nutrient agar (NA) media (Merck, Germany) supplemented with 2, 4, 6, 8, 10, 11, 11.5, 12, 12.5 and 13% NaCl, respectively. The plate containing NA without external NaCl was used as the control sample. The plates were incubated at room

Figure 1. A: Location of the study zone in Cojocna, Romania; B: the habitat of *P. triandra* in Cojocna; C: young *P. triandra* plants

temperature with colonies appearing 3-4 days after inoculation.

2.3. Identification of salt-tolerant rhizobacteria using a 16S rRNA gene sequence

To identify the rhizosphere of bacterial species, strains exhibiting the highest salt tolerance were selected, namely 11.5, 12 and 12.5% NaCl. Thirty colonies were selected for DNA isolation, PCR and gene sequencing of their 16S rRNA gene. Having extracted the total genomic DNA (QIAGEN, Germany), a fragment of the 16S rRNA gene was amplified by PCR using the 16S rRNA universal primers (27F: 5′-AGAGTTTGATCCTGGCTCAG-3′ and 1492R: 5′-GGTTACCTTGTTACGACTT-3′). The PCRs were mixed using a Bioline PCR kit with the polymerase MyTaq Red Mix (Bioline, Meridian Bioscience, Memphis, TN) in a final volume of 50 µl. The PCRs were performed using a MultiGene OptiMax thermal cycler (Labnet, Cary, NC) under the following cycling conditions: 5 mins. at 95°C, followed by 30 cycles lasting

Table 1. Identified rhizosphere bacteria and the salt concentration facilitating their optimum growth

No.	PGPR name	NaCl tolerance (%)
1.	*Bacillus hwajinpoensis* FJAT-46935	12.5
2.	Bacillus sp. LS-X7	12.5
3.	Bacillus sp. EBW4	12.0
4.	Bacillus sp. YTM5	11.5

30s each at 94°C, 30s each at 55°C and 1.5 mins. each at 72°C followed by a final extension step at 72°C for 7 mins. 5 µl aliquots of each reaction were analyzed on 1% (*w*/*v*) agarose gel in TBE buffer, stained with Midori Green Advance nucleic acid staining solution (NIPPON Genetics EUROPE, Düren, Germany). The resulting ~1500 bp PCR product was purified using an Agarose Gel Extraction Kit (Jena Bioscience, Jena, Germany) according to the manufacturer's protocol and sent for sequencing at the genomic sequencing service provider Macrogen (South Korea, http://dna.macrogen.com/eng). BLAST analysis and gene sequencing were also performed by Macrogen.

3. Results and Discussion

3.1. Determination of the NaCl tolerance of the rhizobacteria P. triandra

Rhizobacteria isolated in close proximity to the roots of *P. triandra* could survive in a media supplemented with up to 12.5% NaCl (*Fig.2*). 46 bacterial colonies were able to grow in the presence of salinities as high as 11.5, 12 and 12.5% NaCl. The number of bacterial colonies grown in saline media decreased as the NaCl concentration increased. A total number of 26, 12 and 8 bacterial isolates survived in salinities of 11.5, 12 and 12.5% NaCl, respectively. The 8 most salt-tolerant bacterial isolates survived in the presence of 12.5% NaCl. Based on their highest level of salt tolerance and diverse morphology, 30 isolates were selected for molecular identification.

3.2. Identification of salt-tolerant rhizobacteria

The bacterial 16S rRNA gene sequence analysis determined that of the 30 selected isolates, 26 belonged to the Bacillus genus (Bacillus sp. strains EBW4, LS-X7, YTM5) with one of them identified as the *B. hwajinpoensis* strain FJAT-46935. The other four isolates could not be identified. The names of the isolates and their highest salinity tolerance are presented in *Table 1*.

The important role of some of the identified *P. triandra* rhizobacteria in enhancing plant growth, yield and salt tolerance has been described previously [14]. A plant growth-promoting effect of the rhizosphere bacterial strain Bacillus sp. EBW4 was reported by Utkhede and Smith in 1992 [15], who highlighted an

Figure 2. Bacterial isolates growing on NA media supplemented with 12.5% NaCl

increase in the growth of apple trees and fruit yield after applying Bacillus sp. EBW4. Another PGPR identified is *B. hwajinpoensis*, which was also characterized as a halotolerant rhizobacterial species with plant growth-promoting traits by Ferreira et al. (2021) [16]. Furthermore, many other Bacillus sp. strains were also described as ST-PGPRs. Experiments with several plant species proved that a diverse range of Bacillus strains such as *B. pumilus*, *B. paramycoides and B. amyloliquefaciens* exhibit elevated salinity tolerance following the induction of a series of salt-tolerance mechanisms in plants, e.g. enhance antioxidant enzyme activity and reduce lipid peroxidation [16-19]. Ferreira et al. (2021) described the plant growth-promoting characteristics of salt-tolerant Bacillus sp., e.g. production of indole-3-acetic acid (IAA) and siderophores, enhanced 1-aminocyclopropane-1-carboxylic acid (ACC) deaminase activity as well as phosphate solubilization [16]. Moreover, Nawaz et al. (2020) studied the individual or synergistic effects of ST-PGPRs on wheat growth as well as yield under saline conditions and found that these bacteria may be used as bioinoculants to enhance crop yield in saline environments [20].

Our findings regarding the Bacillus sp. strains LS-X7 and YTM5 in the rhizosphere of the salt-tolerant *P. triandra* populated by numerous ST-PGPR species are novel, moreover, it is hypothesized that these strains are also potential candidates for ST-PGPR activity along with the other described species and Bacillus strains. The potential ST-PGPR function of the aforementioned strains requires further investigation, namely analysis of their ACC deaminase activity, phytohormone production and plant-microbe interactions, which are the goals of our future studies.

In summary, based on our results and prior findings, the root microbiome of the halophyte *P. triandra* is likely to be a useful source for the isolation, discovery and characterization of yet unknown ST-PGPRs providing tools with further applications with regard to inducing halotolerance in plants of high economic value. Therefore, understanding the salt tolerance mechanisms of halotolerant plants in general, e.g. that of *P. triandra* in our study, may ultimately facilitate the exploitation of

saline areas for agricultural purposes, especially in the Carpathian Basin.

4. Conclusions

P. triandra, similarly to a series of other halophyte species, has evolved various morphological, physiological and biochemical salt adaptation mechanisms to counteract the harmful effects of elevated salinity [6]. The isolation of halotolerant bacteria from the rhizosphere of this species indicates that plant-microbe cohabitation may influence the adaptive strategy of the plant. Although further investigations are necessary to characterize the novel identified bacterial strains and demonstrate their PGPR ability, our results are promising. Therefore, the identified ST-PGPR species from the rhizosphere of *P. triandra* could possibly be used to improve the salinity tolerance of non-halophyte species such as many common crops threatened by the salinization of arable land worldwide.

Acknowledgements

REFERENCES

[1] Shrivastava, P.; Kumar, R.: Soil Salinity: A serious environmental issue and plant growth promoting bacteria as one of the tools for its alleviation, *Saudi J. Biol. Sci.,* 2015 **22**(2), 123–131, DOI: 10.1016/j.sjbs.2014.12.001

[2] Rengasamy, P.: Transient salinity and subsoil constraints to dryland farming in Australian sodic soils: an overview, *Anim. Prod. Sci.,* 2002 **42**(3), 351–361, DOI: 10.1071/EA01111

[3] Munns, R.; Tester, M.: Mechanisms of salinity tolerance, *Annu. Rev. Plant Biol.,* 2008 **59**(1), 651–681, DOI: 10.1146/annurev.arplant.59.032607.092911

[4] Tavakkoli, E.; Rengasamy, P.; McDonald, G.K.: High concentrations of Na^+ and Cl^- ions in soil solution have simultaneous detrimental effects on growth of faba bean under salinity stress, *J. Exp. Bot.,* 2010 **61**(15), 4449–4459, DOI: 10.1093/jxb/erq251

[5] Arzani, A.: Improving salinity tolerance in crop plants: a biotechnological view, *In Vitro Cell. Dev. Biol.,* 2008 **44**(5), 373–383, DOI: 10.1007/s11627-008-9157-7

[6] Podar, D.; Macalik, K.; Réti, K.O.; Martonos, I.; Török, E.; Carpa, R.; Weindorf, D.C.; Csiszár, J.; Székely, G.: Morphological, physiological and biochemical aspects of salt tolerance of halophyte *Petrosimonia triandra* grown in natural habitat, *Physiol. Mol. Biol. Plants,* 2019 **25**(6), 1335–1347, DOI: 10.1007/s12298-019-00697-x

[7] Zhang, X.; Yin, H.; Chen, S.; He, J.; Guo, S.: Changes in antioxidant enzyme activity and transcript levels of related genes in *Limonium sinense* Kuntze seedlings under NaCl stress, *J. Chem.,* 2014 **2014,** 1–6, DOI: 10.1155/2014/749047

[8] Ghanem, A-M.F.M.; Mohamed, E.; Kasem, A.M.M.A.; El-Ghamery, A.A.: Differential salt tolerance strategies in three halophytes from the same ecological habitat: Augmentation of antioxidant enzymes and compounds, *Plants,* 2021 **10**(6), 1100, DOI: 10.3390/plants10061100

[9] Bhattacharyya, P.N.; Jha, D.K.: Plant growth-promoting rhizobacteria (PGPR): Emergence in agriculture, *World J. Microbiol.,* 2011 **28**(4), 1327–1350, DOI: 10.1007/s11274-011-0979-9

[10] Jha, B.; Gontia, I.; Hartmann, A.: The roots of the halophyte *Salicornia brachiata* are a source of new halotolerant diazotrophic bacteria with plant growth-promoting potential, *Plant Soil,* 2011 **356**(1-2), 265–277, DOI: 10.1007/s11104-011-0877-9

[11] Grover, M.; Ali, S.Z.; Sandhya, V.D.; Rasul, S.; Venkateswarlu, B.: Role of microorganisms in adaptation of agriculture crops to abiotic stresses, *World J. Microbiol.,* 2011 **27**(5), 1231–1240, DOI: 10.1007/s11274-010-0572-7

[12] Egamberdieva, D.; Wirth, S.; Bellingrath-Kimura, S.D.; Mishra, J.; Arora, N.K.: Salt-tolerant plant growth promoting rhizobacteria for enhancing crop productivity of saline soils, *Front. Microbiol.,* 2019 **10**, 2791, DOI: 10.3389/fmicb.2019.02791

[13] Ayub, M.A.; Ahmad, H.R.; Ali, M.; Rizwan, M.; Ali, S.; Zia-ur-Rehman, M.; Waris, A.A.: Chapter 3 - Salinity and its tolerance strategies in plants, In: Tripathi, D.K.; Singh, V.P.; Chauhan, D.K.; Sharma, S.; Prasad, S.M.; Dubey, N.K.; Ramawat, N.: Plant Life Under Changing Environment (Academic Press) 2020 pp. 47–76, DOI: 10.1016/B978-0-12-818204-8.00003-5

[14] Székely, G.; Barta, C.: Plant growth promoting rhizobacteria – biotechnological tools to improve cereal yield, *Hung. J. Ind. Chem.,* 2022 **50**(1), 11–14, DOI: 10.33927/hjic-2022-03

[15] Utkhede, R.S.; Smith, E.M.: Promotion of apple tree growth and fruit production by the EBW-4 strain of *Bacillus subtilis* in apple replant disease soil, *Can. J. Microbiol.,* 1992 **38**(12), 1270–1273, DOI: 10.1139/m92-209

[16] Ferreira, M.J.; Cunha, A.; Figueiredo, S.; Faustino, P.; Patinha, C.; Silva, H.; Sierra-Garcia, I.N.: The root microbiome of *Salicornia ramosissima* as a seedbank for plant-growth promoting halotolerant bacteria, *Appl. Sci.,* 2021 **11**(5), 2233, DOI: 10.3390/app11052233

[17] Mahmood, A.; Amaya, R.; Turgay, O.C.; Yaprak, A.E.; Taniguchi, T.; Kataoka, R.: High salt tolerant plant growth promoting rhizobacteria from the common ice-plant *Mesembryanthemum crystallinum* L, *Rhizosphere,* 2019 **9**(9), 10–17, DOI: 10.1016/j.rhisph.2018.10.004

[18] Sharma, A.; Dev, K.; Sourirajan, A.; Choudhary, M.: Isolation and characterization of salt-tolerant bacteria with plant growth-promoting activities from aaline agricultural fields of Haryana, India, *J. Genet. Eng. Biotechnol.,* 2021 **19**(1), 99, DOI: 10.1186/s43141-021-00186-3

[19] Ali, Q.; Ayaz, M.; Mu, G.; Hussain, A.; Yuanyuan, Q.; Yu, C.; Xu, Y.; Manghwar, H.; Gu, Q.; Wu, H.; Gao, X.: Revealing plant growth-promoting mechanisms of Bacillus strains in elevating rice growth and its interaction with salt stress, *Front. Plant Sci.,* 2022 **13**, 994902, DOI: 10.3389/fpls.2022.994902

[20] Nawaz, A.; Shahbaz, M.; Asadullah; Imran, A.; Marghoob, M.U.; Imtiaz, M.; Mubeen, F.: Potential of salt tolerant PGPR in growth and yield augmentation of wheat (*Triticum aestivum* L.) under saline conditions, *Front. Microbiol.,* 2020 **11,** 2019, DOI: 10.3389/fmicb.2020.02019

INVESTIGATIONS INTO THE USAGE OF THE MINERAL ALGINITE FERMENTED WITH *LACTOBACILLUS PARACASEI* FOR COSMETIC PURPOSES

Pál Tóth[1] and Áron Németh[1]*

1 Department of Applied Biotechnology and Food Science, Budapest University of Technology and
  Economics, Műegyetem rkp. 3, Budapest, 1111, HUNGARY

A remarkable interplay between the skin and the fermentation of lactic acid bacteria (LAB) occurs. The lactate and amino acids in the supernatant of this bacteria help to hydrate the skin. The fermentation broth of lactic acid bacteria, generally referred as "lactic acid bacteria ferment" according to International Nomenclature of Cosmetic Ingredients (INCI), has been used to make a variety of cosmetic components. The goal of this study was to evaluate new approaches to assess ferment filtrates (also known as cell-free fermentation broths) that could be used in cosmeceuticals. Despite years of research on the production of lactic acid, aesthetic evaluations have not yet been performed. First, the *Lactobacillus paracasei* strain NCAIM B.01525 was employed in our research. Furthermore, a fermentation broth was produced containing the Hungaricum mineral alginite and the impact of hydration on human skin tested. The influence of alginite on the fermentation of LAB was also examined. According to the results of the trials, although alginite might double and triple biomass and specific growth rates, respectively, it cannot facilitate hydration of the skin. These results might contribute to the development of more widely accessible, environmentally-friendly cosmetic components in the future.

Keywords: human skin, dermatoscope, moisturizing effect

1. Introduction

The use of cosmetics dates back 7,000 years to Ancient Egypt and were later used in the Roman Empire, for example, according to some legends, Cleopatra bathed in goats' milk to preserve the youthfulness of her skin. Later, milk baths became popular in the English royal court, for instance, Catherine Parr, the last queen of the House of Tudor, and later Elizabeth I, Queen of England, regularly used a milk bath to preserve their beauty. In today's modern world, using natural ingredients in cosmetics has come to the fore again. Although our laboratory has been dealing with lactic acid producers for many years, to date, no measurements have been made in terms of cosmetics.

The structure of the skin and the composition of the stratum corneum (SC) are shown in *Fig. 1*, including the natural moisturizing factor (NMF). The skin consists of two main layers, namely the dermis and epidermis. The epidermis is further divided into two main layers, that is, the viable epidermis and the stratum corneum (SC), which is the outermost layer mainly consisting of dead cells. The essential function of the SC is to act as a barrier, preventing dehydration caused by water loss from the body. The SC contains 30% NMF, which

consists of 40% amino acids such as serine, glycine and alanine as well as 12% lactate, which is capable of retaining water in the stratum corneum [2].

On the other hand, lactic acid bacteria (LAB) are generally defined as Gram-positive, non-spore-forming, catalase-negative, aerotolerant, acid-tolerant, nutrient-demanding and strictly fermentative organisms that lack cytochromes as well as produce lactic acid as the main end product of carbohydrate metabolism [3]. LAB contains cell wall-bound proteinase that initiates the transformation of extracellular proteins into oligopeptides [4]. The protease activity as well as
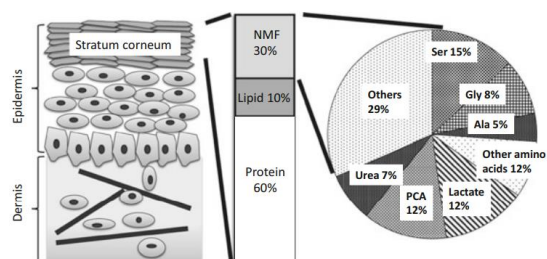

Figure 1. Composition of the skin and its natural moisturizing factor (NMF), where PCA is pyrrolidone carboxylic acid [1]

catabolic production of proteins and peptides enable LAB to produce amino acids in the fermentation broth [5]. Since many amino acids are contained in various LAB-fermented foods such as cheese [6], sausage [7] and even Japanese sake [8], a LAB-fermented ingredient contains large amounts of lactic acid and amino acids, which together form the NMF. Therefore, these ingredients exert a hydration effect when they are applied on the skin. Furthermore, a particular combination of a substrate and a strain of LAB could provide another beneficial functional impact on the skin.

Our goal was to investigate how the mineral alginite affects fermentation and moisturization of the skin. Another aim of this study was to screen for new methods to evaluate the ferment filtrate, i.e. cell-free broth, in terms of usage in cosmeceuticals.

2. Experimental

2.1. Fermentation

The planned experiment concerning the production of lactobacillus ferment filtrate was performed using a strain of *Lactobacillus paracasei* from the National Collection of Agricultural and Industrial Microorganisms (NCAIM, Hungary), namely NCAIM Lactobacillus paracasei B.01525.

The fermentations were conducted in 250 ml shake flasks and 10 ml BacTrac impedance tubes (SY-LAB, Austria - *Fig. 2*) at 37°C. Only the shake flasks were shaken at 150 rpm. The fermentations could be monitored online using a SY-LAB BacTrac 4100 microbiological analyzer due to changes in the impedance of the medium (M%) and on the surface (E%) of the electrodes by following the same method previously reported by Áron Németh [9]. The measurements were performed using the BacTrac analyzer and the results displayed by BacMonitor Y 1.39Er software. Since the BacTrac program only shows curves and does not give the corresponding points, these points had to be extracted in a different way. The curves were saved as QRP files, which were converted into JPEG format using SmartQRP software. The JPEG files had already been recognised by DigitizeIt, which made it easy to determine the points associated with the curves. The points were copied into a Microsoft Excel spreadsheet and curves were fitted to the points using SigmaPlot 2001 software for Windows version 7.0. The generalized logistic equation by Verhulst-Pearl was used [10].

The nutrient solution was the following Marie-Rogosa-Sharpe medium: peptone (10.0 g/l), yeast extract (5.0 g/l), beef extract (10.0 g/l), glucose (20.0 g/l), KH_2PO_4 (2.0 g/l), sodium acetate (5.0 g/l), magnesium sulfate (0.2 g/l), manganese sulfate (0.05 g/l), Tween 80 (1.08 g/l) and ammonium citrate (2.0 g/l). The fermentations with alginite were supplemented with 10g/l of alginite.

During the fermentation, the changes in glucose and lactic acid concentrations were monitored by a Waters
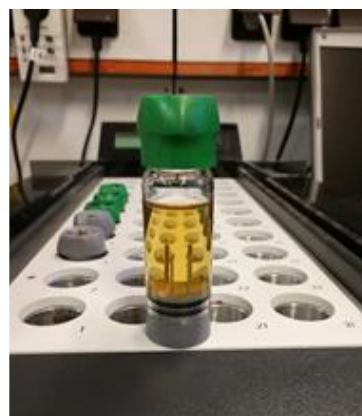

Figure 2. BacTrac and its vials with electrodes

Breeze HPLC system consisting of a Bio-Rad Aminex HPX-87H Column, Waters 717 Plus Autosampler and Waters 2414 RI detector. After appropriate dilution steps, the samples were mixed with a 0.2 µm-pore-size mixed ester syringe filter (ViaLab Magyarország Kft.).

The dry matter was measured as follows: the contents of the BacTrac tubes, that is, 10 ml of fermentation broth, were loaded into Falcon Conical Centrifuge Tubes and centrifuged at 6000 rpm for 10 mins. using a Hermle Z200A centrifuge. The supernatant was then decanted before the cells were suspended in distilled water and centrifuged once more. The supernatant was decanted again and the biomass poured into the crystallization cup with 2-3 ml of distilled water before being dried relatively quickly using our Sartorius MA35 moisture analyzer.

2.2. Determination of moisture content

The short-term/immediate hydration effect of the ferment filtrates was determined by taking triplicate measurements using a dermatoscope (*Fig. 3*). On the forearm of the subject, three 1 cm^2 areas were marked out onto which 20 µl of fermented juice was pipetted. After 5 mins., these areas were wiped with a dry hand towel and then the hydration on that part of the subject's skin was measured at given intervals with the installed Corneometer (capacitance) sensor. In order to establish a basis for comparison, the hydration of the subject's skin

Figure 3. Measuring with a dermatoscope

was recorded before measurements were taken and the values displayed here corrected according to this value.

3. Results and Discussion

3.1. BacTrac results

The effect of alginite on the kinetics of LAB fermentation was also investigated. The fermentations were monitored by BacTrac online by replicating both setups three times, that is, in the presence and and absence of alginite, supplemented with a non-inoculated (blank) reference. The reference BacTrac tube contained the medium MRS and 10 g/l of non-inoculated alginite. The replicates were compared by excluding outliers from further processing and their
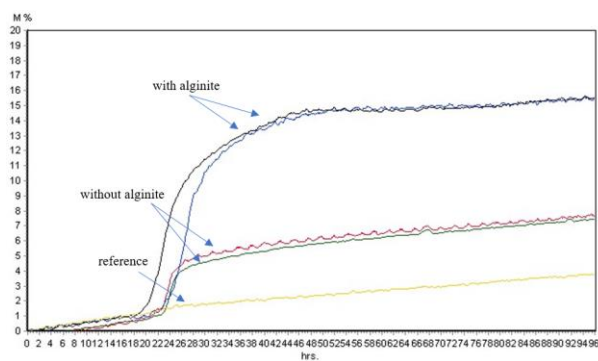

Figure 4. *Lactobacillus paracasei* fermentations in BacTrac tubes

curves are presented in *Fig. 4*. The resulting curves clearly show the impedance of *Lactobacillus paracasei* fermentations in the presence of alginite during the declining growth phase is twice as high as that of non-alginite fermentations. Furthermore, the specific growth rate was also determined to quantitatively compare the effect of alginite on fermentation kinetics as is presented in *Fig. 5*.
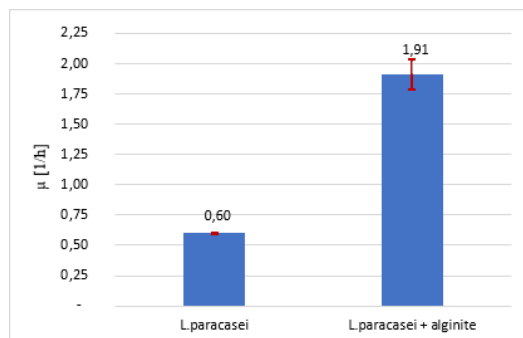

Figure 5. Specific growth rates of *L. paracasei* fermentations

The specific growth rates also differ significantly between the normal and alginite fermentations, namely 0.6 and 1.9 l/h, respectively (*Fig. 5*). Therefore, the specific growth rate of fermentation with alginite is three times higher than without.
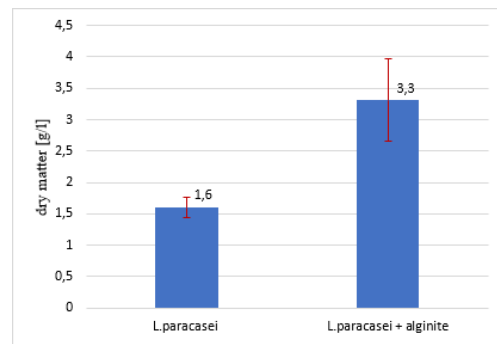

Figure 6. Concentration of dry matter in the *L. paracasei* fermentations

The data obtained from dry matter measurements also indicate that alginite fermentations achieved higher yields (*Fig. 6*).

3.2. Skin hydration

Since a lactic acid-producing strain was investigated, firstly the moisturizing effect of solutions of different lactic acid concentrations, namely 5, 10, 15 and 20 g/l of lactic acid in distilled water, was determined by a dermatoscope. How skin hydration changes over time once the given concentration of the lactic acid solution had been reduced is represented in *Fig. 7*. It is clearly visible that the level of hydration rapidly decreases over time but eventually stabilizes after ca. 35 mins.
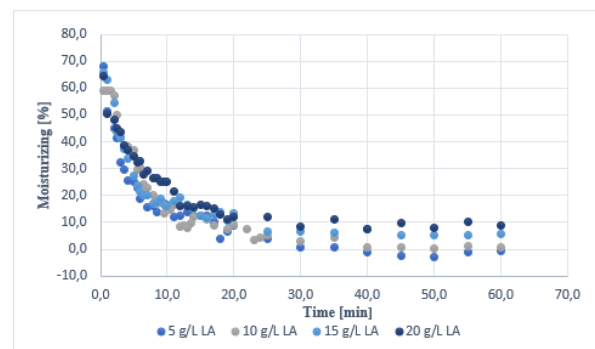

Figure 7. The moisturizing effect of the lactic acid (LA) solutions

Since the initial phase is difficult to quantify, the steady-state values after 30, 35, 40 and 45 minutes were used before being plotted against concentration as presented in *Fig. 8*. The trend is clear, that is, as the concentration of lactic acid increases, so does the moisturizing effect. The effect of the 5g/l lactic acid solution is so minimal that it has a relatively mild dehydration effect on the skin. A trendline was fitted to the points ($R^2 > 0.99$) and from the resulting equation, the hydration effect of the fermentation broth was predicted based on its lactic acid content.

While our technique for measuring the moisturizing effect is first described and applied here, the lactic acid sting test (LAST), which also measures capacitance

using a Corneometer (similarly to our dermatoscope's Corneometer) is highly comparable to it [11]-[13].

The only two differences are that the cited authors applied the ferment filtrates to the facial skin, to nasolabial folds to be exact, where the hydration effect was 6 times higher in contrast to on the forearm in our study, and that they only reported the measured level of hydration after 10 mins., which according to our time profile varies rapidly over time suggesting it may be more reliable.
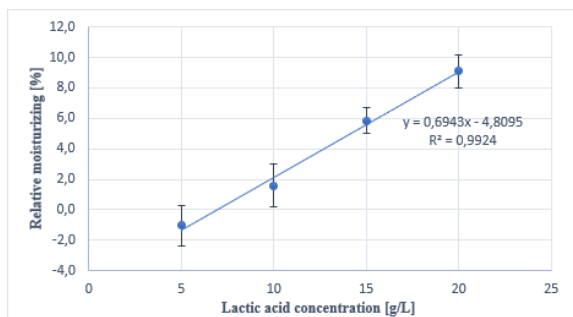

Figure 8. Steady-state moisturizing effects of LA solutions

Overall, a correlation with regard to the lactic acid solutions is observed between our results and those from the cited studies.

The effect on skin hydration of the *Lactobacillus paracasei* fermented broths was also measured and plotted against time (*Fig. 9*). A comparison concerning the steady-state values of the fermentation samples in the presence and absence of alginite is presented in *Fig. 10*. According to the results, the samples containing alginite were less hydrating than the cell-free fermentation broth. This may be due to the higher concentrations of lactic
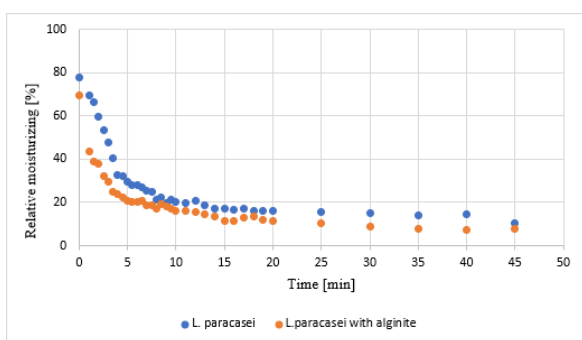

Figure 9. A comparison of the moisturizing effect of *Lactobacillus paracasei* ferment filtrates

acid produced in the alginite-free fermentation broth, namely 23.8 g/l and 28.8 g/l, respectively. By applying the equation in *Fig. 5*, hydration values of 15.2 and 11.7% were predicted for the alginite-free and alginite-containing fermentation broths, respectively, based on these lactic acid concentrations. Although the measured results in both cases are slightly lower, the difference is insignificant.
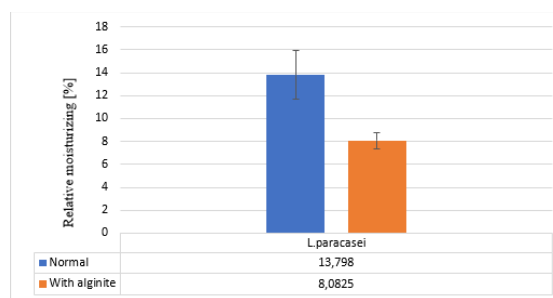

Figure 10. Lactobacillus paracasei ferment filtrates moisturizing comparison in steady state

4. Conclusion

The current study investigated the effects of the mineral alginite on the fermentation of Lactobacillus paracasei and its moisturizing effects on the skin. This study also aimed to test novel approaches for evaluating ferment filtrates (also known as cell-free fermentation broths) for use in cosmeceuticals. According to studies on the process, alginite increases the specific growth rate and dry matter content during fermentation. While the latter doubled, from 1.6 to 3.3 g/l to be exact, the former tripled from 0.60 to 1.91 l/h. Based on these encouraging findings, it was predicted that the hydration effect of the filtrate in the presence of alginite would outweigh that without. However, dermatoscopic measurements provided evidence to the contrary. The measured hydration levels of the alginite-free and alginite-containing fermentation broths were 13.9 and 8.1%, respectively.

Our future studies will focus on the effects of fermented broths containing alginite on additional aesthetic aspects such as antioxidants, skin whitening or the inhibition of the enzyme hyaluronidase.

REFERENCES

[1] Izawa, N.; Sone, T.: Cosmetic ingredients fermented by lactic acid bacteria, In: Microbial Production: From Genome Design to Cell Engineering, (Springer, Tokyo) 2014, pp. 233–242, DOI: 10.1007/978-4-431-54607-8_20

[2] Spier, H.W.; Pascher, G.: Zur analytischen und funktionellen Physiologie der Hautoberfl äche (Analytical and functional physiology of the skin surface), *Hautarzt*, 1956, **7**(2), 55–60, PMID: 13318589

[3] Axelsson, L.: Lactic acid bacteria: classification and physiology, In: Salminen, S.; von Wright, A. (eds) Lactic acid bacteria: Microbiological and functional aspects, (Marcel Dekker, Inc., New York) 1998, pp. 1–71, ISBN: 0-8247-5332-1

[4] Savijoki, K.; Ingmer, H.; Varmanen, P.: Proteolytic systems of lactic acid bacteria, *Appl. Microbiol. Biotechnol.*, 2006, **71**, 394–406, DOI: 10.1007/s00253-006-0427-1

[5] Lee, K.; Lee, J.; Kim, Y.H.; Moon, S.H.; Park, Y.H.: Unique properties of four lactobacilli in amino acid production and symbiotic mixed culture for lactic acid biosynthesis, *Curr. Microbiol.*, 2001, **43**, 383–390, DOI: 10.1007/s002840010324

[6] Visser, S.: Proteolytic enzymes and their relation to cheese ripening and flavor: an overview, *J. Dairy Science*, 1993, **76**, 329–350, DOI: 10.3168/jds.S0022-0302(93)77354-3

[7] Hierro, E.; de la Hoz, L.; Ordóñez, J.A.: Contribution of the microbial and meat endogenous enzymes to the free amino acid and amine contents of dry fermented sausages, *J. Agric. Food Chem.*, 1999, **47**, 1156–1161, DOI: 10.1021/jf980834p

[8] Iwano, K.; Takahashi, K.; Ito, T.; Nakazawa, N.: Search for amino acids affecting the taste of Japanese sake, *J. Brew. Soc. Jpn.*, 2004, **99**(9), 659–664, DOI: 10.6013/jbrewsocjapan1988.99.659

[9] Németh, Á.: Investigations into succinic acid fermentation, *Hung. J. Ind. Chem.*, 2019, **47**(2), 1–4, DOI: 10.33927/hjic-2019-13

[10] Edwardsa, W.H.; Wilke, C.R.: Mathematical representation of batch culture data, *Biotechnol. Bioeng.*, 1968, **10**, 205–232, DOI: 10.1002/bit.260100208

[11] Pan, Y.; Ma, X.; Song, Y.; Zhao, J.; Yan, S.: Questionnaire and lactic acid sting test play different role on the assessment of sensitive skin: A cross-sectional study, *Clin. Cosmet. Investig. Dermatology*, 2021, **14**, 1215–1225, DOI: 10.2147/CCID.S325166

[12] An, S.; Lee, E.; Kim, S.; Nam, G.; Lee, H.; Moon, S.; Chang, I.: Comparison and correlation between stinging responses to lactic acid and bioengineering parameters, *Contact Derm.*, 2007, **57**(3), 158–162, DOI: 10.1111/j.1600-0536.2007.01182.x

[13] Wu, Y.; Wang, X.; Zhou, Y.; Tan, Y.; Chen, D.; Chen, Y.; Ye, M.: Correlation between stinging, TEWL and capacitance, *Skin Res. Technol.*, 2003, **9**(2), 90–93, DOI: 10.1034/j.1600-0846.2003.00026.x

HUNGARIAN JOURNAL OF
INDUSTRY AND CHEMISTRY
HJIC

Separation of Dissolved Gases from Aqueous Anaerobic Effluents Using Gas-Liquid Membrane Contactors

MERVE VISNYEI[1*], PÉTER BAKONYI[1], NÁNDOR NEMESTÓTHY[1] AND KATALIN BÉLAFI-BAKÓ[1]

1 Research Group on Bioengineering, Membrane Technology and Energetics; University of Pannonia; Egyetem u. 10; Veszprém; H-8200; HUNGARY

This study aimed to evaluate a gas-liquid membrane contactor for recovering the dissolved gases of methane (CH_4) and carbon dioxide (CO_2) from model aqueous anaerobic effluents. For this purpose, synthetic effluents were prepared by using the gas mixtures of SE-1: 100/0, SE-2: 0/100 and SE-3: 50/50 CH_4/CO_2 vol.% as well as DI water. The units in which the synthetic effluent was prepared were coupled with a dense hollow fiber membrane module by employing argon gas at atmospheric pressure. The desorption of the gases CH_4 and CO_2 dissolved in the effluents was investigated with a countercurrent flow of the liquid on the lumen side. The effect of the sweep gas flow rate on the removal rate was also investigated. The results showed that the recovery rate of CH_4 was slightly affected by increasing the sweep gas flow rate, while the recovery rate of CO_2 was enhanced considerably. By applying a sweep gas flow rate of 20 mL/min, the recovery rate of both gases from SE-3 exceeded 50%.

Keywords: gas separation; membrane contactor; biogas recovery; anaerobic effluent

1. Introduction

Anaerobic wastewater treatment is a widely used technology to convert organic waste into well-stabilized sludge. Compared to aerobic systems, the major advantages of anaerobic-based ones are that the process produces higher-quality effluent and has the potential to be a net energy producer by utilizing energy from the biogas produced. Raw biogas mainly consists of CH_4 and CO_2, moreover, may contain small quantities of hydrogen sulphide, moisture and siloxanes [1]. The composition of biogas can vary depending on the operating conditions and concentrations of organic compounds in the treated water. Typically, although the methane content in biogas is within the range of 50-70%, it can be as high as 90% depending on its interaction with the aqueous phase of the carbon dioxide [2]-[3]. Furthermore, important benefits of anaerobic treatment include the requirement of less nutrients as well as lower energy consumption and higher organic loads than most conventional biological treatments. Membranes are crucial for the separation of biomass and effluent as they enable higher concentrations of organic compounds to be used in reactors, generation less sludge as well as increase the rate of biogas production [4]. Therefore, an anaerobic membrane bioreactor system has emerged as a potential alternative technology for wastewater treatment by coupling anaerobic bioreactors with membrane separation, facilitating easy scaling up and selective

separation with low energy consumption [5]. Biogas as a renewable fuel consisting of 50-70% CH_4 and 30-50% CO_2 can be produced with this method [6]. Since the treatment process occurs in a completely closed environment, it is crucial that the dissolved gases in the produced effluent are in equilibrium with the biogas in the headspace, resulting in a significant quantity of dissolved CH_4 and dissolved CO_2 being lost in the effluent solution [7]-[8]. Both dissolved gases are desorbed into the environment and contribute towards greenhouse gas emissions. Several researchers have reported that a considerable amount of the methane generated is dissolved and wasted in the liquid phase [1]-[2], [9]-[12].

Methane loss as a function of the temperature of bodies of municipal wastewater containing an average soluble COD of 200 mg/L is presented in *Fig.1*. Since the
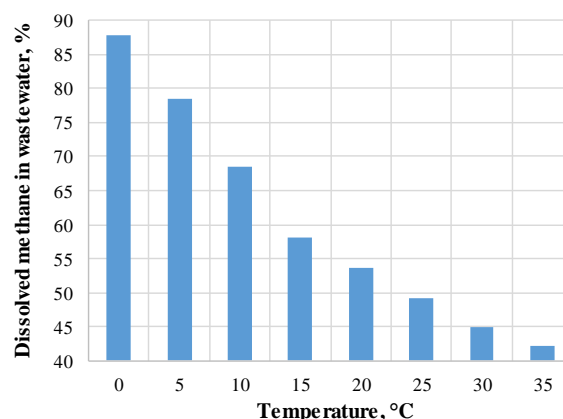

Figure 1. Dissolved methane in the wastewater as a function of temperature

solubility of methane increases as the temperature decreases, the amount of dissolved methane is higher, even as high as 88% at 0°C, at lower temperatures. Methane is a greenhouse gas, its global warming potential is estimated to be 28–36 times higher than that of CO_2 over 100 years [13], moreover, is flammable with a lower explosive limit of 5 vol.% [2]. Consequently, the importance of recovering and utilizing methane entrapped in effluent during biogas production is significant in order for anaerobic treatment systems to be sustainable.

The membrane degassing technology using gas-liquid membrane contactors (GLMCs) has emerged as a potential approach for recovering entrapped methane in fermentation liquor [7]. Preferably, GLMCs are assembled into hollow fiber membrane modules since they yield a higher gas desorption rate by providing high volumetric mass transfer coefficients [14].

The goal of this research was to determine the recovery rates of CH_4 and CO_2 gas dissolved in synthetic effluents by applying a non-porous hollow fiber membrane. The effect of gas and liquid flow rates on the removal rate was also investigated.

2. Experimental

Pure CH_4 (98%)/CO_2 (99%) and deionized water were used to prepare the synthetic effluents (SEs) in glass bottles with a volume of 5 L. A peristaltic pump was used to displace the air from the bottle to create an anaerobic environment, which was confirmed with a dissolved oxygen analyzer. Saturation was achieved by bubbling CH_4 (SE-1), CO_2 (SE-2) or a mixture of CH_4 and CO_2 (50-50%: SE-3) into the deionized water for 3 hours.

The composition of the headspace was monitored by a Hewlett Packard HP 5890 Series II gas chromatograph equipped with a thermal conductivity detector (TCD). A capillary CarboPLOT® column was employed (Agilent Technologies, length: 60 m, ID: 0.32 mm, film thickness: 1.5 mm) with Ar (99.9 %) as a carrier gas at a flow rate of 15 mL/min. The applied split ratio was 100:1. The temperatures of the injector, column oven and detector were 130, 90 and 115°C, respectively. At the saturation point, the concentration of CH_4/CO_2 in the headspace was in a steady state. Once stability had been ensured, deoxygenated and CH_4/CO_2-saturated water was pumped against the membrane by a peristaltic pump. The units in which the synthetic effluent was prepared were coupled with a PermSelect® silicone, non-porous hollow-fiber membrane module with a surface area of 1.0 m^2. The membrane was operated with a countercurrent flow of the liquid on the lumen side to examine the desorption of CH_4 and CO_2 gases dissolved in the effluents. Argon (99.9%) was used as a sweep gas in the experiments.

The concentration of the outlet gas at the membrane module was measured by the gas chromatograph at regular intervals. Henry's law and the liquid flow rates were used to calculate the mass flow rate of gases entering the membrane module, while based on the ideal gas law, results obtained from GC and gas flow rates were used to calculate the mass flow rate of gases exiting from the membrane module. Based on the results obtained, the recovery rates of CH_4/CO_2 were calculated.

3. Results and Discussion

Based on the preliminary experiments, in this research, the liquid flow rate used was 15 mL/min, adjusted by a peristaltic pump and monitored with a balance. The sweep gas flow rate varied from 5-60 mL/min and was adjusted by a control valve as well as measured with a soap film flowmeter.

Recovery rates of CH_4/CO_2 from SE-1/SE-2 as a function of the sweep gas flow rate at a liquid flow rate of 15 mL/min are shown in *Tables 1 and 2* as well as summarized in *Fig.2*.

Table 1. Recovery rates of CH_4 from SE-1 as a function of the sweep gas flow rate

Liquid flow rate (mL/min)	Sweep gas flow rate (mL/min)	Recovery rate of CH_4 (%)
15	5	57.1
15	10	58.0
15	20	58.6
15	60	35.9

Table 2. Recovery rates of CO_2 from SE-2 as a function of the sweep gas flow rate

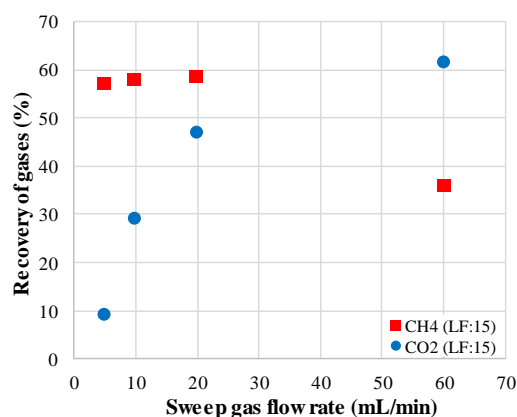| Liquid flow rate (mL/min)	Sweep gas flow rate (mL/min)	Recovery rate of CO_2 (%)
15	5	9.2
15	10	29.0
15	20	47.0
15	60	61.6

Figure 2. Recovery rates of CH_4/CO_2 from SE-1 and SE-2 as a function of the sweep gas flow rate

The results showed that the recovery rate of CH4 at a sweep gas flow rate of 5-20 mL/min was almost constant (57.1-58.6%) and rapidly decreased to 35.9% by increasing the gas flow rate to 60 mL/min. Similar effects of the gas flow rate on the recovery ratios of the gases have been reported by Cookney et al. [15], where increasing the gas flow rate had little effect on the mass transfer coefficient of CH4 due to mass transfer controlled by the resistance in the liquid phase. Rongwong et al. [7], [16] also reported that the CH4 concentration is diluted in the outlet gas in the case of high gas flow rates, which was also observed in this study. Although the recovery rate of CO2 was increased by increasing the sweep gas flow rate, these values were much lower than those of CH4 except for at a gas flow rate of 60 mL/min.

SE-3 was prepared by purging a mixture of CH4 and CO2 gases (50:50) into deionized water for 3 hours to investigate the impact of this mixture on the recovery rate of the membrane module. The results were compared with those obtained from synthetic effluents prepared with pure gases. The recovery rates of CO2 and CH4 as a function of the sweep gas flow rate are given in *Table 3* and *Fig.3*.

Table 3. Recovery rates of gases from SE-3 as a function of sweep gas flow rate

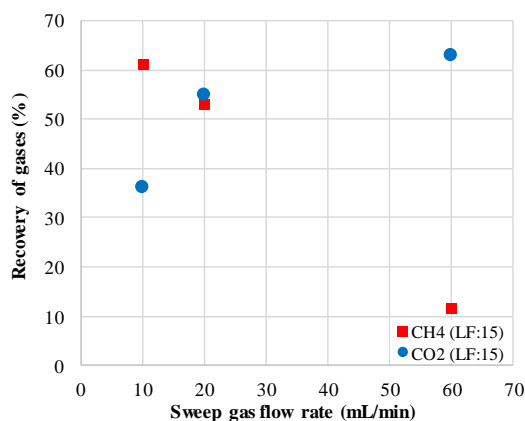| Liquid flow rate (mL/min)	Sweep gas flow rate (mL/min)	Recovery rate of CH4 (%)	Recovery rate of CO2 (%)
15	10	61.3	36.2
15	20	53.1	55.0
15	60	11.9	62.9

Figure 3. Recovery rates of CH4 and CO2 from SE-3 as a function of sweep gas flow rate

The results from SE-3 showed a similar tendency to those obtained in the case of individual gases. The recovery rate of CO2 was increased from 36.2 to 62.9% by increasing the sweep gas flow rate, while these values

for CH4 at a gas flow rate of 10-20 mL/min were 53.1-61.3% but dropped drastically to 11.9% by applying a gas flow rate of 60 mL/min. At the latter gas flow rate, the recovery rate of the membrane module with regard to CH4 from SE-1 was 35.9%, therefore, the presence of CO2 in the synthetic effluent may have a negative effect on the recovery of CH4. Nevertheless, by applying a sweep gas flow rate of 20 mL/min, the recovery rate of both gases from SE-3 exceeded 50%.

4. Conclusions

The anaerobic digestion of wastewater is a commonly used technology to produce biogas by converting organic waste into well-stabilized sludge. Since the process takes place in a completely closed environment, it is crucial that the dissolved gases in the produced effluent are in equilibrium with the biogas in the headspace, leading to a significant quantity of dissolved CH4 and dissolved CO2 being lost in the effluent solution. As a result, the recovery of dissolved CH4 is critical to increase anaerobic energy production while minimizing the environmental impact of greenhouse gases. In this study, synthetic effluents were prepared by purging CH4/CO2 into deionized water. A membrane contactor was employed as a mass transfer device for measuring the recovery rates of CH4 and CO2 gases dissolved in synthetic effluents by applying a non-porous hollow fiber membrane. The effect of the sweep gas flow rate on the removal rate was also investigated. The results showed that the recovery rate of CH4 was slightly affected by increasing the sweep gas flow rate, while the recovery rate of CO2 was enhanced considerably.

Acknowledgements

REFERENCES

[1] Visnyei, M.; Bakonyi, P.; Bélafi-Bakó, K.; Nemestóthy, N.: Integration of gas–liquid membrane contactors into anaerobic digestion as a promising route to reduce uncontrolled greenhouse gas (CH4/CO2) emissions, *Bioresour. Technol.*, 2022, **364**, 128072, DOI: 10.1016/J.BIORTECH.2022.128072

[2] Henares, M.; Izquierdo, M.; Penya-Roja, J.M.; Martínez-Soria, V.: Comparative study of degassing membrane modules for the removal of methane from Expanded Granular Sludge Bed anaerobic reactor effluent, *Sep. Purif. Technol.*, 2016, **170**, 22–29, DOI: 10.1016/j.seppur.2016.06.024

[3] Velasco, P.; Jegatheesan, V.; Thangavadivel, K.; Othman, M.; Zhang, Y.: A focused review on membrane contactors for the recovery of dissolved methane from anaerobic membrane bioreactor (AnMBR) effluents, *Chemosphere*, 2021, **278**, 130448, DOI: 10.1016/j.chemosphere.2021.130448

[4] Chen, C.; Guo, W.; Ngo, H.H.; Lee, D. J.; Tung, K. L.; Jin, P.; Wang, J.; Wu, Y.: Challenges in biogas production from anaerobic membrane bioreactors, *Renew. Energy*, 2016, **98**, 120–134, DOI: 10.1016/J.RENENE.2016.03.095

[5] Aslam, M.; Ahmad, R.; Yasin, M.; Khan, A.L.; Shahid, M.K.; Hossain, S.; Khan, Z.; Jamil, F.; Rafiq, S.; Bilad, M.R.; Kim, J.M.: Anaerobic membrane bioreactors for biohydrogen production: Recent developments, challenges and perspectives, *Bioresour. Technol.*, 2018, **269**, 452–464, DOI: 10.1016/J.BIORTECH.2018.08.050

[6] Luo, G.; Wang, W.; Angelidaki, I.: A new degassing membrane coupled upflow anaerobic sludge blanket (UASB) reactor to achieve in-situ biogas upgrading and recovery of dissolved CH_4 from the anaerobic effluent, *Appl. Energy*, 2014, **132**, 536–542, DOI: 10.1016/J.APENERGY.2014.07.059

[7] Rongwong, W.; Goh, K.; Bae, T.H.: Energy analysis and optimization of hollow fiber membrane contactors for recovery of dissolve methane from anaerobic membrane bioreactor effluent, *J. Memb. Sci.*, 2018, **554**, 184–194, DOI: 10.1016/j.memsci.2018.03.002

[8] Sohaib, Q.; Kalakech, C.; Charmette, C.; Cartier, J.; Lesage, G.; Mericq, J.P.: Hollow-fiber membrane contactor for biogas recovery from real anaerobic membrane bioreactor permeate, *Membranes (Basel)*, 2022, **12**(2), 112-118, DOI: 10.3390/membranes12020112

[9] Pauss, A.; Andre, G.; Perrier, M.; Guiot, S.R.: Liquid-to-Gas mass transfer in anaerobic processes: Inevitable transfer limitations of methane and hydrogen in the biomethanation process, *Appl. Environ. Microbiol.*, 1990, **56**(6), 1636–1644, DOI: 10.1128/AEM.56.6.1636-1644.1990

[10] Souza, C.L.; Chernicharo, C.A.L.; Aquino, S.F.: Quantification of dissolved methane in UASB reactors treating domestic wastewater under different operating conditions, *Water Sci. Technol.*, 2011, **64**(11), 2259–2264, DOI: 10.2166/WST.2011.695

[11] Cookney, J.; Cartmell, E.; Jefferson, B.; McAdam, E.J.: Recovery of methane from anaerobic process effluent using poly-di-methyl-siloxane membrane contactors, *Water Sci. Technol.*, 2012, **65**(4), 604–610, DOI: 10.2166/wst.2012.897

[12] Lobato, L.C.S.; Chernicharo, C.A.L.; Souza, C.L.: Estimates of methane loss and energy recovery potential in anaerobic reactors treating domestic wastewater, *Water Sci. Technol.*, 2012, **66**(12), 2745–2753, DOI: 10.2166/wst.2012.514

[13] Paolini, V.; Petracchini, F.; Segreto, M.; Tomassetti, L.; Naja, N.; Cecinato, A.: Environmental impact of biogas: A short review of current knowledge, *J. Environ. Sci. Health A*, 2018, **53**(10), 899–906, DOI: 10.1080/10934529.2018.1459076

[14] Younas, M.; Tahir, T.; Wu, C.; Farrukh, S.; Sohaib, Q.; Muhammad, A.; Rezakazemi, M.; Li, J.: Post-combustion CO_2 capture with sweep gas in thin film composite (TFC) hollow fiber membrane (HFM) contactor, *J. CO2 Util.*, 2020, **40**, 101266, DOI: 10.1016/J.JCOU.2020.101266

[15] Cookney, J.; Mcleod, A.; Mathioudakis, V.; Ncube, P.; Soares, A.; Jefferson, B.; McAdam, E.J.: Dissolved methane recovery from anaerobic effluents using hollow fibre membrane contactors, *J. Memb. Sci.*, 2016, **502**, 141–150, DOI: 10.1016/j.memsci.2015.12.037

[16] Rongwong, W.; Wongchitphimon, S.; Goh, K.; Wang, R.; Bae, T.H.: Transport properties of CO_2 and CH_4 in hollow fiber membrane contactor for the recovery of biogas from anaerobic membrane bioreactor effluent, *J. Memb. Sci.*, 2017, **541**, 62–72, DOI: 10.1016/j.memsci.2017.06.090

INVESTIGATION OF THE PYROLYSIS OF ANIMAL MANURE IN A LABORATORY-SCALE TUBULAR REACTOR: THE EFFECT OF THE PROCESS TEMPERATURE AND RESIDENCE TIME

MARIA ELENA LOZANO FERNANDEZ[1], SZABINA TOMASEK[1]*, CSABA FÁYKÖD[2] AND ANDREA SOMOGYI[3]

1 Research Centre for Biochemical, Environmental and Chemical Engineering, Department of MOL Hydrocarbon and Coal Processing, University of Pannonia, Egyetem u. 10, Veszprém, 8200, HUNGARY
2 Felső-Bacska Storage Windpark Ltd., Arany János út 200, Fadd, 7133, HUNGARY
3 Solver Unio Ltd., Ábel Jenő u. 8, Budapest, 1113, HUNGARY

This paper focuses on the pyrolysis of animal manure in a laboratory-scale tubular reactor between 300 and 900°C at nitrogen flow rates of 1 and 5 dm³/h. During the experiments, it was found that both the temperature and nitrogen flow rate had significant effects on the product yields and compositions. The highest gas yield and syngas content were observed at 900°C at a nitrogen flow rate of 1 dm³/h. In this case, since the gaseous product was characterized by a H_2/CO ratio of 0:5, its quality must be improved prior to being used for synthesis. The composition of the solid residue was also affected by the pyrolysis parameters. Based on the hydrogen/carbon and oxygen/carbon ratios, it was concluded that both the water-gas shift and Boudouard reactions were the most critical.

Keywords: cattle manure, pyrolysis, tubular reactor, product yield, composition

1. Introduction

The rapid growth of the world's population is leading to a significant rise in the demand and consumption of food, including meat and animal-derived products. As a consequence, farms and this sector generate huge amounts of waste such as livestock manure, sewage sludge and poultry litter [1]-[2]. The inadequate management of manure and sewage sludge causes serious health and environmental issues, e.g. water and air pollution as well as the emission of greenhouse gases and heavy metals in addition to the spread of pathogens. The composition of this residue includes a wide variety of chemical and biological compounds which are associated with the specific species of animals and age ranges amongst other factors. The residue consists of a complex mixture of compounds, mainly microbiota, lignocellulose, proteins as well as a significant amount of inorganic matter such as S, N, P, K, Ca, Mg and Cl. Additionally, heavy metals such as Cu, Pb, Cd, Zn and Mn can be found in the residue due to the use of antibiotics and hormones supplied to the animals [3]-[5]. Some of the practices concerning the disposal of sewage sludge and manure include landfilling, agricultural utilization, composting, anaerobic digestion and thermochemical conversion [6]. One of the most traditional and practical alternatives is the usage of these residues in agricultural land due to the high content of N and P which are essential elements required in plant fertilization. However, nowadays, this practice has diminished due to the enormous amount of waste generated, exceeding the nutritional requirements of the soil. Environmental regulations establish limits on the values allowed for the usage of sewage sludge in agriculture. The excessive use of manure on land causes problems such as contamination of the subsoil and surface, odors as well as the emission of greenhouse gases and ammonia [5,7-10].

Therefore, new alternatives for the proper management of this type of waste have been explored as well as studied more comprehensively in an attempt to solve the environmental and social impacts [8]. For example, thermal conversion techniques such as pyrolysis and gasification could be alternatives for transforming the residue into valuable products such as oil, char and gaseous products. Additional advantages of these techniques are that the huge volume generated is reduced, microorganisms are degraded and pathogenic organisms destroyed [1,9-10]. It is important to take into consideration that the percentage of humidity in the residues in the material is high and should be reduced while using the thermal techniques. The material could

be dried through natural, mechanical and thermal drying techniques [11]. Depending on the thermal degradation technique applied, the composition of the feedstock; process conditions, e.g. temperature and heating rate; as well as product distribution and its composition will vary [11]. For example, during pyrolysis, degradation in the absence of oxygen occurs at high temperatures. Through pyrolysis, the feedstock decomposes to form char, oil and light non-condensable gases [11]. In the case of the raw material containing a large amount of hemicellulose and cellulose, a product consisting of a higher percentage of gases could be expected, while lignin contributes towards the formation of char. Regarding the temperature, the formation of char is favored by low temperatures, while that of oil and volatile gaseous components is more likely at high temperatures [12]. The products can be further utilized depending on their characteristics. Char has interesting physical properties, for example, a high surface area, microporosity as well as high adsorption and ion exchange capacities. Char potentially could be used as an adsorbent, a catalyst, in power plants or as a fertilizer. Char obtained from manure is rich in elements such as K, P, Ca and Mg [10], [12]. In the oil fraction, hydrocarbons are produced but the pyrolysis oil from manure and sewage sludge is not regarded as of high quality since the oil produced contains oxygen, which gives rise to the production of compounds such as alcohols, ketones, aldehydes and esters that decrease the quality of the product [1]. The gas produced contains a mixture of CO, CO_2, CH_4, H_2 and some light hydro-carbons (C_2H_2, C_2H_4, C_2H_6 and C_3H_8) [13]. The gas may be valuable because the energy it contains could be used in gas turbines and power plants or its compounds applied as a feedstock to be processed into a more added-value chemical product [13]-[14]. Despite the wide range of possible uses of the products, relatively few studies have investigated the pyrolysis of cattle manure. Consequently, limited information about the product yields and compositions is available.

In light of the above, this study focuses on the pyrolysis of cattle manure within the temperature range of 300-900°C using nitrogen flow rates of 1 and 5 dm^3/h as well as on the impact of the process parameters.

2. Materials and methods

2.1. Raw material

Cattle manure was used as a feedstock for the pyrolysis experiments. Before the experiments, the raw material was dried at 110°C to constant mass.

To determine the physical and chemical properties, the proximate and ultimate analyses of cattle manure (*Table 1*) were carried out. As data show, the raw material is characterized by 40.6% ash, 53.5% volatile compounds and 0.3% water content.

The C, H, N, S and O contents were determined by a Carlo Erba-type elemental analyzer and in order to identify the inorganic compounds, e.g. Ca, P, S, Si, Na,

Table 1. Proximate and ultimate analyses of cattle manure

	Parameter	Value (%)
Proximate analysis	Fixed carbon	5.59
	Ash content	40.68
	Volatile organic compounds	53.43
	Water content	0.30
Ultimate analysis	C	24.80
	H	3.00
	N	2.90
	S	1.30
	O	45.30
	Others (Ca, P, S, Si, Na, Mg, Fe, Al)	22.70

Mg, Fe and Al, Energy Dispersive X-Ray Analysis was performed (Shimadzu EDX).

2.2. Pyrolysis experiments

Pyrolysis was performed in a laboratory-scale horizontal tubular reactor (*Fig.1*). The cattle manure was placed in the center of a glass wool tube. The experiments were performed at 300, 500, 700 and 900°C. A N_2 atmosphere was used and the flow rates established were 1 and 5 dm^3/h. The heating rate used for this experiment was 100°C/min. The reaction system was equipped with a scrubber and silica gel-filled tube, where the gaseous products were purified to remove possible impurities and dried. At the end of the reaction, the product yields were estimated by measuring and calculating their difference in mass.
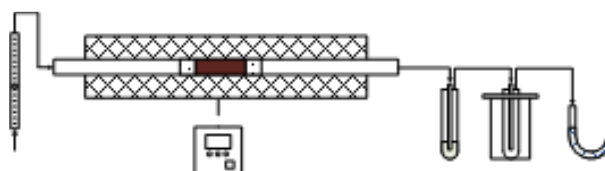

Figure 1. Experimental setup

2.3. Product analysis

The composition of the gaseous products was determined by a DANI-type gas chromatograph using a flame ionization and thermal conductivity detectors. The equipment contained two capillary columns (Rtx-1 PONA (100 m x 0.25 mm x 0.5 μm) and Carboxen TM-1006 PLOT (30 m x 0.53 mm)). Regarding the isothermal conditions of the PONA capillary column, the injector and detector temperatures were both 230°C. In terms of the Carboxen TM-1006 PLOT capillary column, the applied heating program was as follows: 35°C for 18 mins before being heated to 120°C at a heating rate of 15°C/min and maintained at 120°C for 2 mins. The

retention times of the components were determined using gas mixtures and individual components.

3. Results and Discussion

3.1. Product yields

The product yields of the pyrolysis experiments are summarized in *Fig.2*. During the experiments, only gas and char were formed. As expected, the gas yields and amount of solid residue produced increased and decreased, respectively, as a function of the reaction temperature. During the pyrolysis process, a series of complex reactions took place.
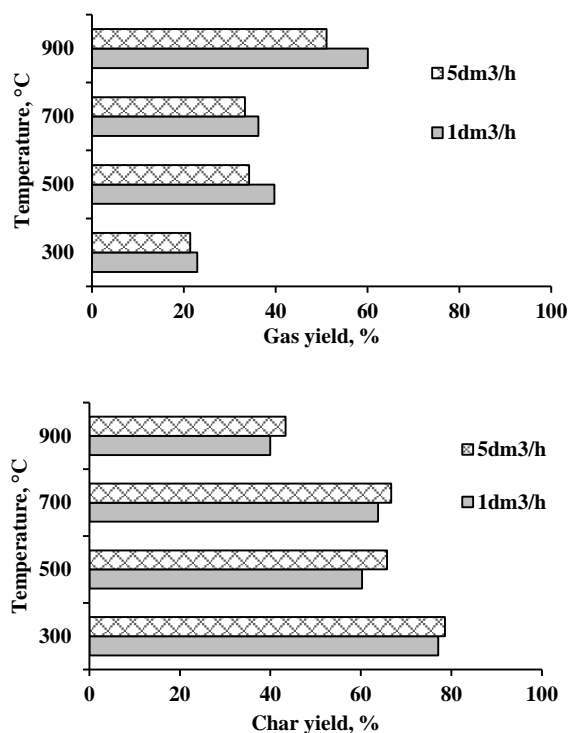

Figure 2. Product yields of pyrolysis

Up to 200°C, to all intents and purposes, only the water was removed from the cattle manure (*Fig.3*). In the torrefaction stage, since cellulose, hemicellulose and lignin were only slightly degraded, the final product was a solid carbonaceous material. This stage was followed by the pyrolysis process, where a significant reduction in mass resulted. In addition, a sharp peak appeared at approximately 300°C in the derivative thermogravimetric diagram (DTG), indicating that the reduction in mass occurred at a high speed. It is well known that cellulose degradation occurs between300 and 350°C, while protein decomposes between 450 and 660°C. In addition, deamination also took place.

During the pyrolysis stage, approximately 30% of the initial mass was lost. Above 600°C, another significant proportion of mass, ~25%, was lost. This reduction in mass was related to the degradation of chains of lignin, carbon and minerals. It was also observed that
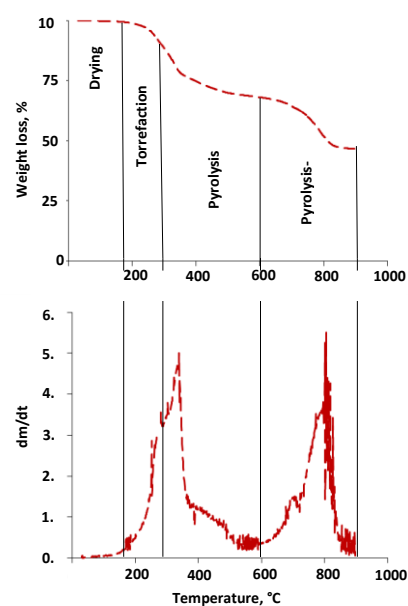

Figure 3. Thermogravimetric results with regard to the raw material

the rate at which the mass reduced was low and relatively stable. This effect could be attributed to the minerals and possible carbonated forms. Additionally, it is worth mentioning that within this temperature range, CO_2 was also formed. CO_2 acts as an oxygen donor, promoting the Boudouard reaction and, therefore, the formation of CO. Another peak is also visible at 800°C in the DTG curve, which can be attributed to the devolatilization of the char and decomposition of the mineral matter. At the end of the test, that is, at a temperature of 900°C, the percentage of mass consisting of ash and fixed carbon remaining in the crucible was the same as that reported during the proximate analysis.

It is important to note that the N_2 flow rate also had an effect on the product yields. The lower flow rates facilitated the formation of the gaseous products. Given the longer residence time, the volatile vapors resuting from the pyrolysis exited the reactor more slowly, so they had sufficient time to degrade more comprehensively.

3.2. Composition of the gaseous products

Although the gaseous products consisted of H_2, CO, CO_2 and CH_4, C_2-C_6 hydrocarbons were also formed (*Fig.4*). H_2 was formed by dehydrogenation, however, it could have formed as a result of the reforming reactions. CO may be related to the reactions that facilitated the cleavage of bonds in the ether groups and decarbonylation from proteins [15]-[16].

As *Fig.4* shows, the formation of CO considerably increased above 700°C and the highest level was obtained at 900°C. This large increase was attributed to the Boudouard reaction, which has already been referred to in the thermogravimetric analysis. The Boudouard reaction can also be catalyzed by carbonates present in the manure [17]. The increase in CO can also be justified by a reaction between CO_2 and other compounds generated during pyrolysis, the reduction of CO_2 to CO
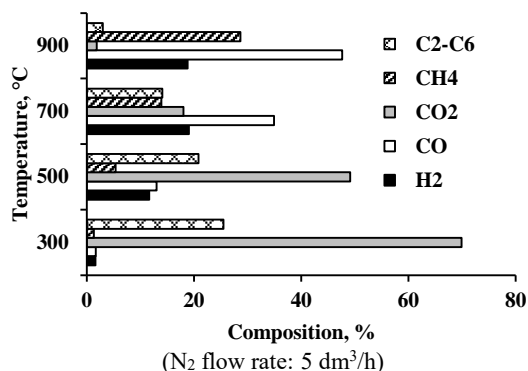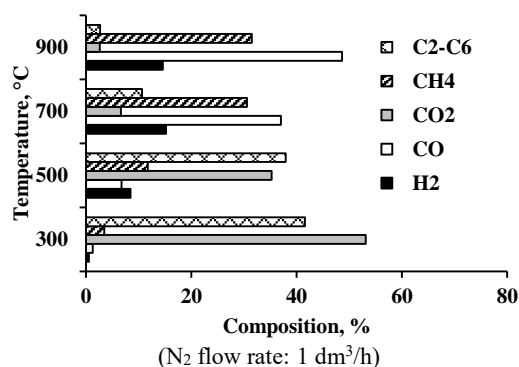
Figure 4. Composition of the gas products

and simultaneously the oxidation of the carbon of the pyrolysis product through a homogeneous reaction [18].
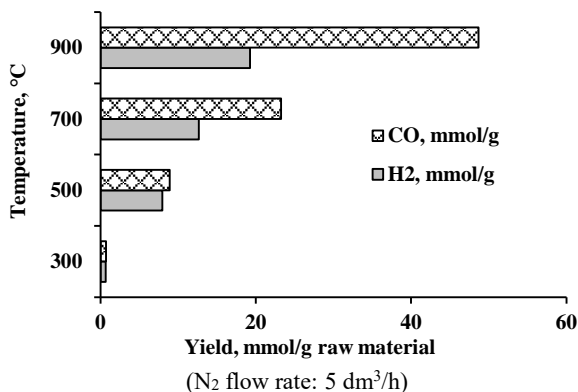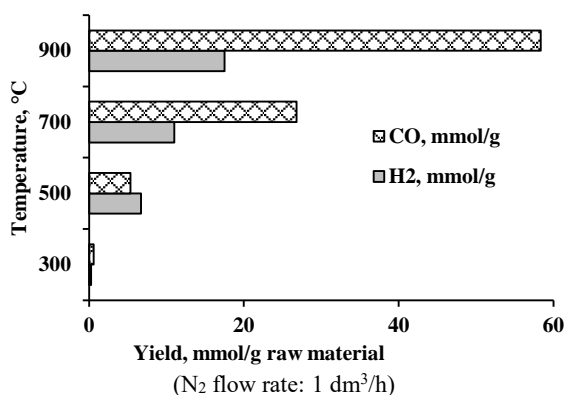

Figure 5. Syngas yields

The quality of the gaseous product can be defined in terms of its chemical composition and calorific value. *Fig.5* represents the content of syngas, namely H_2 and CO, in the product.

From the results, it is remarkable that the production of syngas only took place above 500°C and the yield increased in proportion to the temperature. The highest syngas yields (~80%) were observed at 900°C. It is important to emphasize that the N_2 flow rate also had an effect on the syngas yield. The yield of syngas was higher at lower N_2 flow rates, in the same manner as the overall gas yield.

The H_2/CO ratio of syngas (*Fig.6*) is extremely important. The typical initial ratios for the transformation of methanol into chemicals are >2:1 for light olefins; <2:1 for diesel; 1.5:1 for aldehydes, higher alcohols and dimethyl ether; 1:1 for oxygen-containing alcohols and acetic acid; and 1:2 for polycarbonate [19]-[20]. As data in *Fig.6* show, although the ratio of H_2/CO at 500°C was approximately 1, at 700 and 900°C it was below 0.6.
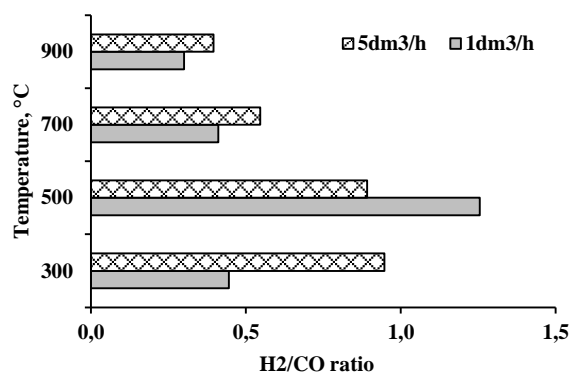
Figure 6. H_2/CO ratios of syngas

The heating values of the gases were also estimated. As is depicted in *Fig.7*, at lower temperatures (300 or 500°C) and an N_2 flow rate of 1dm³/h, the calorific value of the gas mixture was higher (~30 MJ/m³), meanwhile, at higher N_2 flow rates, the heating value of the gaseous product was about 15 MJ/m³ at the same temperatures.

Figure 7. Heating values of the gaseous products

This can be explained by the fact that a higher percentage of light hydrocarbons is present, the individual components of which provide a higher

calorific value than the other compounds present in the mixture [21].

Another interesting correlation is the difference in the proportions of different elements contained in the gas as well as the resultant study and proposition of possible reaction mechanisms at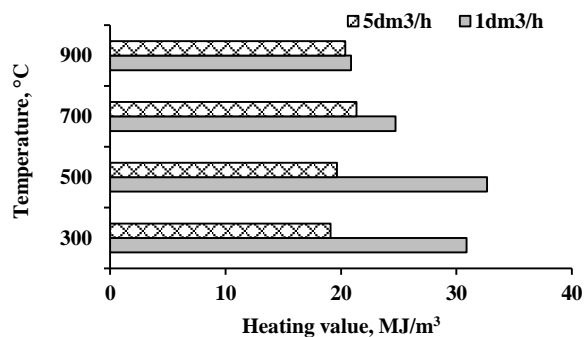 different temperatures. The trends observed when the ratio of components were estimated are summarized in *Table 2*. From the process, the water-gas shift reaction and Boudouard reaction are some of the critical reactions that took place [14].

3.3. Char

According to the International Biochar Initiative (IBI), the char obtained from the pyrolysis experiments can be regarded as biochar [22], in which the C content is greater than 10% except for during the tests carried out at 900°C.

Table 2. The proportions of different elements

Component ratio	N_2 flow rate: 1 dm^3/h	N_2 flow rate: 5 dm^3/h	Relationship	Proposed reaction
H_2/CO	Optimum (highest peak at 500°C)	Optimum (highest peak at 500°C)	Higher ratio at a flow rate of 5 dm^3/h (except for at 500°C)	$C_n H_m + H_2 \rightarrow \dfrac{n+m}{2H_2} + nCO$ $CO + H_2O \rightarrow CO_2 + H_2$
CO/CO_2	Increasing	Increasing	Higher ratio at a flow rate of 5 dm^3/h	$C + CO_2 \rightarrow 2CO$
H_2/CH_4	Optimum (highest peak at 500°C)	Optimum (highest peak at 500°C)	Higher ratio at a flow rate of 5 dm^3/h	$C + H_2 \rightarrow CH_4$
CO/CH_4	Optimum (highest peak at 700°C)	Increasing	Higher ratio at a flow rate of 5 dm^3/h	$CO + 3H_2 \rightarrow CH_4 + H_2O$
CO_2/CH_4	Decreasing	Decreasing	Higher ratio at a flow rate of 5 dm^3/h	$CO_2 + 4H_2 \rightarrow CH_4 + 2H_2O$ $2CO + 2H_2 \rightarrow CH_4 + CO_2$

To determine the possible applications of char, it is recommended to evaluate the relationship between the proportions of some elements. For example, the C/N ratio could be a positive parameter to determine the microbial activity should this residue be used in soils. Another aspect possibly worth evaluating and analyzing is the H/C and O/C ratios of the manure as well as the char obtained in each test (*Table 3*). The ratios are valuable for understanding the reaction mechanisms during

pyrolysis under specific conditions [15]. The atomic ratios show that the process of carbonization changed the chemical compositions by removing functional groups. Due to the cleavage of the functional groups, the nitrogen contents significantly decreased, moreover, as a result of the formation of CO, CO_2 and CH_4, the carbon contents also reduced.

Table 3. Elemental analysis of the char products

| | Cattle manure | at N_2 flow rate of 1 dm^3/h | | | | at N_2 flow rate of 5 dm^3/h | | | |
		300°C	500°C	700°C	900°C	300°C	500°C	700°C	900°C
Elements content (%)									
C	24.8	23.40	20.20	20.90	6.30	23.50	20.50	18.90	7.20
H	3.00	1.80	0.70	0.30	0.80	1.60	0.60	0.30	0.80
N	2.90	2.50	1.50	1.00	0.40	2.30	1.60	0.80	0.80
S	1.20	1.50	1.40	1.40	2.50	1.40	1.60	1.40	2.90
O	45.30	48.20	53.50	53.70	67.30	48.50	53.10	55.80	65.60
Al	0.60	0.99	0.98	1.55	1.39	0.72	1.06	1.48	1.57
Ca	14.12	12.61	12.91	12.83	15.74	12.36	12.40	11.92	14.74
Cl	0.71	0.82	0.70	0.84	0.21	0.63	0.67	0.78	0.40
Fe	0.60	0.55	0.18	0.39	0.54	0.72	0.53	0.53	0.52
K	1.76	3.39	2.90	3.22	1.18	2.75	2.93	2.58	1.31
Mg	1.19	1.11	1.19	1.55	0.96	1.11	1.13	1.23	0.91
Mn	0.03	0.03	0.04	<0.001	<0.001	0.05	0.03	0.04	<0.001
P	2.16	1.40	1.99	2.32	0.96	1.93	2.09	2.05	1.17
Si	1.48	1.81	1.82	0.00	1.71	2.42	1.86	2.09	2.09
Atomic ratios									
C/N	8.6	9.4	13.5	20.9	15.8	10.2	12.8	23.6	9.0
H/C	0.10	0.08	0.03	0.01	0.13	0.07	0.03	0.02	0.11
O/C	1.8	2.1	2.6	2.6	10.7	2.1	2.6	2.9	9.1

4. Conclusions

In this study, cattle manure was pyrolysed in a horizontal tubular reactor between 300 and 900°C at N_2 flow rates of 1 and 5 dm³/h. During the experiments, 20-60% gaseous and 40-80% solid carbonaceous residues were formed. The gas yields increased in proportion to the reaction temperature and residence time, while the amount of char decreased. The decomposition process resulted in the formation of H_2, CO, CO_2, CH_4 and C_2-C_6 hydrocarbons. Syngas was only produced above 500°C. The ratio of H_2/CO at 500°C was 1, while at 700 and 900°C, the proportion of CO was greater than that of H_2. At lower temperatures (300 or 500°C) and at an N_2 flow rate of 1dm³/h, the calorific value of the gas mixture was higher (~30 MJ/m³) than at the higher N_2 flow rate and same temperatures (~15 MJ/m³). The process of carbonization changed the chemical composition of the raw material by removing functional groups, which also indicates the occurrence of the water-gas shift and Boudouard reactions.

Acknowledgement

REFERENCES

[1] Naqvi, S.R.; Tariq, R.; Shahbaz, M.; Naqvi, M.; Aslam, M.; Khan, Z.; Mackey, H.; Mckay, G.; Al-Ansari, T.: Recent developments on sewage sludge pyrolysis and its kinetics: Resources recovery, thermogravimetric platforms, and innovative prospects, *Comput. Chem. Eng.*, 2021, **150**, 107325, DOI: 10.1016/j.compchemeng.2021.107325

[2] Burton, C.H.; Turner, C.: Manure management: Treatment strategies for sustainable agriculture, 2nd edition (Silsoe Research Institute, Bedford, UK), 2003, ISBN: 0953128261

[3] Su, G.; Ong, H.C.; Mohd Zulkifli, N.W.; Ibrahim, S.; Chen, W.H.; Chong, C.T.; Ok, Y.S.: Valorization of animal manure via pyrolysis for bioenergy: A review, *J. Clean. Prod.*, 2022, **343**, 130965, DOI: 10.1016/j.jclepro.2022.130965

[4] Havukainen, J.; Nguyen, M.T.; Hermann, L.; Horttanainen, M.; Mikkilä, M.; Deviatkin, I.; Linnanen, L.: Potential of phosphorus recovery from sewage sludge and manure ash by thermochemical treatment, *Waste Manage.* , 2016, **49**, 221–229, DOI: 10.1016/j.wasman.2016.01.020

[5] Bernal, M.P.; Alburquerque, J.A.; Moral, R.: Composting of animal manures and chemical criteria for compost maturity assessment. A review, *Bioresour. Technol.*, 2009, **100**(22), 5444–5453, DOI: 10.1016/j.biortech.2008.11.027

[6] Hušek, M.; Moško, J.; Pohořelý, M.: Sewage sludge treatment methods and P-recovery possibilities: Current state-of-the-art, *J. Environ. Manage.*, 2022, **315**, 115090, DOI: 10.1016/j.jenvman.2022.115090

[7] Djandja, O.S.; Yin, L.-X.; Wang, Z.-C.; Duan, P.-G.: From wastewater treatment to resources recovery through hydrothermal treatments of municipal sewage sludge: A critical review, *Process Saf. Environ. Prot.*, 2021, **151**, 101–127, DOI: 10.1016/j.psep.2021.05.006

[8] Ruiz-Gómez, N.; Quispe, V.; Ábrego, J.; Atienza-Martínez, M.; Murillo, M.B.; Gea, G.: Co-pyrolysis of sewage sludge and manure, *Waste Manage.*, 2017, **59**, 211–221, DOI: 10.1016/j.wasman.2016.11.013

[9] Zhu, Y.; Zhai, Y.; Li, S.; Liu, X.; Wang, B.; Liu, X.; Fan, Y.; Shi, H.; Li, C.; Zhu, Y.: Thermal treatment of sewage sludge: A comparative review of the conversion principle, recovery methods and bioavailability-predicting of phosphorus, *Chemosphere*, 2022, **291**, 133053, DOI 10.1016/j.chemosphere.2021.133053

[10] Rangabhashiyam, S.; Lins, P.V.D.S.; Oliveira, L.M.T.D.M.; Sepulveda, P.; Ighalo, J.O.; Rajapaksha, A.U.; Meili, L.: Sewage sludge-derived biochar for the adsorptive removal of wastewater pollutants: A critical review, *Environ. Pollut.*, 2022, **293**, 118581, DOI: 10.1016/j.envpol.2021.118581

[11] Gao, N.; Kamran, K.; Quan, C.; Williams, P.T.: Thermochemical conversion of sewage sludge: A critical review, *Prog. Energy Combust. Sci.*, 2020, **79**, 100843, DOI: 10.1016/j.pecs.2020.100843

[12] Ippolito, J.A.; Cui, L.; Kammann, C.; Wrage-Mönnig, N.; Estavillo, J.M.; Fuertes-Mendizabal, T; Cayuela, M.L.; Sigua, G.; Novak, J.; Spokas, K.; Borchard, N.: Feedstock choice, pyrolysis temperature and type influence biochar characteristics: a comprehensive meta-data analysis review, *Biochar*, 2020, **2**(4), 421–438, DOI: 10.1007/s42773-020-00067-x

[13] Hoang, S.A.; Bolan, N.; Madhubashani, A.M.P.; Vithanage, M.; Perera, V.; Wijesekara, H.; Wang, H.; Srivastava, P.; Kirkham, M.B.; Mickan, B.S.; Rinklebe, J.; Siddique, K.H.M.: Treatment processes to eliminate potential environmental hazards and restore agronomic value of sewage sludge: A review, *Environ. Pollut.*, 2022, **293**, 118564, DOI: 10.1016/j.envpol.2021.118564

[14] Burra, K.G.; Hussein, M.S.; Amano, R.S.; Gupta, A.K.: Syngas evolutionary behavior during chicken manure pyrolysis and air gasification, *Appl. Energy*, 2016, **181**, 408–415, DOI: 10.1016/j.apenergy.2016.08.095

[15] Zhou, S.; Liang, H.; Han, L.; Huang, G.; Yang, Z.: The influence of manure feedstock, slow pyrolysis, and hydrothermal temperature on manure thermochemical and combustion properties, *Waste Manage.*, 2019, **88**, 85–95, DOI: 10.1016/j.wasman.2019.03.025

[16] Li, Q.; Lin, H.; Fan, H.; Zhang, S.; Yuan, X.; Wang, Y.; Xiang, J.; Hu, S.; Bkangmo Kontchouo, F.M.; Hu, X.: Co-pyrolysis of swine manure and pinewood sawdust: Evidence of cross-interaction of the volatiles and profound impacts on product characteristics, *Renew. Energ.*, 2021, **179**, 1370–1384, DOI: 10.1016/j.renene.2021.07.104

[17] Choi, D.; Oh, J.-I.; Baek, K.; Lee, J.; Kwon, E.E.: Compositional modification of products from Co-Pyrolysis of chicken manure and biomass by shifting carbon distribution from pyrolytic oil to syngas using CO_2, *Energy*, 2018, **153**, 530–538, DOI: 10.1016/j.energy.2018.04.084

[18] Cho, S.-H.; Jung, S.; Tsang, Y.F.; Lin, K.-Y.A.; Jeon, Y.J.; Kwon, E.E.: Strategic way for valorization of manure into chemicals and fuels, *J. Clean. Prod.*, 2021, **322**, 129109, DOI: 10.1016/j.jclepro.2021.129109

[19] Hua, Y.; Wang, J.; Min, T.; Gao, Z.: Electrochemical CO_2 conversion towards syngas: Recent catalysts and improving strategies for ratio-tunable syngas, *J. Power Sources*, 2022, **535**, 231453, DOI: 10.1016/j.jpowsour.2022.231453

[20] Zhao, S.; Li, H.; Wang, B.; Yang, X.; Peng, Y.; Du, H.; Zhang, Y.; Han, D.; Li, Z.: Recent advances on syngas conversion targeting light olefins, *Fuel*, 2022, **321,** 124124, DOI: 10.1016/j.fuel.2022.124124

[21] Sánchez, M.E.; Martínez, O.; Gómez, X.; Morán, A.: Pyrolysis of mixtures of sewage sludge and manure: A comparison of the results obtained in the laboratory (semi-pilot) and in a pilot plant, *Waste Manage.*, 2007, **27**(10), 1328–1334 DOI: 10.1016/j.wasman.2006.07.015

[22] Kim, S.-S.; Agblevor, F.A.; Lim, J.: Fast pyrolysis of chicken litter and turkey litter in a fluidized bed reactor, *J. Ind. Eng. Chem.*, 2009, **15**(2), 247–252 DOI: 10.1016/j.jiec.2008.10.004

BEHAVIOR OF CONTROL AND INHIBITIVE POLYASPARTIC COATINGS USING ALKYLAMMONIUM AND ZINC PHOSPHATE CORROSION INHIBITORS IN SOIL

ABDU ELHOUD[1]* AND TIM VAN EVERBROECK[1]

1 CHEMSYSTEMS, Ambachtsstraat 15, Malle, 2390, Belgium

This study is part of an anti-corrosion coating development project at CHEMSYSTEMS. The corrosion performance was assessed through erosion, immersion and soil corrosion experiments. The erosion results have previously been published. This article discusses the impact of soil on control polyaspartic coatings used to protect concrete and the modified polyaspartic coating intended to protect underground steel substrates. The modified polyaspartic coating was boosted with a micaceous iron oxide barrier, a liquid alkylammonium corrosion inhibitor, a powdered zinc phosphate corrosion inhibitor and a novel hardener. The surface finish of the steel samples was of a milled and blasted nature (SA 2.5). The coating was applied directly to the metal without the application of a primer or second layer of coating. The average thickness of the coating was 220±10 μm as a direct-to-metal protection system. The experiments were conducted in soil at room temperature (RT) and 35°C over 30 days. The experimental results of the control polyaspartic coating loaded on steel substrates exhibited severe blistering. The polyaspartic coating dispersed with a liquid alkylammonium inhibitor also exhibited blistering, whereas the modified polyaspartic coating with a zinc phosphate corrosion inhibitor showed an adequate degree of resistance to the impact of soil under the evaluated conditions. The results confirmed that the presence of a zinc phosphate corrosion inhibitor in combination with a micaceous iron oxide barrier improved the resistance of the coating to the evaluated soils in which it was positioned and at the investigated temperatures.

Keywords: soil, polyaspartic coating, corrosion inhibitor, iron oxide barrier

1. Introduction

Carbon steels with desirable mechanical properties are widely used in infrastructure, including in underground assets such as pillars, foundations, storage tanks and pipelines. In the field, these structures are more likely to degrade and rust due to direct contact with the soil, especially if no protection system is provided to hinder the effect of the corrosive elements. Corrosion due to soil is influenced by the temperature, moisture content, oxygen content, environmental pH, microbial activity and soluble salts. Soil moisture contains a wide range of chemicals which have penetrated through the soil surface. Some examples of these chemicals are salts, e.g. chlorides, nitrates, nitrites, sulfates, etc., and heavy metals, e.g. cadmium, chromium, copper, iron, manganese, nickel, lead, zinc, etc. Along with the influence of microbial activity and environmental factors such as temperature, pH, conductivity and dissolved oxygen concentration, salts and heavy metals make the study of soil moisture an interesting topic as they are related to the corrosion of underground metal structures [1]. Jiao Chen et al. 2015 [2] studied the soil corrosion of steel as a function of anions in the soil, namely total soluble salts, Cl^-, SO_4^{2-} and HCO_3^-, and soil nutrition, that is, moisture content, organic matter, total nitrogen, alkaline hydrolysable nitrogen, available phosphorus and available potassium.

Many attempts have been made in this regard to reduce the risk of soil corrosion on submerged steel and concrete structures. Organic, inorganic and metal coatings such as Zn, Al and Ni are considered to be very effective means to protect submerged assets from premature corrosion and degradation [3]-[4]. Corrosion inhibitors in powdered and liquid forms have been incorporated into coatings to enhance their antirust and adhesive characteristics when applied to substrates. Zinc phosphate is commonly dispersed into coating formulae during manufacturing and effectively reduced the tendency of a coating to fail and substrates to rust. Nevertheless, although further investigations are still favorable to evaluate the efficiency of corrosion inhibitors in coatings exposed to soil, in this study, an attempt was made to compare the efficiency of two types of corrosion inhibitors in combination with iron oxide coatings for the purpose of developing control and inhibited polyaspartic coatings in soils at room temperature (RT) and 35°C applied to milled-surface-finished and sandblasted steels (SA 2.5).

2. Materials and experiments

The study was carried out on polyaspartic coatings applied to structural steel plates. The tested plates composed of hot-rolled steel grade S235, which was chosen due to its wide range of applications in infrastructure projects in Belgium and throughout Europe, were manufactured by ASK Romein Malle NV, a steel company based in Malle, Belgium. The control polyaspartic coating was designed to protect concrete structures, whereas the modified polyaspartic coating containing inhibitors and a barrier was planned to prevent steel from corroding. The surface finish of the steel panels, as received from the supplier, was milled and blasted (SA 2.5). Before blasting, the mill scale was removed by immersing the steel plates in 10% H_2SO_4 for 30 minutes at 60°C before being cleaned and dried by acetone to ensure a suitable steel surface before blasting. Sand blasting was carried out using a blasting cabinet, while blast cleaning was performed using granular aluminum oxide abrasive media. The steel samples were 150 x 80 x 2 mm rectangular plates. An example of the surface morphology of both the milled and blasted steel surface finishes are displayed in *Figs.1a* and *1b*, respectively.
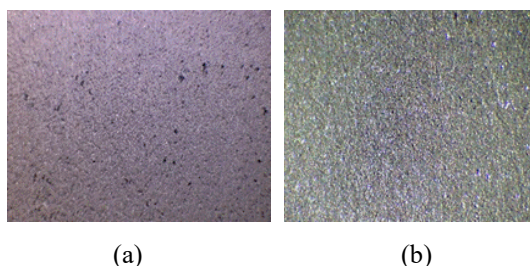

(a)   (b)

Figure 1. Photographs of a) milled steel finish, b) blasted steel finish

Polyaspartic coatings consist of two components. Component (A), which also contains a corrosion inhibitor and an oxide barrier, is the active material, while component (B) is the hardener. The required amount of component (A) was added to component (B) and mixed for 120 seconds before being applied to the steel. One layer of each coating was applied to each steel sample using an ERICHSEN 358 spiral film applicator and left for one day before being buried in the soil. The edges of the steel samples were well covered with tape to avoid premature failure of the coating or rusting of the steel plates. The edges of the steel plates were carefully smoothened and curved. During the coating, extra layers were applied to the edges, moreover, a strong tape was placed over them to prevent them from rusting and the coating from failing. An example of a coated steel panel is displayed in *Fig.2*. The soil used in this study was loamy sandy soil according to the Belgian soil analysis report [5] collected from arable, residential and light industrial flattened land located in Malle in the Vlaanderen region of Belgium. The average climate of the soil in the region of Vlaanderen is temperate maritime with an average 800 mm of precipitation falling annually.
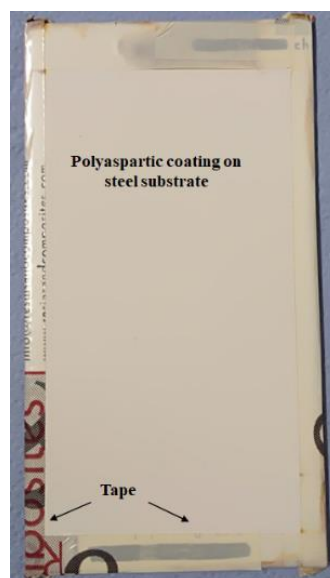

Figure 2: Materials used in the soil experiment: an example of a coated steel panel

In many locations, the concentration of heavy metals in the soil and groundwater still exceeds environmental quality standards due to the use of ash material for road stabilization, which has also resulted in the spread of heavy metals. The actual carbon content of arable land parcels in Flanders is considered to be fairly good. Salinization is a minor concern in the region of the tested soil because it is regarded as being situated far from the coastline [5].

The soil was collected at a depth of 0.5 m and filtered using sieves of two different mesh sizes to remove dirt and purify the soil (*Fig.3*).
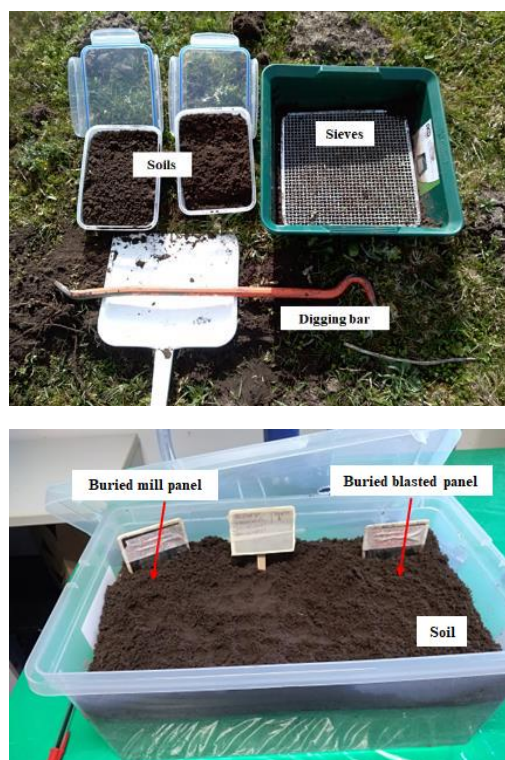

Figure 3: Soil experiment materials: soil collection and coated steel samples buried in soil

The pH of the soil was controlled before each experiment and measured to be between 6.5 and 7.0. The tested samples were placed in soil in a plastic container (*Fig.3*) for 30 days at both room temperature and 35°C using an oven. The resistance of the coating to soil attack was evaluated by identifying any forms of coating damage and defects as well as signs of rust on the steel using visual and macroscopic inspection techniques.

3. Results and Discussion

Optical observations of the control and inhibited polyaspartic coatings loaded onto milled and blasted steel panels after having been buried in soil for 30 days at RT and 35°C are displayed in *Figs.4-15*. The coatings exhibited varying degrees of blistering and, in some cases, some rusting was also present following the test. The experimental results are presented and discussed according to the type of coating applied and the experimental conditions.

3.1. Control polyaspartic coating in soil at RT and 35°C

The macroscopic observations after soil experiments had been conducted on the control polyaspartic coating applied to the milled and blasted surface finished steel panels are depicted in *Figs.4-7*. A cluster of blisters on the control polyaspartic coating applied to the milled surface finished steel after a soil experiment had been conducted at RT can be seen in *Fig.4*. Furthermore, cracking of the blisters is also clearly visible as indicated by the arrows, where rust can be observed under the peeled off blisters. Additional clustered and isolated open blisters on the control polyaspartic coating tested in soil at 35°C are presented in *Fig.5*.

Blisters in isolated spherical shapes of the control polyaspartic coating applied to the blasted, surface finished steel panels are documented in *Figs.6-7*. However, in *Fig.6*, the surface morphology contains a collection of smaller blisters on the control polyaspartic coating applied to the blasted, surface finished steel after the soil experiments had been conducted at RT. On the other hand, in *Fig.7*, bigger blisters on the control
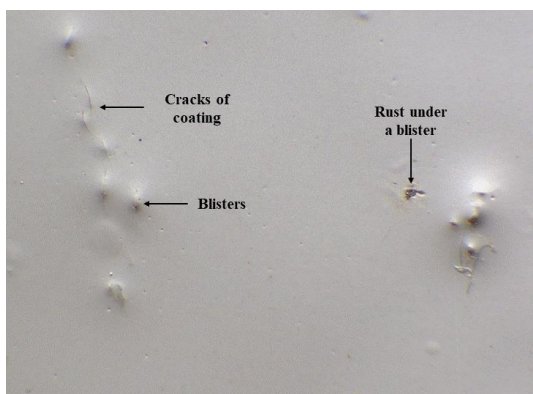

Figure 4. *C*ontrol polyaspartic coating, milled steel panel, RT

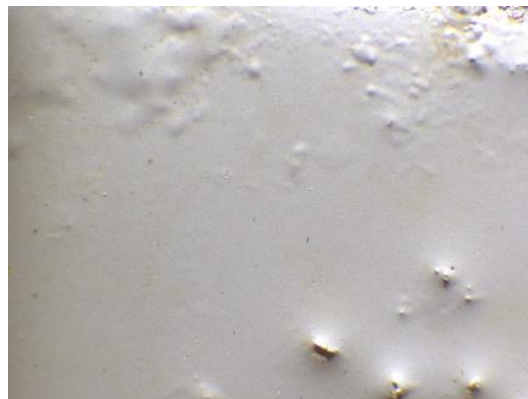polyaspartic coating are visible following the soil experiments at 35°C.

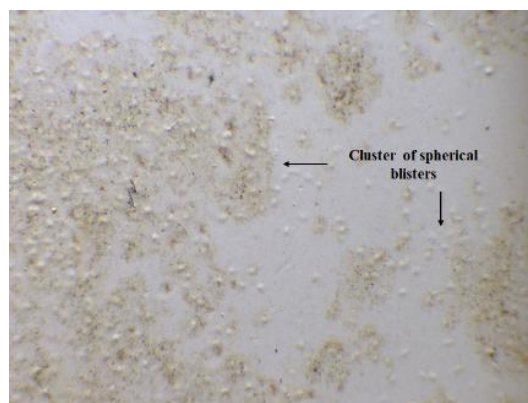*Figure 5.* Control polyaspartic coating, milled steel panel, 35°C

Figure 6. Control polyaspartic coating, blasted steel panel, RT
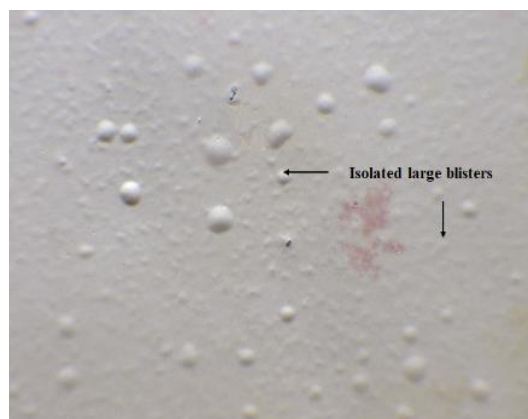

Figure 7. Control polyaspartic coating, blasted steel panel, 35°C

3.2. Polyaspartic coating loaded with an alkylammonium corrosion inhibitor tested in soil at RT and 35°C

Corrosion inhibitors are used to reduce the risk of corrosion on metal substrates in aqueous media by forming a barrier film or controlling the corrosion reactions of the corrosion cell. Alkylammonium salt inhibitors exhibit excellent biocidal and anticorrosive properties [6]. Corrosion inhibitors have been added to coating systems as one of the direct additives or in capsular form in the smart coating. Although the addition of a corrosion inhibitor to a coating system is primarily intended to improve its degradation resistance, adhesion between the film coating and metal substrate may also be improved to some extent. Nevertheless, some corrosion inhibitors have a tendency to degrade in microbial cultures such as soils.

In this regard, the performance of the alkylammonium inhibitor in the examined polyaspartic coating submerged in soil is presented in this section. Surface morphological observations of the polyaspartic coating incorporated with the alkylammonium inhibitor and micaceous iron oxide barrier following soil corrosion experiments at RT and 35°C are displayed in *Figs.8-11*. In *Fig.8*, it can be seen that the liquid alkylammonium inhibitor reduced but did not prevent the formation of blisters on the polyaspartic coating applied to the milled surface finished steel panels tested in soil at RT. Perforations through the coatings of the alkylammonium corrosion inhibitor and iron oxide barrier were visible after having been immersed in soil for 30 days at RT.

For clear verification, the images of the perforations were inverted horizontally and vertically as documented in *Figs.8a and 8b*, respectively. Since these perforations were not observed when the coating was applied and before it was immersed in the soil, they may have resulted from the corrosion reactions occurring underneath the coating or the coating substances reacting with the soil causing leaching of coating contents such as the corrosion inhibitors. Groups of blisters and the iron oxide barriers on black spots distributed over the surface of the coating layer can be seen in *Fig.8c*.

As for the samples tested in soil at 35°C presented in *Fig.9*, damage to the coating was in the form of wider bulging blisters, moreover, iron oxide barriers were visible. The effect of the surface finish of the steel panels on the organic inhibitor polyaspartic coating was not noticeable.

However, the degree of blistering still visible on the coating applied to the blasted panels as well as tested in soil at RT and 35°C is illustrated in *Figs.10 and 11*, respectively. The experiments in this study simulated to a certain extent the performance of both steel structures immersed in soil and coatings as one of the most commonly used protection systems for underground assets. In this regard, the examined soils at RT and 35°C were found to threaten the control polyaspartic coating and polyaspartic coating dispersed with the alkylammonium corrosion inhibitor. This outcome is proven by the penetration and accumulation of the

a) Coating surface: Horizontal position image

b) Coating surface: Vertical position image
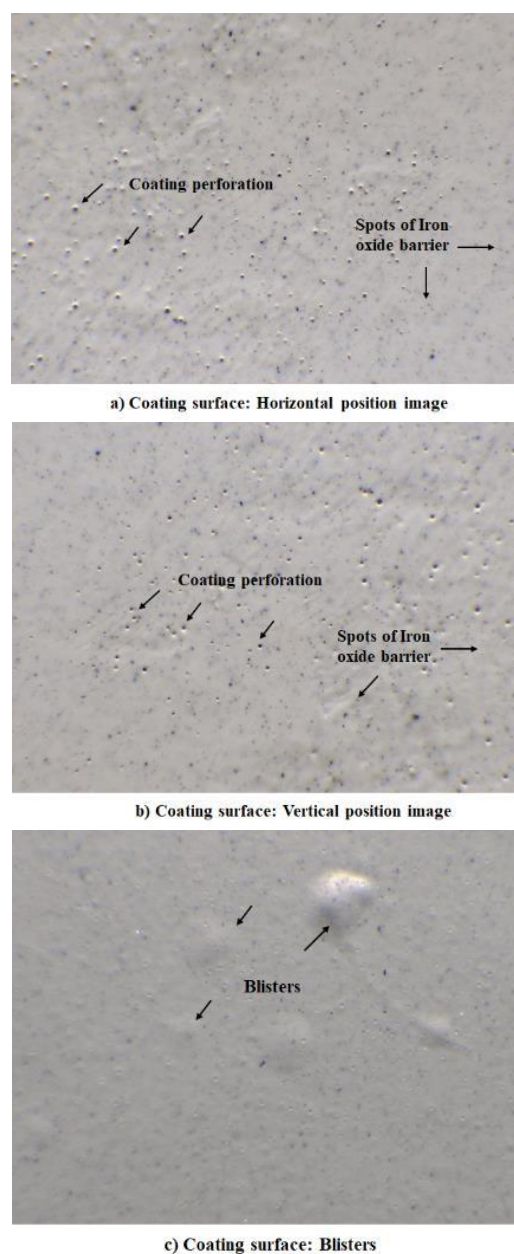

c) Coating surface: Blisters

Figure 8. Polyaspartic coating (alkylammonium corrosion inhibitor + iron oxide barrier), milled steel panel, RT
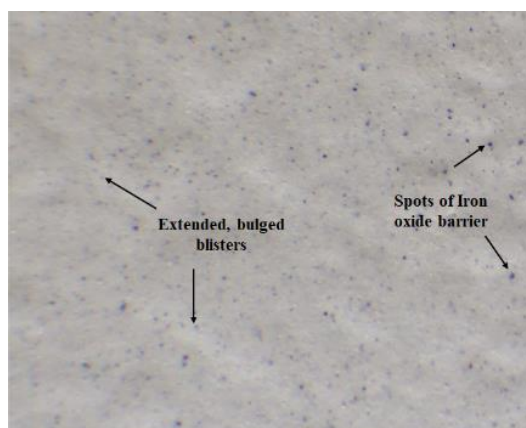

Figure 9. Polyaspartic coating (alkylammonium corrosion inhibitor + iron oxide barrier), milled steel panel, 35°C

aggressive elements in moisture through the coating matrix, whereas the visual and macroscopic interpretations confirmed the existence of a mass of blisters and cracks in the control coating.

The identified blisters in the coating are most likely

Figure 10. Polyaspartic coating (alkylammonium corrosion inhibitor + iron oxide barrier), blasted steel panel, RT
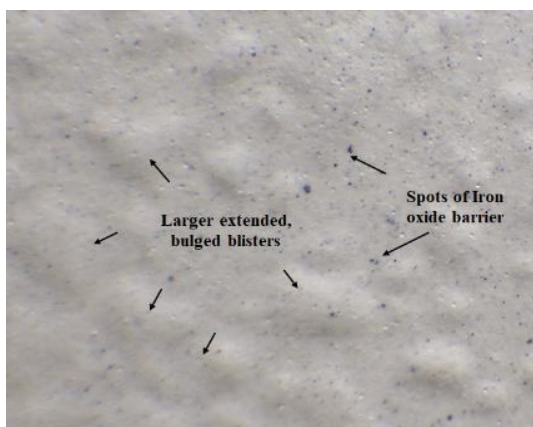

Figure 11. Polyaspartic coating (alkylammonium corrosion inhibitor + iron oxide barrier), blasted steel panel, 35°C

caused by a combination of factors such as saline conditions as well as the presence of sulfate, bacteria and sulfide. The role of such parameters, in addition to chemical, mechanical and biological activities, in the corrosion of buried steel on top of the degradation of other materials are discussed elsewhere [2,7-8]. Furthermore, the microbial culture of the soil has a tendency to cause the biodegradation of the alkylammonium salt that exists in the chains of some corrosion inhibitors in the main structure. This type of biodegradation has been studied by several previous researchers, who summarized that a closely packed nitrogen atom yields biodegradable alkylammonium salts. However, its degree of resistance improves significantly in correlation with the number of long alkyl chains associated with the nitrogen atom [9].

3.3. Polyaspartic coating loaded with a zinc phosphate corrosion inhibitor tested in soil at RT and 35°C

Figs.12-15 depict the macroscopic observations of a polyaspartic coating containing a zinc phosphate inhibitor and a micaceous iron oxide barrier applied to milled and blasted steel panels. It was clearly observed that the combination of zinc phosphate and the iron oxide barrier in the polyaspartic coating significantly inhibited the formation of blisters. The optical photographs of the polyaspartic coating tested in soil at RT and 35°C on the milled surface finished and blasted surface finished steel panels are strongly in line with the presence of the zinc phosphate corrosion inhibitor and iron oxide barrier, since neither blisters nor rust were recorded. Only flakes of the iron oxide barrier dispersed in the matrix of the polyaspartic coating are visible. The experimental results show that the dispersion of the zinc phosphate corrosion inhibitor and iron oxide barrier in the polyaspartic coating led to the development of its resistance to soil attack without exhibiting any considerable indications of deterioration. The resistance of this type of coating to the soil is attributed to the effectiveness of the zinc phosphate corrosion inhibitor, which reacted with and bonded to the steel substrate, forming a zinc phosphate protective layer and an iron oxide barrier composed of the phosphating
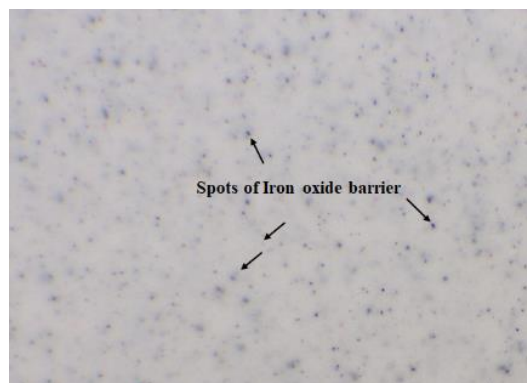

Figure 12. Polyaspartic coating (zinc phosphate corrosion inhibitor + iron oxide barrier), milled steel panel, RT
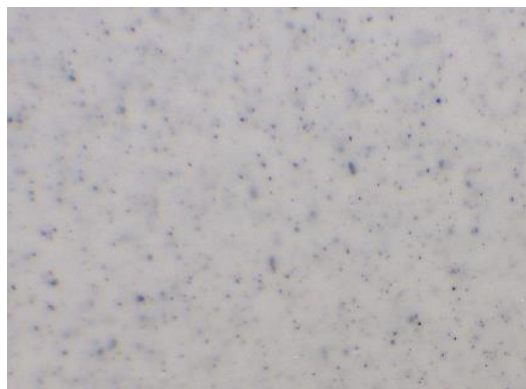

Figure 13. Polyaspartic coating (zinc phosphate corrosion inhibitor + iron oxide barrier), milled steel panel, 35°C
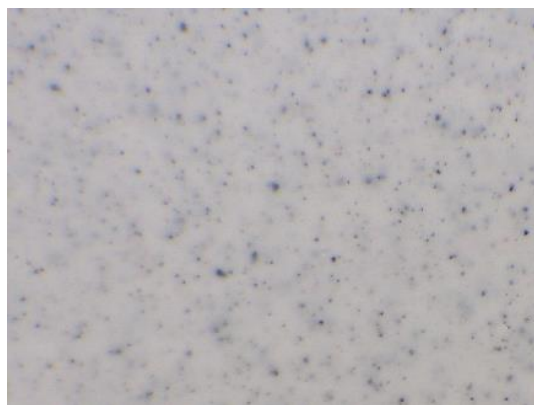
Figure 14. *P*olyaspartic coating (zinc phosphate corrosion inhibitor + iron oxide barrier), blasted steel panel, RT
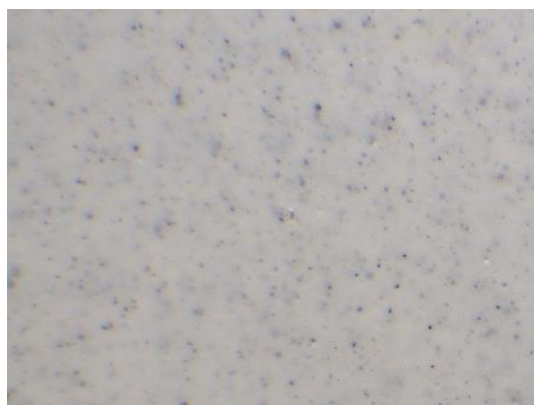

Figure 15. *P*olyaspartic coating (zinc phosphate corrosion inhibitor + iron oxide barrier), blasted steel panel, 35°C

film containing $FePO_4$, Fe_2O_3 and FeO. The effectiveness of both the zinc phosphate and barrier are in agreement with the findings of several studies that investigated epoxy and waterborne acrylic coatings [10].

3.4. Mechanism of blister formation

Blistering phenomena are associated with the absorption of water into the coating. Two of the most common types of coating blisters are: 1) osmotic blisters associated with the diffusion of water through the coating due to the presence of soluble salts on substrates or interlayers; 2) non-osmotic blisters due to swelling and buckling of the coating associated with the absorption of water in the coating [11]. In *Figs.4 and 5*, rust is observed under blisters in the control coating on the milled surface finished steel panels. The blisters on the milled surface finished steel panels can be classified as osmotic blisters because the milled layer might contain impurities resulting in a weak degree of adhesion of the coating to the substrate, thereby leading to the possible formation of blisters given the presence of the penetrated moisture. However, since the same coating on blasted steel yielded isolated blisters, as can be seen in *Figs.6 and 7* after soil experiments were conducted at RT and 35°C, it seems that the steel finish controlled the formation of blisters on the control polyaspartic coating. Horizontal and vertical

flip images of perforations in the alkylammonium coating on milled steel plates following soil tests at RT are depicted in *Figs.8a and 8b*, respectively. These can be explained by either corrosion reactions beneath the coating leading to osmotic blisters and subsequently perforations or reactions between the soil and the contents of the coating yielding perforations in the coating due to leaching of some of its contents such as the corrosion inhibitor. Nevertheless, examination of the coating before being buried in the soil did not exhibit perforations, which were only seen after the soil tests. The same sample in *Fig.8c* shows a group of unperforated blisters.

The hypothesis for the formation of blisters recorded in the experimental results is schematically described in *Fig.16*. How moisture from the soil penetrated through the coating is outlined in *Fig.16a*; with regard to the control coating, which does not contain inhibitive pigments or a coating loaded with the alkylammonium corrosion inhibitor, the moisture can easily pass through the coating into the substrate causing blistering. However, the presence of the zinc phosphate corrosion inhibitor and the iron oxide barrier protected the coating against soil attack (*Fig.16b*). Anyway, high-tech investigative techniques such as SEM could be applied in future studies to better understand the behavior of polyaspartic coatings in soils.

a)

b)

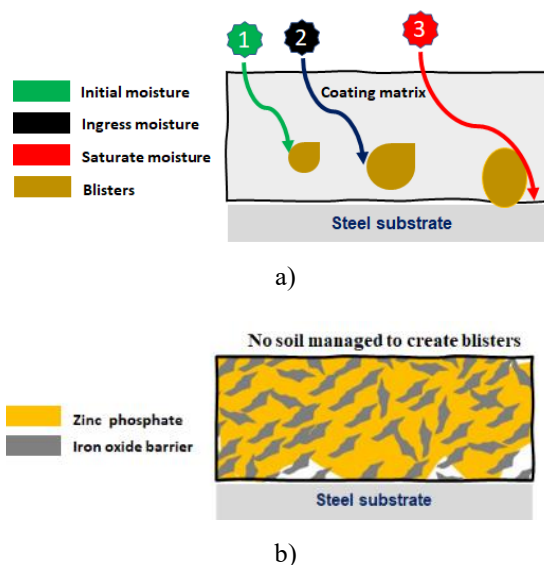*Figure 16.* A schematic diagram representing the formation of blisters in the control and inhibitive coatings: a) control coating and b) zinc phosphate + iron oxide barrier inhibitive coating

4. Conclusions

Since the content of the coating and temperature are important factors controlling the impact of soil on the performance of coatings and its reliability, the following conclusions have been drawn:

- Increasing the soil temperature from RT to 35°C increased the severity of blistering in the control polyaspartic coating and polyaspartic coating loaded with the alkylammonium corrosion inhibitor after 30-day-long soil experiments due to the high degree of moisture absorption.
- The advantages of applying the zinc phosphate corrosion inhibitor and the micaceous iron oxide barrier are significant in eliminating the soil risk to buried steel.
- This coating efficiently protects milled surface finished steel as well as blasted steel in soil experiments conducted over 30 days at RT and 35°C.
- The newly invented coating formula may well be applied as a protection system for steel assets submerged in soil in industry and the infrastructure sectors.
- The soil experimental results of the polyaspartic coating containing the zinc phosphate corrosion inhibitor supported the final remarks that this type of coating exhibits a good degree of resistance to erosion when immersed, as determined in earlier stages of this project.

Future studies should include experimentally measuring and examining the soil parameters as well as physical testing, which could not be examined at this stage of the project:

1. Soil parameters such as soil type, pH variation, bacterial activity, water content and soil resistivity.
2. Physical and mechanical testing of coatings, e.g. with regard to their compatibility with protective coatings and cathodic protection, cathodic disbondment, flexibility, cracking resistance, electrical and insulation resistance as well as compressive and tensile strength.
3. Thermal resistance and permeability of the coating in the simulation of anticipated working environments.

Acknowledgements

REFERENCES

[1] Emori, W.; Okafor, P.C.; Bassey, V.M.: Physicochemical characteristics of soil moisture and their effects on the corrosion behavior of buried mild steel in Calabar metropolis, Nigeria, *J. Environ. Prot.* 2018, **9**, 801–814, DOI: 10.4236/jep.2018.97050

[2] Chen, J.; Chen, Z.; Ai, Y.; Xiao, J.; Pan, D.; Li, W.; Huang, Z.; Wang, Y.: Impact of soil composition and electrochemistry on corrosion of rock-cut slope nets along railway lines in China, *Sci. Rep.*, 2015, **5**, 14939, DOI: 10.1038/srep14939

[3] Putra, R.; Muhammad; Huzni, S.; Ali, N.; Fonna, S.: Effect soil resistivity in mapping potential corrosion in underground pipelines area, *AIP Conf. Proc.*, 2018, **1977**, 040011, DOI: 10.1063/1.5042981

[4] Jiang, C.; Cheng, X.: Anti-corrosion zinc phosphate coating on building steel via a facile one-step brushing method, *Electrochem. Commun.*, 2019, **109**, 106596, DOI: 10.1016/j.elecom.2019.106596

[5] Van Liedekerke, M., Gentile, A., Barceló-Cordón, S., Soil country analyses: Belgium (Joint Research Centre Report 2009), DOI 10.2788/27334

[6] Brycki, B.; Szulc, A.: Gemini surfactants as corrosion inhibitors. A review, *J. Mol. Liq.*, 2021, **344**, 117686, DOI: 10.1016/j.molliq.2021.117686

[7] Yahaya, N.; Lim, K.S.; Noor, N.M.; Othman, S.R.; Abdullah, A.: Effects of clay and moisture content on soil-corrosion dynamic, *Malays. J. Civ. Eng.*, 2011, **23**(1), 24–32, DOI: 10.11113/mjce.v23.15809

[8] Abdulameer, E.A.; Al-Uqaily, R.A.H.; Al-Bayaty, S.A.H.: The effect of both moisture and clay content on the soil corrosion process for different periods of time as a geomorphological study in Al-Kut city, *IOP Conf. Ser.: Earth Environ. Sci.*, 2022, **961**(1), 012083, DOI: 10.1088/1755-1315/961/1/012083

[9] van Ginkel, C.G.; Kolvenbach, M.: Relations between the structure of quaternary alkyl ammonium salts and their biodegradability, *Chemosphere*, 1991, **23**(3), 281–289, DOI: 10.1016/0045-6535(91)90184-F

[10] Hao, Y.; Liu, F.; Han, E.-H.; Anjum, S.; Xu, G.: The mechanism of inhibition by zinc phosphate in an epoxy coating, *Corros. Sci.*, 2013, **69**, 77–86, DOI: 10.1016/j.corsci.2012.11.025

[11] Li, J.C.M.; Him, L.K.; Chang, B.T.A.: Blister initiation mechanism of FBE coatings, *NACE-International Corrosion Conference Series*, 2019, 13508, ISSN: 03614409

HUNGARIAN JOURNAL OF
INDUSTRY AND CHEMISTRY
HJIC

STUDY ON ADSORPTION OF ESSENTIAL OILS ON POLYLACTIC ACID MICROPARTICLES

LILLA VIRÁG[1*], RÓBERT BOCSI[1] AND DÓRA PETHŐ[1]

1 Research Centre for Biochemical, Environmental and Chemical Engineering, Faculty of
   Engineering, University of Pannonia, Egyetem u. 10, Veszprém, 8200, HUNGARY

Polylactic acid (PLA) is a biodegradable polymer that is widely used in medical devices, drug delivery systems, fibers for packaging containers and textiles. However, given that interactions between the polymer and the materials in contact with it affect its applications, it is important to study its adsorption and diffusion properties. The adsorption capacity of different polylactic acid particles regarding different additives, e.g. essential oils (*Thymus vulgaris, Melissa officinalis* and *Foeniculum vulgare*), was investigated. PLA microparticles of various sizes were prepared by a solvent emulsification evaporation method. In this study, the specific adsorption of essential oils on PLA microparticles was also investigated, which is related to the solubility parameters of essential oils. The experiments were performed using three different solutions of essential oils and ethanol as a solvent. Two sets of PLA microparticles were prepared with different solvents using three different particle sizes. PLA microparticles exhibited different adsorption properties depending on the solvent that was used for their production. Samples of particles prepared using the solvent dichloromethane had a higher essential oil uptake than those prepared with chloroform. The uptake of essential oil solution did not change significantly (~60%) by varying either the type of solvent used for PLA preparation or PLA particle size. The solubility of the essential oils affects the specific adsorption of essential oils on the microparticles. Among the components of the Hansen solubility parameters (HSPs), the polarity of essential oils is strongly related to adsorption.

Keywords: polylactic acid, microparticles, essential oil adsorption, Hansen solubility parameters

1. Introduction

Biodegradable polymers are important feedstocks in industry as they offer an environmentally-friendly alternative to fossil-based polymers in biomedical, agricultural and household applications [1]. PLA is an aliphatic polyester as well as one of the most commercially available, bio-based, biodegradable and biocompatible polymers. PLA is commonly considered for different applications such as in drug delivery systems, tissue engineering, packaging and textiles. The fields of application of this polymer are limited by certain properties, e.g. its low mechanical strength or hydrophobicity [2]-[3]. Different additives, e.g. essential oils, can be incorporated into biodegradable polymers to improve their functional properties [4]. Different types of essential oils such as thyme, cinnamon, oregano and basil are incorporated into biodegradable polymer films, e.g. for the development of food packaging films to enhance antimicrobial properties [5]. Essential oils also act as plasticizers in polymers. Due to their plasticizing properties, the structural and mechanical properties of such polymers can be altered [6], thereby also changing the sorption properties of PLA.

Interactions between essential oils and PLA have been studied by several researchers (Dusankova et al., Martins et al., Dicastillo et al.) using different processing methods [7]-[9] and are mainly determined by the composition of the essential oil and its polarity.

Dusankova et al. studied PLA microspheres containing different components of essential oils. They found that the more polar components adsorb better in the microspheres than the more apolar ones, as PLA itself is polar [7]. Martins et al. came to a similar conclusion. When the incorporation and release of the components of the essential oils thymol and p-cymene were studied, the diffusion rate of these components through the PLA matrix differed significantly (diffusion coefficient was 1.99×10^{-16} m^2/s for thymol and 4.34×10^{-16} m^2/s for p-cymene), which could be explained by their difference in polarity [8].

In our work, the adsorption properties of polylactic acid particles regarding different essential oils like those from lemon balm, fennel and thyme were investigated. The microparticles were prepared by a solvent emulsification evaporation method [10]. The structure of the polymer particles formed is critical, as their particle size distribution and porosity influence their adsorption properties. The properties of the particles that are

Sample name	PLA-solution – solvent type	Average size, μm
PLA_DKM_50	Dichloromethane (DKM)	57±12
PLA_DKM_100		116±21
PLA_DKM_200		207±57
PLA_K_50	Chloroform (K)	56±14
PLA_K_100		121±31
PLA_K_200		198±40

produced by the solvent emulsification evaporation method are mostly affected by the concentration of the PLA solution, type and amount of surfactant as well as the mixing speed. Besides the concentration of the PLA solution, its composition is also important [11]. The organic solvent in which PLA is dissolved will affect the structure of the microparticles produced [10], [12]. Shi et al. found that PLA particles prepared using chloroform as the solvent were less porous than those prepared in ethyl acetate [12].

Consequently, in our work, the adsorption of essential oils on PLA microparticles as a function of the PLA particle size was investigated. To modify the particle size distribution, the concentration of PLA solution was changed during the emulsification method.

2. Experimental

2.1. Materials

NatureWorks Ingeo Biopolymer 3D850 PLA granules, dichloromethane (>99.8%, Fisher), chloroform (technical grade, stabilized with ~0.6% of ethanol, VWR) and polyvinyl alcohol (fully hydrolyzed, M_w approx. 60,000; Merck) were used to prepare the PLA microparticles. To measure the degree of adsorption, ethanol (99.8% G.R., ISO reagent, Lach-Ner, s.r.o.) and three kinds of essential oils: *Melissa officinalis* (from lemon balm, Neuston Healthcare Kft.), *Foeniculum vulgare* (from fennel, Neuston Healthcare Kft.) and *Thymus vulgaris* (from thyme, Neuston Healthcare Kft.) were used.

2.2. Methods

Microparticles were prepared based on a solvent emulsification evaporation method. The particles were prepared as follows: firstly, 200 ml of PLA solution of a given concentration (2.5, 5.0 and 7.5 wt. %) using dichloromethane or chloroform as a solvent; secondly, the solution was added to 400 ml of 1 wt. % polyvinyl alcohol (PVA) solution. The emulsion was stirred with a magnetic stirrer at 820 rpm for 24 or 48 hours, depending on the solvent used (dichloromethane or chloroform, respectively). After filtering and washing, the solid particles were dried in a Binder FD 53 oven at 50 °C for 24 hours.

To determine the average diameter and size distribution of the particles, an image was taken using an optical microscope (Lacerta, zoom: 40x). The particle size was determined from the images using the program ImageJ.

To measure the degree of adsorption, 1.000 g of PLA particles were weighed on an Ohaus Adventurer AR3130 analytical balance in a pre-weighed dry test tube, then 2.000 g of a 1.00 mg/ml ethanolic solution of essential oil was added to it. The microparticles were soaked for 24 hours before the samples were separated by filtration.

The essential oil concentrations of the residual ethanolic solutions were analyzed by UV-Vis spectrophotometry. The absorption spectra of the samples were recorded between 200 and 800 nm using an Agilent Cary 60 UV-Vis Spectrophotometer.

Differential scanning calorimetry (DSC) was performed with a NETZSCH DSC 214 Polyma differential scanning calorimeter. The measurements were carried out under a 60 ml/min N_2 flow rate according to the following protocol: first the sample was heated from 20 to 200 °C at a heating rate of 10 °C/min before being cooled from 200 to 20 °C at a cooling rate of 10 °C/min then reheated from 20 to 200 °C at the same heating rate.

Notation was applied to the samples, e.g. *PLA_K_100_EL*. The first letter refers to the solvent that was used for PLA preparation (*DKM* for dichloromethane and *K* for chloroform), the number refers to the size of the microparticles (*Table 1*). At the end of the sample identification, the first letter refers to the type of solvent used for essential oil solution (*E* for ethanol) and the last letter refers to the essential oil, namely *L* for lemon balm, *T* for thyme and *F* for fennel.

3. Results and Discussions

3.1. Microparticle properties

The properties of the microparticles such as their particle size distribution are shown in *Fig.1*. As the concentration of the PLA solution increased, the size of the particles produced also increased. The correlation between the concentration of PLA solution and the diameter of the particles is linear. The solvent emulsification evaporation method mainly produced spherical particles that did not aggregate (*Fig.2*).

3.2. Solution uptake by microparticles

Regarding the uptake of ethanolic solution of essential oil by the particles prepared from a PLA solution prepared in dichloromethane, it was concluded that the solution uptake increases slightly by 10% on average as the particle size increases. However, the presence of essential oils in the solutions did not significantly affect the solution uptake of the particles. For a given particle size, the solution uptake was practically the same for all examined solutions. The average solution uptake by
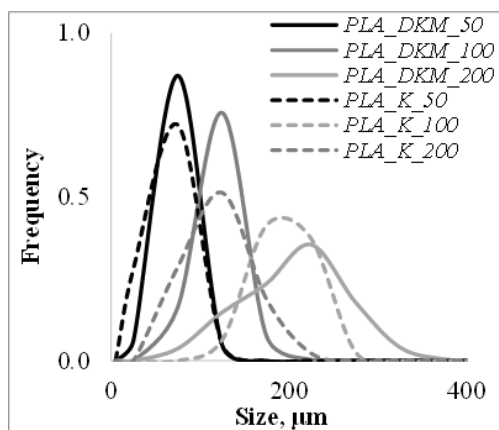
Figure 1. Particle size distribution of the different PLA microparticles

Figure 2. Images of the microparticles:
a.) PLA_K_100 and b.) PLA_DKM_100

particles 50, 100 and 200 μm in diameter is ~60, ~66 and ~75%, respectively.

3.3. Adsorption of essential oils on microparticles

The different types of PLA microparticles exhibited different adsorption properties (Figs.3 and 4) regarding various essential oils.

It was found that in the case of lemon balm, the uptake of essential oils by PLA_DKM particles from ethanolic solutions and the specific amount of the essential oil adsorbed increased as the particle size increased, while the degree of uptake and adsorption decreased in the case of ethanolic solutions of thyme and fennel. Lemon balm essential oil yielded an outstanding result. In this case, by increasing the particle size from 50 to 100 μm and then to 200 μm, the degree of essential oil uptake increased by 19% and then by a further 16%.

It was concluded that the effect of PLA_K particle size on the specific adsorption of thyme and fennel essential oils is insignificant, there is no correlation between the amount of essential oil adsorbed and the particle size. However, in the case of the lemon balm
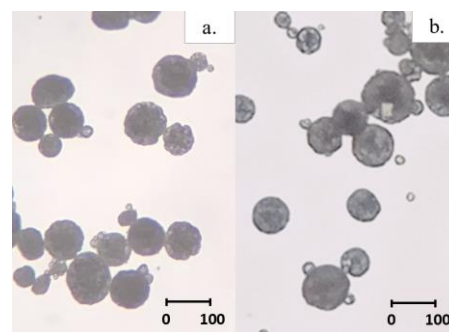
essential oil, the degree of specific adsorption increased as the particle size increased.

In general, it was concluded that for PLA_DKM particles, the essential oil uptake mainly resulted from the differences between the microparticles (degree of crystallinity, size, porosity) and the types of essential oils present in the solutions. Nonetheless, in the case of PLA_K particles, the specific amount of essential oil adsorbed on the surface or in the pores of the particles did not change significantly as the particle size changed, rather each essential oil was adsorbed differently on the particles. The particles prepared by using dichloromethane as a solvent had a higher specific essential oil adsorption (0.8-3.4 mg EO/g PLA) than particles prepared in chloroform (0.6-1.6 mg EO/g PLA). Variation in the adsorption properties of the particles was probably caused by the differences in their structure. The different solvents used in the production process caused the particles to solidify at different rates, leading to possible differences in their internal structure and porosity.

3.4. The correlation between adsorption properties in light of the Hansen solubility parameters (HSPs)

Adsorption properties are affected by the composition and properties of the adsorbate. The connection between
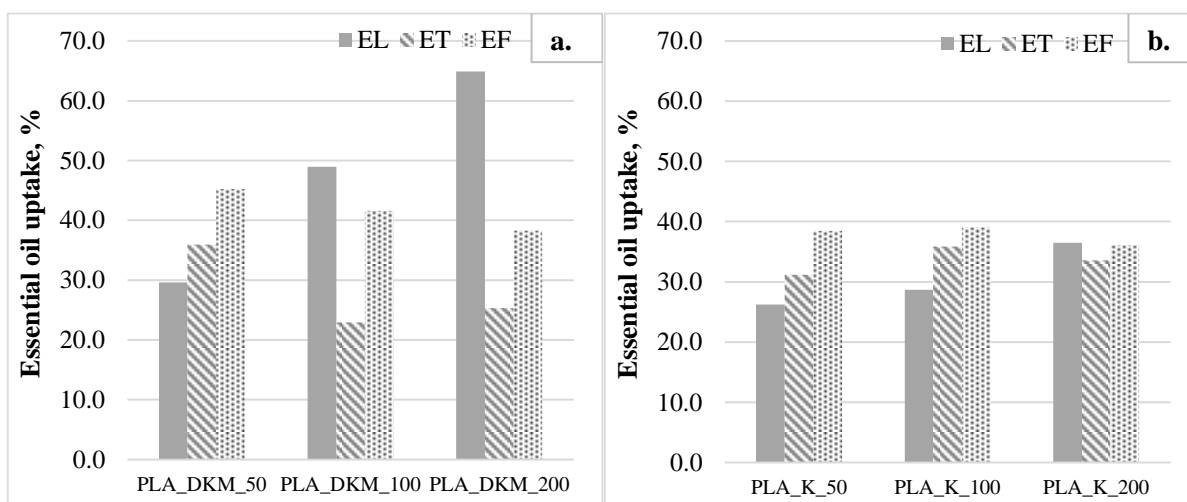

Figure 3. Essential oil uptake (%) by the microparticles in the case of a.) particles prepared in dichloromethane and b.) particles prepared in chloroform
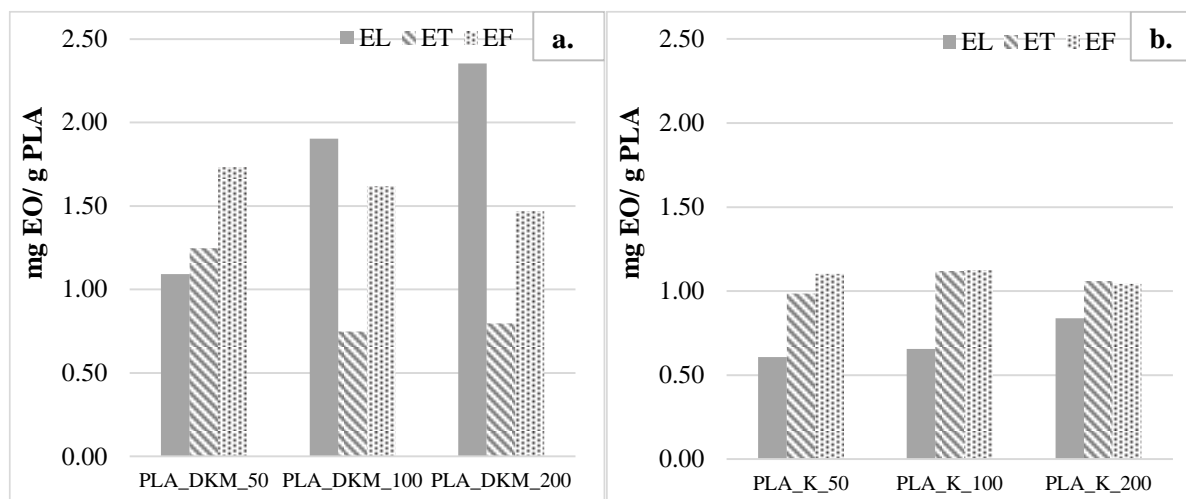
Figure 4. Specific adsorption of essential oil (EO) on microparticles (mg EO/g PLA) in the case of a.) particles prepared in dichloromethane and b.) particles prepared in chloroform

the solubility of essential oils and the adsorption properties of PLA was investigated. Solubility can be characterized by the HSPs, which describe the affinity of the polymer for different organic substances. Hansen total solubility parameter (δ_t) is composed of three parameters, one indicating the contribution to the dispersion forces (δ_d), another characterising the polar interactions (δ_p) and one more demonstrating the formation of H-bonds (δ_h). These solubility parameters can be determined using different methods such as the group contribution method (Hoftyzer-Van Krevelen method) [13]-[15].

The specific amount of essential oil adsorbed on PLA can be related to the total solubility parameter or one of its components. Since different essential oils have different solubility parameters depending on their composition (*Table 2*), the specific adsorption on PLA is different for different essential oils.

A correlation between the adsorbed amount of the essential oil and $\Delta\delta_{p,EO}$ was observed. ($\Delta\delta_{p,EO}$ shows how much the δ_p of an essential oil differs from that of PLA.) In the case of *PLA_DKM* particles, the specific adsorption decreased as $\Delta\delta_{p,EO}$ increased (*Fig.5*). In contrast, it was found that the specific amount of essential oil adsorbed on *PLA_K* particles deviated in the case of $\Delta\delta_{p,EO}$ less than 5.5 (MPa$^{1/2}$).

3.5. Thermal properties of the PLA particles

DSC was used to evaluate the thermal properties of the samples. The glass transition (T_g), cold crystallization

(T_{cc}) and melting temperatures (T_m) of the PLA particles were determined during the second heating of the DSC measurement.

The degree of crystallinity ($X_C\%$) was calculated from the enthalpy of melting (ΔH_m) and the enthalpy of cold crystallization (ΔH_{cc}), taking into account an enthalpy of melting (ΔH_m^0) of 94 kJ/kg for 100% crystalline *PLA* [16]-[17]:

$$X_C\% = [(\Delta H_m - \Delta H_{cc})/\Delta H_m] \times 100 \qquad (1)$$

Both types of PLA particles exhibited two exothermic, cold crystallization peaks and an endothermic melting peak (*Fig.6*). For both *PLA_DKM* and *PLA_K* particles, the glass transition occurred at ~61°C (61.3±0.6 and 60.9±0.3°C, respectively) and the melting at 177°C (177.3±0.8 and 176.6±0.3°C, respectively). However, a difference is observed in the cold crystallization temperatures between the two types of particles. For the *PLA_K* and *PLA_DKM* particles, the first cold crystallization peaks appeared at 96.7±0.6°C and 104.4±0.2°C, respectively. The probable reason for this is that during the emulsification method, the particles solidified at different rates based on the organic solvent used for the PLA solution. As the particles solidified at different rates, their structure and porosity vary. The thermal properties of the granules did not change even when the concentration of the PLA solution was changed during their preparation. The degree of crystallinity of the *PLA_K* particles was approximately 25.0±0.7%, while that of *PLA_DKM* was different. The degree of

Table 2. Hansen solubility parameters (HSPs) of the materials

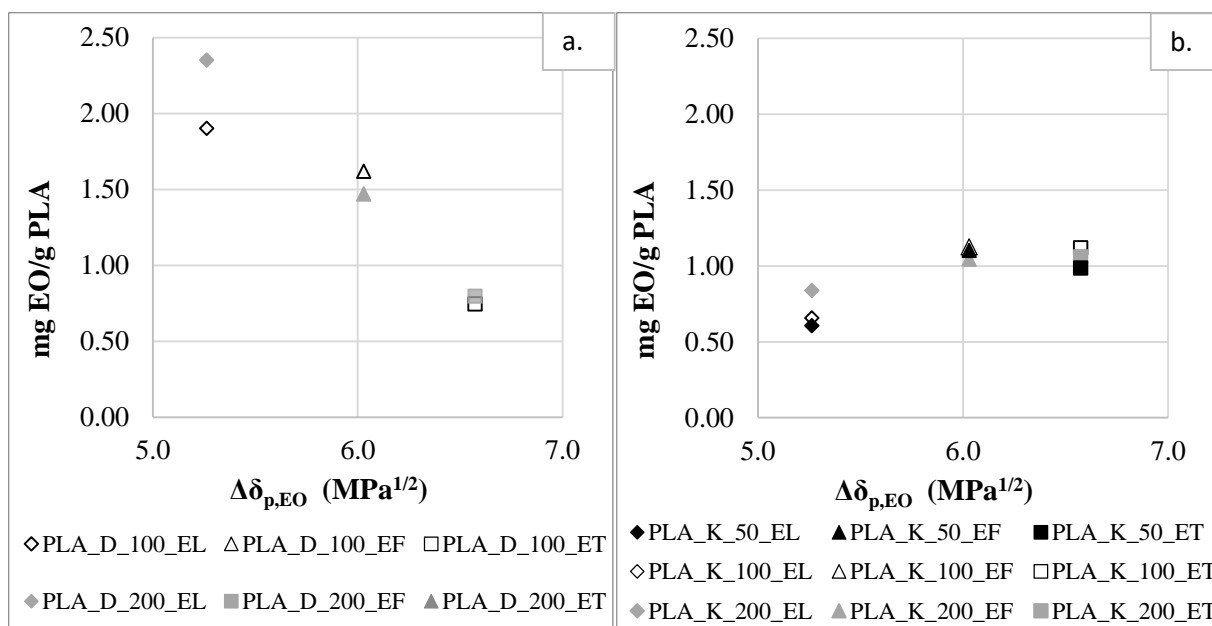| Material	δ_d (MPa$^{1/2}$)	δ_p (MPa$^{1/2}$)	δ_h (MPa$^{1/2}$)	δ_t (MPa$^{1/2}$)
PLA	18.6	9.9	6.0	21.9
Ethanol	15.1	8.4	18.3	25.2
Lemon balm essential oil	16.4	4.6	5.1	17.8
Thyme essential oil	21.5	3.3	9.6	23.8
Fennel essential oil	24.3	3.9	28.0	37.3

Figure 5. Correlation between the HSPs and the specific adsorption of essential oil (EO) on microparticles (mg EO/ g PLA) in the case of a.) particles prepared in dichloromethane and b.) particles prepared in chloroform
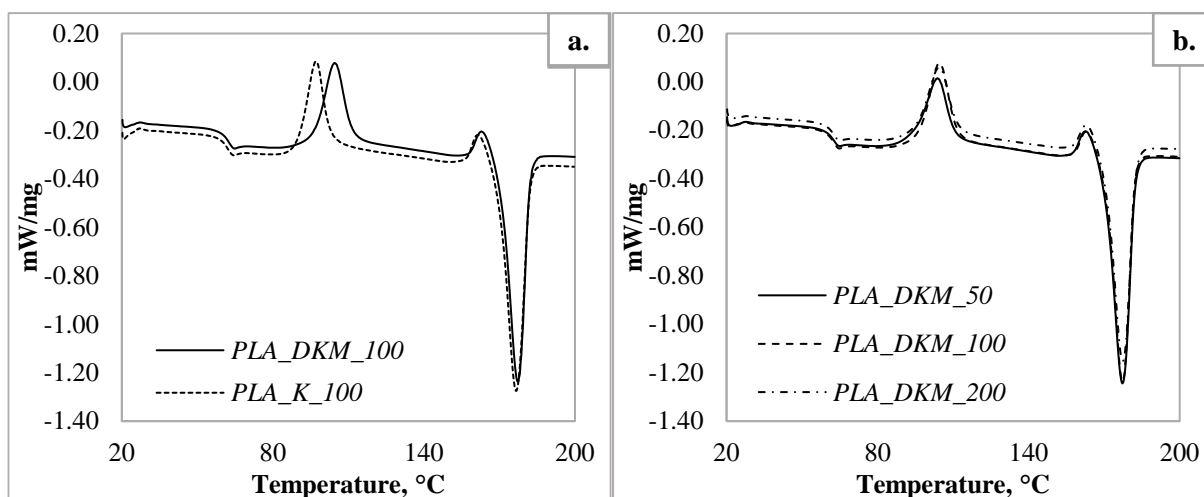

Figure 6. The second heating DSC curves of the PLA granules and microparticles in the case of a.) their different types and b.) their different sizes

crystallinity of the *PLA_DKM_50*, *PLA_DKM_100* and *PLA_DKM_200* particles was 24.3±0.4, 19.6±0.7 and 21.5±0.8, respectively.

After the degree of adsorption was measured, the thermal properties of the microparticles did not change due to their interaction with the essential oils (*Fig.7*). However, the adsorption of essential oils had an effect on the degree of crystallinity of the particles, as the degree of crystallinity of the *PLA_DKM* particles increased by ~2% and that of *PLA_K_50* particles increased to ~30%.

The degree of crystallinity of the *PLA_K_100* and *PLA_K_200* particles was not influenced by which essential oil was used.

Based on the results, it was found that the thermal properties of the PLA microparticles are affected by the type of solvent used during their preparation rather than by the concentration of the PLA solution used. It was concluded that the thermal properties of the microparticles were not changed by the adsorption of

essential oils. Therefore, the amount of essential oil adsorbed was insufficient to cause a significant change to the PLA structure.

4. Conclusion

In our work, the adsorption properties of polylactic acid particles for lemon balm, fennel and thyme essential oils were investigated. The adsorption of these essential oils on the PLA particles was investigated as a function of particle size (50, 100 and 200 μm).

It was concluded that the adsorption of essential oils is affected by both differences between types of microparticles (degree of crystallinity, size, porosity) and the types of essential oils present in the solutions of *PLA_DKM* samples. Although the specific amount of essential oil adsorbed on the surface or in the pores of *PLA_K* particles did not change significantly as the
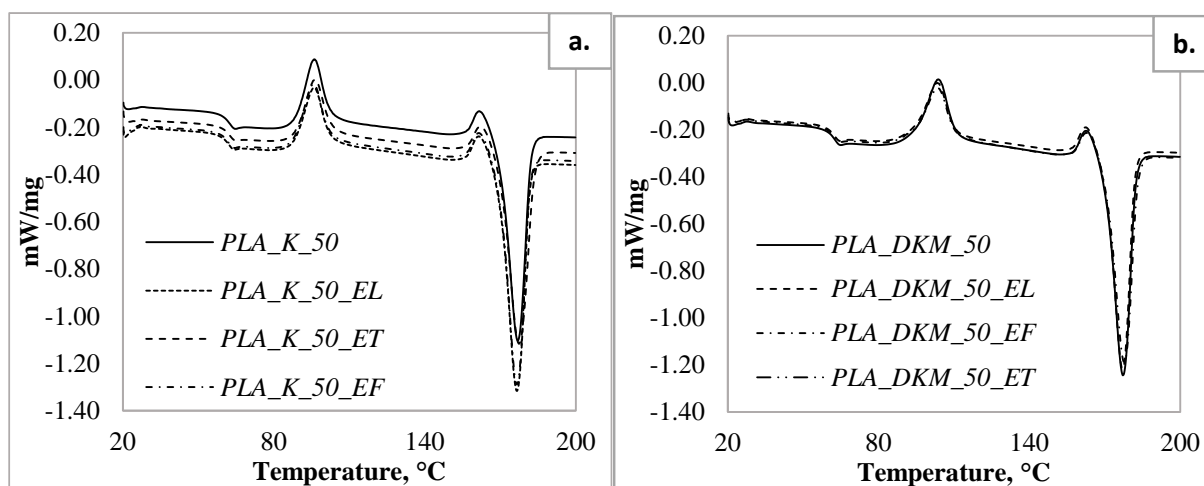
Figure 7. The second heating DSC curves of the PLA microparticles after measuring the adsorption of a.) particles prepared in chloroform and b.) particles prepared in dichloromethane.

particle size varied, the degree of adsorption of the essential oils on the particles varied. The particles that were prepared in dichloromethane as a solvent, exhibited a higher specific adsorption of 0.8-3.4 mg EO/g PLA compared to particles prepared in chloroform of 0.6-1.6 mg EO/g PLA. The difference in the adsorption properties of the particles is probably caused by variations in their structure. The different solvents used in the production process caused the particles to solidify at various rates, which may lead to differences in their internal structure and porosity.

The reason for differences in the degree of adsorption of the essential oils is variation in the composition of the essential oil solutions, which is characterized by the HSPs. In ethanolic solutions, a correlation between the adsorbed amount of the essential oil and the δ_p component of the total HSPs was observed.

Based on the results, it was determined that the thermal properties of the PLA microparticles are affected by the type of solvent used during their preparation rather than by the concentration of PLA solution applied. It was concluded that the thermal properties of the microparticles were not affected by the degree of adsorption.

REFERENCES

[1] Ranakoti, L.; Gangil, B.; Mishra, S.K.; Singh, T.; Sharma, S.; Ilyas, R.A.; El-Khatib, S.: Critical review on polylactic acid: Properties, structure, processing, biocomposites, and nanocomposites, *Materials*, 2022, **15**(12), 4312, DOI: 10.3390/ma15124312

[2] Li, G.; Zhao, M.; Xu, F.; Yang, B.; Li, X.; Meng, X.; Teng, L.; Sun, F.; Li, Y.: Synthesis and biological application of polylactic acid, *Molecules*, 2020, **25**(21), 5023, DOI: 10.3390/molecules25215023

[3] Nofar, M.; Sacligil, D.; Carreau, P.J.; Kamal, M.R.; Heuzey, M.C.: Poly (lactic acid) blends: Processing, properties and applications, *Int. J. Biol. Macromol.*, 2019, **125**, 307–360, DOI: 10.1016/j.ijbiomac.2018.12.002

[4] Qin, Y.; Li, W.; Liu, D.; Yuan, M.; Li, L.: Development of active packaging film made from poly (lactic acid) incorporated essential oil, *Prog. Org. Coat.*, 2017, **103**, 76–82, DOI: 10.1016/j.porgcoat.2016.10.017

[5] Ahmed, J.; Hiremath, N.; Jacob, H.: Antimicrobial, rheological, and thermal properties of plasticized polylactide films incorporated with essential oils to inhibit *Staphylococcus aureus* and *Campylobacter jejuni*, *J. Food Sci.*, 2016, **81**(2), 419–429, DOI: 10.1111/1750-3841.13193

[6] Tarach, I.; Olewnik-Kruszkowska, E.; Richert, A.; Gierszewska, M.; Rudawska, A.: Influence of tea tree essential oil and poly(ethylene glycol) on antibacterial and physicochemical properties of polylactide-based films, *Materials*, 2020, **13**(21), 4953, DOI: 10.3390/ma13214953

[7] Dusankova, M.; Pummerova, M.; Sedlarik, V.: Microspheres of essential oil in polylactic acid and poly(methyl methacrylate) matrices and their blends, *J. Microencapsul.*, 2019, **36**(3), 305–316, DOI: 10.1080/02652048.2019.1623337

[8] Martins, I.M.; Rodrigues, S.N.; Barreiro, M.F.; Rodrigues, A.E.: Release studies of thymol and p-cymene from polylactide microcapsules, *Ind. Eng. Chem. Res.*, 2012, **51**(35), 11565–11571, DOI: 10.1021/ie301406f

[9] de Dicastillo, C.L.; Villegas, C.; Garrido, L.; Roa, K.; Torres, A.; Galotto, M.J.; Rojas, A.; Romero, J.: Modifying an active compound's release kinetic using a supercritical impregnation process to incorporate an active agent into PLA electrospun mats, *Polymers*, 2018, **10**(5), 479, DOI: 10.3390/polym10050479

[10] O'Donnell, P.B.; McGinity, J.W.: Preparation of microspheres by the solvent evaporation technique, *Adv. Drug Deliv. Rev.*, 1997, **28**(1), 25–42, DOI: 10.1016/S0169-409X(97)00049-5

[11] Singh, B.; Singh, P.; Sutherland, A.J.; Pal, K.: Control of shape and size of poly (lactic acid) microspheres based on surfactant and polymer concentration, *Mater. Lett.*, 2017, **195**, 48–51, DOI: 10.1016/j.matlet.2017.02.068

[12] Shi, X.-D.; Sun, P.-J.; Gan, Z.-H.: Preparation of porous polylactide microspheres and their application in tissue engineering, *Chinese J. Polym. Sci.*, 2018, **36**(6), 712–719, DOI: 10.1007/s10118-018-2079-x

[13] Hansen, C.M.: Hansen solubility parameters: A user's handbook, Second edition, (CRC Press, Boca Raton, FL, USA), 2007, DOI: 10.1201/9781420006834

[14] Van Krevelen, D.W.; Te Nijenhuis, K.: Properties of polymers: Their correlation with chemical structure; Their numerical estimation and prediction from additive group contributions, Fourth edition, (Elsevier, Amsterdam, The Netherlands), 2009, pp. 201–225, ISBN: 978-008054819-7

[15] Sato, S.; Gondo, D.; Wada, T.; Kanehashi, S.; Nagai, K.: Effects of various liquid organic solvents on solvent-induced crystallization of amorphous poly(lactic acid) film, *J. Appl. Polym. Sci.*, 2013, **129**(3), 1607–1617, DOI: 10.1002/app.38833

[16] Saiter, A.; Delpouve, N.; Dargent, E.; Saiter, J.M.: Cooperative rearranging region size determination by temperature modulated DSC in semi-crystalline poly(L-lactide acid), *Eur. Polym. J.*, 2007, **43**(11), 4675–4682, DOI: 10.1016/j.eurpolymj.2007.07.039

[17] Ahmed, J.; Zhang, J.-X.; Song, Z.; Varshney, S.K.: Thermal properties of polylactides: Effect of molecular mass and nature of lactide isomer, *J. Therm. Anal. Calorim.*, 2009, **95**(3), 957–964, DOI: 10.1007/s10973-008-9035-x

HUNGARIAN JOURNAL OF
INDUSTRY AND CHEMISTRY
HJIC

OPTIMIZATION OF *BACILLUS LICHENIFORMIS* DSM13 FOR BIOSURFACTANT PRODUCTION USING RESPONSE SURFACE METHODOLOGY

JESSE JOHN SAKIYO[1] AND ÁRON NÉMETH[1]*

1 Department of Applied Biotechnology and Food Science, Budapest University of Technology and Economics, Műegyetem rkp. 3, Budapest, 1111, HUNGARY

Biosurfactants are surface-active compounds that can reduce surface tension in both aqueous solutions and hydrocarbon mixtures, which in recent times have become more valuable due to their lower toxicity and are generally referred to as green or organic surfactants. Such products are much better than chemical surfactants in terms of their enhanced biodegradation rates and the bioavailability of organic contaminants. Fungi, yeast and bacteria are mainly capable of producing microbial biosurfactants. Bacteria, especially Bacillus, are one of the most frequently applied and studied biosurfactant producers. This study investigated the kinetics of cell growth, the production of biosurfactants as well as the effect of and interactions between the (A) pH within the range of 4.1 to 9.8, (B) glucose concentration between 3.0 and 36.9 g/l, (C) surface tension and (D) emulsification index to maximize biosurfactant production. The analysis was carried out using a central composite design (CCD) model with four factors and five levels. The optimized medium (pH=8 and glucose concentration = 38 g/l) decreased the surface tension to 60 mN/m and increased the product yield up to 2.7 g/l.

Keywords: cell growth, effect of pH, glucose concentration

1. Introduction

Surfactants are surface-active compounds that reduce the surface tension between two liquids. Surfactant molecules are comprised of hydrophobic and hydrophilic, that is, water-hating and water-loving components, respectively. They are also regarded as detergents because of their wetting potential and emulsifying as well as foaming agents. Biosurfactants are also surfactants but from a microbial source. They have proven to be more sustainable due to their ability to leave less of or even no chemical residues after their use. Biosurfactants have been commonly used in industries such as the petroleum, cosmetics, antimicrobial, pharmaceutical and bioremediation industries [1]-[4].

Biosurfactants, also known as biological surfactants, are structurally varied molecules with high surface and emulsifying activities [5]-[6]. Glycolipids, lipopeptides and polymeric biosurfactants are the three major groups of biosurfactants. Biosurfactants have many advantages over conventional surfactants, including their ease of renewability, large-scale production, economic viability, cheaper substrates, more significant degree of foaming, good selectivity, turbidity, good biocompatibility, effectiveness at high temperatures or pH levels, chemical diversity and environmentally-friendliness [7]-[8]. Biodegradation is one of the most effective methods for combating environmental degradation mainly as a result of petroleum hydrocarbons, which pose a significant danger to ecosystems. This includes bacteria that use toxic materials as carbon sources, resulting in the breakdown of polluted components into low-molecular-weight or less harmful chemicals with no adverse effects [9].

Biosurfactants can decrease the surface tension of water to between 35 and 27 mN/m, which has been recorded by biosurfactant-producing bacteria [10]-[11], as well as increase the emulsifying activity from 20 to 30% for different hydrocarbon compounds during experiments on the emulsification index. A CCD was used to create appropriate testing levels for our response surface methodology (RSM). This analysis will create relevant parameters by making observations or taking measurements to determine the best combination of media that produces the desired response as well as characterizing the reaction so the conventional medium optimization strategy of modifying one independent variable while keeping the rest constant can be applied [12].

The main aim of our research is to produce biosurfactants to study their antifungal effects on crops in agriculture. Therefore, the first step is to produce biosurfactants efficiently. For this purpose, media optimization is commenced by using statistical optimization for cell growth in the fermentation broth to

increase the biosurfactant yield, i.e. decrease the surface tension and increase the emulsification index of the biosurfactant produced by *Bacillus licheniformis* DSM13.

2. Materials and Methods

2.1. Microorganism and cultivation of strain

The *Bacillus licheniformis* DSM13 strain was purchased from Hungary's National Collection of Agricultural and Industrial Microorganisms. The biosurfactant fermentations were conducted in 500 ml shake flasks (Erlenmeyer flasks with cotton plugs covered with aluminum foil). The inoculum was incubated for two days at 150 rpm and 37°C in a rotary shaker (New Brunswick Excella E24) by applying an inoculation ratio of 10 %. During the biosurfactant fermentation, the starting total volume, including the inoculum, was 150 ml, with an aeration greater than the working volume.

For the biosurfactant fermentation, a minimal medium was used; 1 liter of minimal media (pH=6) contained 1.0 g NH_4NO_3, 34.0 g glucose (Hungrana Kft., Szabadegyháza, Hungary), 6.0 g KH_2PO_4, 2.7 g Na_2HPO_4, 0.1 g $MgSO_4*7H_2O$, $1.2x10^{-3}$ g $CaCl_2$, $1.65x10^{-3}$ g $FeSO_4*7H_2O$, $1.5x10^{-3}$ g $MnSO_4*4H_2O$ and $2.2x10^{-3}$ g Na-EDTA (Reanal Laborvegyszer Kft., Hungary) Joshi et al. [13]-[14].

2.2. Unoptimized (reference) fermentation

Scale-up tests were conducted in a 1 l benchtop fermenter Biostat Q bioreactor (B Braun Co) filled up to 700 ml. During batch fermentation, the temperature was maintained at 37°C, the agitation rate at 300 rpm and the aeration rate at 0.5 VVM without pH control. A collection vessel was added to the exhaust air of the fermenter to collect the foam produced during the fermentation.

2.3. Statistical analysis of CCD (RSM) for optimization

Using a CCD for two variables, the power of the response surface approach to maximize biosurfactant production by *Bacillus licheniformis* was investigated in this study, which has served as the foundation for the simulated experimental plan and subsequent analysis. The randomized empirical findings were statistically analyzed using the statistical program TIBCO Statistica (version 13 for Windows) to detect the significant differences between the independent variables, namely (A) glucose concentration between 10 and 36 g/l and (B) pH between 4 and 9, to achieve maximum biosurfactant production by *B. licheniformis* DSM13 (*Table 1*).

Table 1. CCD runs showing factors and their levels

Standard run	2**(2) central composite, nc=4 ns=4 n0=2 Runs=10	
	Glucose [g/l]	pH
3	34.00	5.00
8	20.00	9.83
1	10.00	5.00
6	36.97	7.00
7	20.00	4.17
2	10.00	9.00
5	3.03	7.00
4	34.00	9.00
10 (C)	20.00	7.00
9 (C)	20.00	7.00

2.4. Biomass analysis

A CamSpec M501 spectrophotometer was used to determine the biomass content via optical density measurements at a wavelength of 600 nm (OD_{600}).

2.5. Surface tension analysis

Surface tension is the force per unit length measured in Millinewtons per meter (mN/m). The surface tension was measured using a stalagmometer (Wilmad-LabGlass LG-5050-100) according to the method of Czinkóczky et al. [11].

2.6. pH analysis

Initially, the pH of the media was set by adjusting it to several pH values ranging from 4 to 9 with 5M HCl or 6M NaOH. The pH was measured by a METTLER TOLEDO FiveEasy™ pH meter.

2.7. Emulsification index (E24)

The emulsification index measurement applied was established by Plaza et al. [15]. The emulsification index was determined from the supernatant of the fermented broth at intervals corresponding to the sampling frequency during the fermentation. In a test tube, 2 ml of crude oil and 2 ml of cell-free media (supernatant) were introduced and homogenized for 2 minutes by vortexing at 4000 rpm. The emulsifying activity was once more determined after 24 hours as follows: the relative height of the two liquid layers was documented by photos and the pixel size divided to obtain the values of the emulsification index [16]. E24 (%) is defined as [(total height of the emulsified layer) / (total height of the liquid layer) x 100] after 24h of vortexing.

2.8. Isolation and purification of the biosurfactant

Acid precipitation was used to isolate the biosurfactants. The bacterial cells were first removed by centrifugation and the remaining supernatant containing the biosurfactant was acidified with 2M HCl solution until the pH reduced to 2. The mixture was then incubated at 4 °C for 24 hours. The precipitate was collected by centrifugation at 10,000 rpm and 4°C for 30 minutes. The residue was then resolved in distilled water and the pH reset to neutral before being freeze-dried by a Martin Christ Alpha 1-4 LSCbasic lyophilizer [13].

3. Results

3.1. Unoptimized (reference) fermentation

An unoptimized fermentation according to Section 2.2. was carried out and the parameters that were measured during the process are shown in *Fig.1*. The highest reduction in the surface tension (ST) was observed 4 - 30 hours after the fermentation commenced. ST ranged from 75.5 to 68.3 mN/m. After 8 hours, the foam began to overflow and was collected in a vessel for further processing. The collected foam had a ST of 60 mN/m, indicating that the biosurfactants produced are mainly collected in the foam phase.
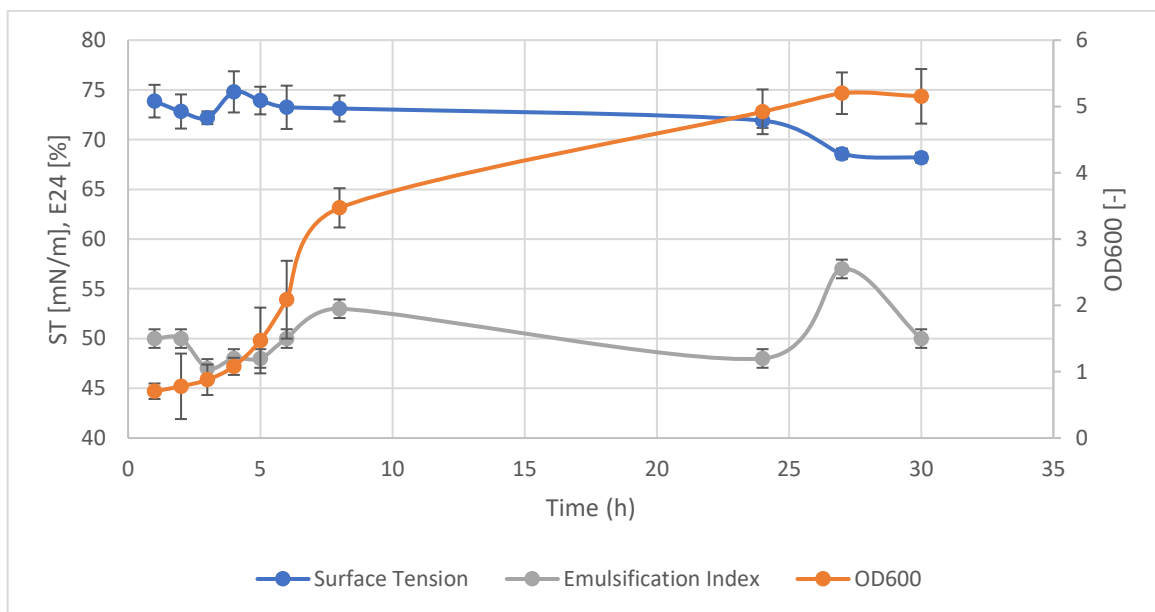

Figure 1. Growth, surface activity and emulsification index (E24) of *Bacillus licheniformis* in a 1 l fermenter during growth on a mineral salt medium

3.2. RSM

The effects of the glucose concentration and pH is shown in *Fig.2*. The highest biomass growth (OD) was recorded at a glucose concentration of 40 g/l and a rather higher pH value of approximately 9 resulting in an optical density of 4.5.

The mixed effect of the pH and glucose concentration regarding the surface tension is shown in *Fig.3*. The minimum surface tension was achieved while fermenting at pH 7.

According to *Fig.4*, the smallest product amount was achieved when the pH was extremely high at 11 and the glucose concentration was the lowest, while at a higher glucose concentration, the highest product yield was still achieved. This indicates that the gradient of the surface is minimal and very high at low and high glucose concentrations, respectively; moreover, depends on the pH. Therefore, the pH was the most important factor leading to an increase in the amount of biosurfactant produced.
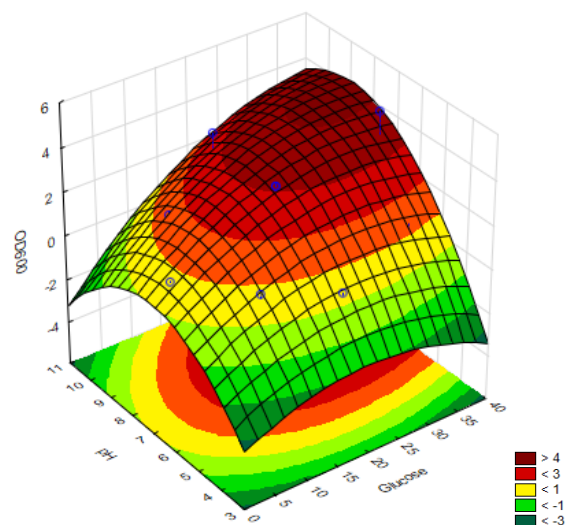

Figure 2. 3D RSM plot of the interactive effects of glucose concentration (g/l) and pH on biomass production

The model predicted the following ideal conditions to maximize the biosurfactant productivity using *Bacillus licheniformis* DSM13: pH=8 and glucose concentration=40g/l. The anticipated optimum point was confirmed experimentally, moreover, the observed and isolated product was 2.7 g/l. These findings show a strong connection between the predicted and actual experimental values, moreover, this model accurately represents biosurfactant production in the presence of *Bacillus licheniformis* DSM13. Since the highest product yield (i.e. lowest surface tension, *Fig.3*) was observed at different conditions, it is recommended to examine product purity in the future as the presence of contaminants can depend on the pH because of pH-dependent precipitation during product isolation.
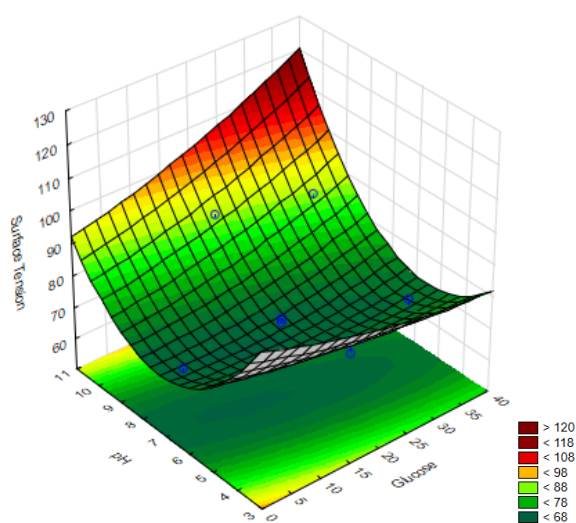

Figure 3. 3D RSM plot of the interactive effects of the glucose concentration (g/l) and pH on the surface tension (mN/m)
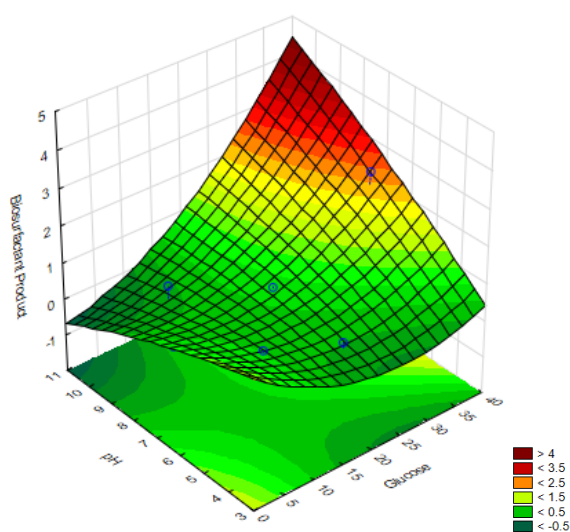

Figure 4. 3D RSM plot of the collaborative effects of the glucose concentration (g/l) and pH on the biosurfactant product

4. Conclusions

Biosurfactants are emerging as suitable alternatives to their predominant, less sustainable, petroleum-derived counterparts. In this study, the CCD, in conjunction with the response surface approach, is used to predict the optimization of *Bacillus licheniformis* DSM13 effectively. An increase in the glucose concentration yielded a high biosurfactant concentration while also increasing the fermentation time. At a lower pH level, the strain achieved a low biomass yield and lower biosurfactant yield but no change in the surface tension was observed. It was observed that the best operating conditions for biosurfactant production with *Bacillus licheniformis* DSM13 was a higher pH (pH=8) and a glucose concentration of 38 g/l. Future process validation to optimize biosurfactant manufacturing techniques is advised as follow-up research.

REFERENCES

[1] Markande, A.R.; Acharya, S.R.; Nerurkar, A.S.: Physicochemical characterization of a thermostable glycoprotein bioemulsifier from *Solibacillus silvestris* AM1, *Process Biochem.*, 2013, **48**(11), 1800–1808, DOI: 10.1016/j.procbio.2013.08.017

[2] Banat, I.M.; Makkar, R.S.; Cameotra, S.S.: Potential commercial applications of microbial surfactants, *Appl. Microbiol. Biotechnol.*, 2000, **53**(5), 495–508, DOI: 10.1007/s002530051648

[3] Sharma, N.; Lavania, M., Lal; B.: Biosurfactant: A next-generation tool for sustainable remediation of organic pollutants, *Front. Microbiol.*, 2022, **12**, 821531, DOI: 10.3389/fmicb.2021.821531

[4] Lai, C.-C.; Huang, Y.-C.; Wei, Y.-H.; Chang, J.-S.: Biosurfactant-enhanced removal of total petroleum hydrocarbons from contaminated soil, *J. Hazard. Mater.*, 2009, **167**(1-3), 609–614, DOI: 10.1016/j.jhazmat.2009.01.017

[5] Abdel-Fattah, Y.R.; Gaballa, A.A.: Identification and over-expression of a thermostable lipase from *Geobacillus thermoleovorans* Toshki in *Escherichia coli*, *Microbiol. Res.*, 2008, **163**(1), 13–20, DOI: 10.1016/j.micres.2006.02.004

[6] Luna, J.M.; Rufino, R.D.; Jara, A.M.A.T.; Brasileiro, P.P.F.; Sarubbo, L.A.: Environmental applications of the biosurfactant produced by *Candida sphaerica* cultivated in low-cost substrates, *Colloids Surf. A Physicochem. Eng. Asp.*, 2015, **480**, 413–418, DOI: 10.1016/j.colsurfa.2014.12.014

[7] Ilori, M.O.; Amobi, C.J.; Odocha, A.C.: Factors affecting biosurfactant production by oil degrading *Aeromonas* spp. isolated from a tropical environment, *Chemosphere*, 2005, **61**(7), 985–992, DOI: 10.1016/j.chemosphere.2005.03.066

[8] Wisdom, A.; Mark, U.; Zeberu, E.; Adeleke, A.: Optimisation of the physical properties of rice husk ash in ceramic materials using the response surface methodology, *Hung. J. Ind. Chem.*, 2021, **49**(1), 23–30, DOI: 10.33927/hjic-2021-04

[9] Donio, M.B.S.; Ronica, F.A.; Viji, V.T.; Velmurugan, S.; Jenifer J.S.C.A.; Michaelbabu, M.; Dhar, P.; Citarasu, T.: *Halomonas* sp. BS4, A biosurfactant producing halophilic bacterium isolated from solar salt works in India and their biomedical importance, *Springerplus*, 2013, **2**(1), 149, DOI: 10.1186/2193-1801-2-149

[10] Czinkóczky, R.; Németh, Á.: The effect of pH on biosurfactant production by *Bacillus subtilis* DSM10, *Hung. J. Ind. Chem.*, 2020, **48**(2), 37–43, DOI: 10.33927/hjic-2020-25

[11] Czinkóczky, R.; Németh, Á.: Techno-economic assessment of *Bacillus* fermentation to produce surfactin and lichenysin, *Biochem. Eng. J.*, 2020, **163**, 107719, DOI: 10.1016/j.bej.2020.107719

[12] Zhang, G.-L.; Wu, Y.-T.; Qian, X.-P.; Meng, Q.: Biodegradation of crude oil by *Pseudomonas aeruginosa* in the presence of rhamnolipids, *J. Zhejiang. Univ. Sci. B.*, 2005, **6**(8), 725–730, DOI: 10.1631/jzus.2005.B0725

[13] Joshi, S.; Bharucha, C.; Jha, S.; Yadav, S.; Nerurkar, A.; Desai, A.J.: Biosurfactant production using molasses and whey under thermophilic conditions, *Bioresour. Technol.*, 2008, **99**(1), 195–199, DOI: 10.1016/j.biortech.2006.12.010

[14] Joshi, A.; Pund, S.; Nivsarkar, M.; Vasu, K.; Shishoo, C.: Dissolution test for site-specific release isoniazid pellets in USP apparatus 3 (reciprocating cylinder): Optimization using response surface methodology, *Eur. J. Pharm. Biopharm.*, 2008, **69**(2), 769–775, DOI: 10.1016/j.ejpb.2007.11.020

[15] Arora, A.; Cameotra, S.S.; Kumar, R.; Balomajumder, C.; Singh, A.K.; Santhakumari, B.; Kumar, P.; Laik, S.: Biosurfactant as a promoter of methane hydrate formation: Thermodynamic and kinetic studies, *Sci. Rep.*, 2016, **6**, 20893, DOI: 10.1038/srep20893

[16] Rahman, K.S.M.; Rahman, T.J.; Lakshmana-perumalsamy, P.; Marchant, R.; Banat, I.M.: The Potential of bacterial isolates for emulsification with a range of hydrocarbons, *Acta Biotechnol.*, 2003, **23**(4), 335–345, DOI: 10.1002/abio.200390043

HUNGARIAN JOURNAL OF
INDUSTRY AND CHEMISTRY
HJIC

UTILIZATION OF AGRO-WASTES IN BIOHYDROGEN FERMENTATION BY VARIOUS MICROORGANISMS

KATALIN BÉLAFI-BAKÓ[1*], GÁBOR TÓTH[1], PÉTER BAKONYI[1] AND NÁNDOR NEMESTÓTHY[1]

1 Research Group on Bioengineering, Membrane Technology and Energetics, University of Pannonia, Egyetem u. 10, Veszprém, 8200, Hungary

Biohydrogen production based on agro-industrial wastes might be an attractive and effective technology for providing an energy source in the future. Dark fermentation is considered to be one of the most suitable biohydrogen formation processes. In this paper, various agro-industrial wastes as well as microorganisms applied for biohydrogen formation are reviewed.

Keywords: anaerobic process, dark fermentation, bioreactor

1. Introduction

Hydrogen produced biologically (biohydrogen) can be considered as a renewable source of energy [1]-[4]. Moreover, it is regarded as one of the most promising, environmentally-friendly "fuels" of the future due to its favourable characteristics, e.g., only water is formed by the combustion of H_2, no environmental pollution is produced, highest energy density of 143 kJ/g. Agro-industrial residues seem to be suitable feedstocks for the production of biohydrogen [5].

Large amounts of solid and liquid waste are formed in agriculture every year, moreover, the majority of it is unutilized. However, promising technologies are available whereby agro-industrial residues are applied to produce value-added products and green energy by biological methods [6]. Liquid wastes are usually found in the form of wastewater. Solid agro-wastes can be classified into four groups [7]:

    (i)   field residues
    (ii) waste of processing
    (iii) livestock waste
    (iv) chemical waste

Field residues generally originate from crop production and consist of the remains of crops, e.g., leaves, stalks, stems, seeds, straw, husks, shells, pulp, roots, woodland waste, etc.

Industrial food processing results in solid wastes which are mainly by-products of and leftovers from various plants, e.g., bagasse, sugarcane molasses, wheat bran, rice bran, groundnut shells, apple pomace, fruit peels, de oiled rice bran cake and oil cakes.

Livestock waste consists of by-products of slaughterhouses or originates from processing, e.g., bones, feathers, shells of crustaceans, as well as bedding/litter, carcasses and damaged feeders.

Chemical waste includes plant protection compounds, e.g., pesticides, insecticides and herbicides, as well as their containers and bottles. However, since these materials cannot be utilized in biological methods, this study focuses on the first three groups of solid wastes.

Biological hydrogen production from agro-industrial wastes includes dark fermentation, photofermentation and microbial electrolysis cells (MEC) [5]. Photofermentation is a process whereby organic substrates are converted into hydrogen by photosynthetic organisms under anoxic conditions. H_2 production in MECs is a bioelectrochemical process, where electrochemical and biological techniques are combined [8]. Given that dark fermentation is one of the most common methods used for hydrogen production from agro-wastes due to its higher hydrogen production rate, it is the focus of this mini-review.

2. Biohydrogen production by dark fermentation

The composition and certain characteristics of agro-wastes are determining factors of biohydrogen production. Generally speaking, although these materials are rich in carbon sources, the majority of them require some sort of pretreatment. The lignin content in particular should be treated to increase the efficiency of

biodegradation and conversion processes [5]-[7]. Pretreatments of agro-industrial residues include:

    (i)   physical,
    (ii)   chemical,
    (iii)   physicochemical and
    (iv)   biological methods.

Physical methods involve ultrasonication, ozonization, thermal- and microwave-assisted techniques as well as size-reduction processes, e.g., milling, grinding, etc.

Chemical methods include acid or alkali treatments, moreover, more recently organic solvents have been applied.

In physicochemical methods, a combination of physical and chemical techniques is used, e.g., steam explosion, hydrothermal treatment and chemical treatment complemented with microwave irradiation.

Biological methods include enzymatic and microbial (whole cell) treatments, where mainly the degradation of biopolymers occurs.

Using these pretreatment methods, higher yields and more efficient hydrogen formation can be achieved.

Dark fermentative biohydrogen production can be carried out by facultative anaerobes and obligate microbes [1], [4]-[5]. In many cases, the suitable types of microorganisms are determined by the substrate applied and mixed microbial consortia are frequently used. Nevertheless, numerous microbes have still been used in dark fermentative biohydrogen production based on agro-wastes, examples of which are listed in *Table 1*:

Table 1: Examples of the utilization of various agro-wastes to produce biohydrogen

Agro-waste	Microorganism	H_2 production rate or yield	Ref.
Sugar and rice mill wastewater	*Acinetobacter junii*	Rate 5.23 mLH_2L^{-1}h^{-1}	[9]
Rice mill wastewater	*Clostridium beijerinckii*	Yield 214.9 mLH_2L^{-1}	[10]
Cheese whey powder	*Enterobacter asburiae*	Yield 1.19 ± 0.01 molH_2mol^{-1}	[11]
Sugarcane molasses	*Eisenia fetida*	Yield 1571.81 mLH_2L^{-1}	[12]
Cashew apple bagasse	*Clostridium roseum*	Yield 15 mmolH_2 L^{-1} hydrolysate	[13]
Fruit and vegetable wastes + seawater	*Thermotoga maritima*	Rate 12.4 mmolh^{-1}L^{-1}	[14]
Fruit wastes (apple, banana, grape, melon, orange)	*consortia from biogas sludge*	Yield 523 mL/g VS (volatile solid)	[15]
Sweet sorghum bagasse	*Caldicellulosiruptor saccharolyticus*	Yield 73.6 mLH_2mmol^{-1} C6 sugars	[16]
Cornstalk	*Thermoanaerobacterium thermosaccharolyticum*	Yield 89.3 mLH_2g^{-1} DB (dry biomass)	[16]
Distillers grains	*Caldicellulosiruptor thermocellum*	Yield 29.2 mLH_2g^{-1} DB	[16]
Fruit and vegetable wastes as well as corn stover	*anaerobic sludge*	Yield 1.91 molH_2mol^{-1} glucose	[17]
Beer lees	*consortia from cow dung compost*	Yield 68.6 mlH_2/g TVS	[18]
Corn straw	*Ethanoligenens harbinense*	Yield 9 mLH_2g^{-1}	[19]
Wheat straw	*consortia from cow dung compost*	Yield 68 mLH_2g^{-1}	[20]
Grass silage	*manure*	Yield 16 mLH_2g^{-1}	[19]
Extracts of sweet lime peel	*anaerobic mixed consortia*	Yield 76.4 ml/g COD	[21]
Palm oil mill effluent	*Thermoanaerobacterium-rich sludge*	Yield 84.4 mLH_2g^{-1}	[22]
Beet pulp	*mixed culture from anaerobic sludge*	Yield 115.6 mLH_2g^{-1} COD	[24]
Sunflower stalks	*Clostridium sp.*	Yield 2.04 molH_2mol^{-1} eq. hexose	[25]
Miscanthus sinensis	*Thermotoga elfii*	Rate 23.99 mLH_2h^{-1}	[16]
Cassava pulp hydrolysate	*mixed culture*	Yield 342 mlH_2g^{-1} COD$_{reduced}$	[26]
Tequila vinasse	*Eisenia fetida*	Yield 1246.36 mLH_2L^{-1}	[12]
Sugarcane bagasse	*Eisenia fetida*	Yield 232.72 mLH_2L^{-1}	[12]

As can be seen, although several types of agro-wastes and microbes have been used for biohydrogen fermentation, the results regarding the yield or production rate of the processes are difficult to compare since their units vary and the data on hydrogen formation is diverse. Moreover, in this study, no information was collected about the treatment of the substrate (if any) nor which kind of bioreactor, set-up or mode of operation was used, making their comparison even more difficult. Therefore, only some special considerations can be discussed in this work.

3. Special considerations

In addition to single microorganisms, mixed consortia are often applied in these processes, which originate from various sources [19], e.g., sludge from biogas production; anaerobic sludges from municipal wastewater treatment plants and cow-dung composts; cattle or dairy residue composts; sludge from palm oil mill effluent; soil, rice and straw composts; fermented soybean meal, etc. Even though these sources usually contain the microbes which are able to form biohydrogen, they need to be acclimated which includes some sort of pretreatment, e.g., heat shock, starving for a couple days, etc., to enrich the suitable microorganisms [3], [28] or sometimes bioaugmentation [10].

In hydrogen-producing consortia, a wide range of species have been isolated [19], e.g., under mesophilic conditions, *Clostridium (C. pasteurianum, C. saccharobutylicum, C. butyricum), Enterobacter (E. aerogenes) and Bacillus*, while under thermophilic conditions, the genera *Thermoanaerobacterium (T. thermosaccharolyticum), Caldicellulosiruptor (C. saccharolyticus, C. thermocellum)* and *Bacillus thermozeamaize*.

Regarding the utilization of certain fruit wastes, some flavor compounds were found to exhibit an antimicrobial effect [15], e.g., a citrus flavor, since D-limonene is able to weaken the fermentation even at very low concentrations (0.01% w/v). Therefore, the undesired effect of these substrates can be diminished by special treatments, e.g., encapsulation of the microbes in a membrane or pretreatment of the feedstock.

4. Conclusions

In biohydrogen production, the application of agro-industrial residues has a great potential since they are renewable, huge amounts of them are formed year by year and have not been utilized. Various types of agro-wastes have been investigated with regard to biohydrogen production using a wide variety of microbes, namely single microorganisms or consortia. Although it seems that both can be effective in terms of fermentation, higher yields and/or production rates could be achieved when carbohydrates – which can be easily uptaken – are present in the initial substrate.

REFERENCES

[1] Azwar, M. Y.; Hussain, M. A.; Abdul-Wahab, A. K.: Development of biohydrogen production by photobiological, fermentation and electrochemical processes: A review, *Renew. Sustain. Energy Rev.,* 2014, **31**, 158–173, DOI: 10.1016/j.rser.2013.11.022

[2] Bharathiraja, B.; Sudharsanaa, T.; Bharghavi, A.; Jayamuthunagai, J.; Praveenkumar, R.: Biohydrogen and biogas – an overview on feedstocks and enhancement process, *Fuel,* 2016, **185**, 810–828, DOI: 10.1016/j.fuel.2016.08.030

[3] Bakonyi, P.; Nemestóthy, N.; Simon, V.; Bélafi-Bakó, K.: Review on the start-up experiences of continuous fermentative hydrogen producing bioreactors, *Renew. Sustain. Energy Rev.*, 2014, **40**, 806–813, DOI: 10.1016/j.rser.2014.08.014

[4] Akhlaghi, N.; Najafpour-Darzi, G.: A comprehensive review on biological hydrogen production, *Int. J. Hydrogen Energy*, 2020, **45**(43), 22492–22512, DOI: 10.1016/j.ijhydene.2020.06.182

[5] Saravanan, A.; Senthil Kumar, P.; Mat Aron, N. S.; Jeevanantham, S.; Karishma, S.; Yaashikaa, P. R.; Chew, K. W.; Show, P. L.: A review on bioconversion processes for hydrogen production from agro-industrial residues, *Int. J. Hydrogen Energy*, 2022, **47**(88), 37302–37320, DOI: 10.1016/j.ijhydene.2021.08.055

[6] Zakaria, Z. A.; Boopathy, R.; Dib, J. R. (Eds): Valorisation of agro-industrial residues - Volume I: Biological approaches, (Springer Nature, Switzerland), 2020, DOI: 10.1007/978-3-030-39137-9

[7] Dey, T.; Bhattacharjee, T.; Nag, P.; Ritika; Ghati, A.; Kuila, A.: Valorization of agro-waste into value added products for sustainable development, *Bioresour. Technol. Rep.,* 2021, **16**, 100834, DOI: 10.1016/j.biteb.2021.100834

[8] Cardena, R.; Kook, L.; Zitka, J.; Bakonyi, P.; Galajdova, B.; Otmar, M.; Nemestothy, N.; Buitron, G.: Evaluation and ranking of polymeric ion exchange membranes used in microbial electrolysis cells for biohydrogen production, *Bioresour. Technol.*, 2021, **319**, 124182, DOI: 10.1016/j.biortech.2020.124182

[9] Murugan, R. S.; Dinesh, G. H.; Raja, R. K.; James Obeth, E. S.; Bora, A.; Samsudeen, N. M.; Pugazhendhi, A.; Arun, A.: Dark fermentative biohydrogen production by *Acinetobacter junii*-AH4 utilizing various industry wastewaters, *Int. J. Hydrogen Energy*, 2021, **46**(20), 11297–11304, DOI: 10.1016/j.ijhydene.2020.07.073

[10] Rambabu, K.; Bharath, G.; Thanigaivelan, A.; Das, D. B.; Show, P. L.; Banat, F.: Augmented biohydrogen production from rice mill wastewater through nano-metal oxides assisted dark fermentation, *Bioresour. Technol.*, 2021, **319**, 124243, DOI: 10.1016/j.biortech.2020.124243

[11] Alvarez-Guzman, C. L.; Cisneros-de la Cueva, S.; Balderas-Hernandez, V. E.; Smolinski, A.; De Leon Rodrıguez, A.: Biohydrogen production from cheese whey powder by *Enterobacter asburiae*: effect of operating conditions on hydrogen yield and chemometric study of the fermentative metabolites, *Energy Rep.*, 2020, **6**, 1170–1180, DOI: 10.1016/j.egyr.2020.04.038

[12] Oceguera-Contreras, E.; Aguilar-Juarez, O.; Oseguera-Galindo, D.; Macıas-Barragan, J.; Bolanos-Rosales, R.; Mena-Enrıquez, M., Arias-García. A.; Montoya-Buelna, M.; Graciano-Machuca, O.; De León-Rodríguez, A.: Biohydrogen production by vermihumus associated microorganisms using agro industrial wastes as substrate, *Int. J. Hydrogen Energy*, 2019, **44**(20), 9856–9865, DOI: 10.1016/j.ijhydene.2018.10.236

[13] Silva, J. S.; Mendes, J. S.; Correia, J. A. C.; Rocha, M. V. P.; Micoli, L.: Cashew apple bagasse as new feedstock for the hydrogen production using dark fermentation process, *J. Biotechnol.*, 2018, **286**, 71–78, DOI: 10.1016/j.jbiotec.2018.09.004

[14] Saidi, R.; Liebgott, P. P.; Gannoun, H.; Gaida, L. B.; Miladi, B.; Hamdi, M.; Bouallagui, H.; Auria, R.: Biohydrogen production from hyperthermophilic anaerobic digestion of fruit and vegetable wastes in seawater: Simplification of the culture medium of *Thermotoga maritima*, *Waste Manage.*, 2018, **71**, 474–484, DOI: 10.1016/j.wasman.2017.09.042

[15] Akinbomi, J.; Taherzadeh, M. J.: Evaluation of fermentative hydrogen production from single and mixed fruit wastes, *Energies*, 2015, **8**(5), 4253–4272, DOI:10.3390/en8054253

[16] Kumar, G.; Bakonyi, P.; Periyasamy, P.; Kim, S. H.; Nemestóthy, N.; Bélafi-Bakó, K.: Lignocellulose biohydrogen: Practical challenges and recent progress, *Renew. Sustain. Energy Rev.*, 2015, **44**, 728–737, DOI: 10.1016/j.rser.2015.01.042

[17] Rodrıguez-Valderrama, S.; Escamilla-Alvarado, C.; Magnin, J. P.; Rivas-Garcıa, P.; Valdez-Vazquez, I.; Rıos-Leal, E.: Batch biohydrogen production from dilute acid hydrolyzates of fruits-and-vegetables wastes and corn stover as co-substrates, *Biomass Bioenergy,* 2020, **140**, 105666, DOI: 10.1016/j.biombioe.2020.105666

[18] Fan, Y.-T.; Zhang, G.-S.; Guo, X.-Y.; Xing, Y.; Fan, M.-H.: Biohydrogen production from beer lees biomass by cow dung compost, *Biomass Bioenergy*, 2006, **30**(5), 493–496, DOI: 10.1016/j.biombioe.2005.10.009

[19] Guo, X. M.; Trably, E.; Latrille, E.; Carrère, H.; Steyer, J.-P.: Hydrogen production from agricultural waste by dark fermentation: A review, *Int. J. Hydrogen Energy*, 2010, **35**(19), 10660–10673, DOI: 10.1016/j.ijhydene.2010.03.008

[20] Fan, Y.-T.; Zhang, Y.-H.; Zhang, S.-F.; Hou, H.-W.; Ren, B.-Z.: Efficient conversion of wheat straw wastes into biohydrogen gas by cow dung compost, *Bioresour. Technnol.*, 2006, **97**(3), 500–505, DOI: 10.1016/j.biortech.2005.02.049

[21] Venkata Mohan, S.; Lenin Babu, M.; Venkateswar Reddy, M.; Mohanakrishna, G.; Sarma, P. N.: Harnessing of biohydrogen by acidogenic fermentation of *Citrus limetta* peelings: effect of extraction procedure and pretreatment of biocatalyst, *Int. J. Hydrogen Energy*, 2009, **34**(15), 6149–6156, DOI: 10.1016/j.ijhydene.2009.05.056

[22] O-Thong, S.; Prasertsan, P.; Intrasungkha, N.; Dhamwichukorn, S.; Birkeland, N.-K.: Optimization of simultaneous thermophilic fermentative hydrogen production and COD reduction from palm oil mill effluent by *Thermoanaerobacterium*-rich sludge, *Int. J. Hydrogen Energy*, 2008, **33**(4), 1221–1231, DOI: 10.1016/j.ijhydene.2007.12.017

[23] Ivanova, G.; Rákhely, G.; Kovács, K. L.: Thermophilic biohydrogen production from energy plants by *Caldicellulosiruptor saccharolyticus* and comparison with related studies, *Int. J. Hydrogen Energy*, 2009, **34**(9), 3659–3670, DOI: 10.1016/j.ijhydene.2009.02.082

[24] Ozkan, L.; Erguder, T. H.; Demirer, G. N.: Effects of pretreatment methods on solubilization of beet-pulp and bio-hydrogen production yield, *Int. J. Hydrogen Energy*, 2011, **36**(1), 382–389, DOI: 10.1016/j.ijhydene.2010.10.006

[25] Monlau, F.; Aemig, Q.; Trably, E.; Hamelin, J.; Steyer, J.-P.; Carrere, H.: Specific inhibition of biohydrogen-producing *Clostridium* sp. after dilute-acid pretreatment of sunflower stalks, *Int. J. Hydrogen Energy*, 2013, **38**(28), 12273–12282, DOI: 10.1016/j.ijhydene.2013.07.018

[26] Phowan, P.; Danvirutai, P.: Hydrogen production from cassava pulp hydrolysate by mixed seed cultures: effects of initial pH, substrate and biomass concentrations, *Biomass Bioenergy*, 2014, **64**, 1–10, DOI: 10.1016/j.biombioe.2014.03.057

[27] Chatellard, L.; Marone, A.; Carrère, H.; Trably, E.: Trends and challenges in biohydrogen production from agricultural waste, in: Biohydrogen production: Sustainability of current technology and future perspective, A. Singh; D. Rathore (Eds.), (Springer, New Delhi), 2017, pp. 69–95, DOI: 10.1007/978-81-322-3577-4_4

[28] Rózsenberszki, T.; Koók, L.; Bakonyi, P.; Nemestóthy, N.; Bélafi-Bakó, K.: Comparative study on anaerobic degradation processes of pressed liquid fraction of organic solid waste, *Hung. J. Ind. Chem.*, 2021, **49**(1), 31–35, DOI: 10.33927/hjic-2021-05

HUNGARIAN JOURNAL OF
INDUSTRY AND CHEMISTRY
HJIC

EVALUATION OF PC-FMEA USING NETWORK ANALYSIS

EDINA UNGVÁRI[1*], ISTVÁN GÁBOR GYURIKA[1]

1 Department of Mechanics, University of Pannonia, H-8200 Veszprém, Hungary

Abstract – PC-FMEA is a method that combines the pairwise comparison and basic FMEA (Failure Modes and Effects Analysis) methods. Using the pairwise comparison, which of the risks is more severe, common or noticeable can be determined. The results evaluated by the pairwise comparison can be modeled with networks, where the risks can be ranked according to the criteria using the PageRank and weighted in-degree values. Applying these two solutions together, a form of risk assessment can be created where risks are assessed by pairwise comparisons and the results analyzed using network research tools. The resulting method also provides two types of evaluations to rank the risks and also facilitates visualization. This study aimed to develop the application of PC-FMEA in network research.

Keywords: Network science, PC-FMEA, risk assessment, pairwise comparison

1. Introduction

Failure Modes and Effects Analysis (FMEA) is a method of identifying and fully understanding the potential causes as well as effects of failures on systems or end users with regard to a given product, process or project [1]. FMEA is a risk assessment method that is widely used in several fields [2], particularly in the automotive industry, to formalize a complete set of actions, thereby reducing the risk associated with a system or manufacturing and assembly process [3]. In FMEA, each failure is ranked in order of its Risk Priority Number (RPN), which is calculated by multiplying the values of the three risk factors for failure, namely severity, probability of occurrence and probability of detection before the effects of the failure are realized, moreover, is represented by numbers, generally between 1 (in the case of no or a negligible risk) and 10 (in the worst-case scenario) [4]. The new method is based on a reference table, which gives the most critical risk. The FMEA team takes into account previous FMEAs, test results of similar items, experience with comparable systems and sources of information. A subjective element of this ranking will over time arise as the FMEA always includes new parts and all sources of risk must be reexamined. However, the FMEA team should be as objective as possible by using the criteria from the scales to help determine the appropriate ranking. Therefore, the FMEA team defines the classification of the failure modes based on their experience and knowledge [5].

To eliminate subjectivity, an improved method has been developed in which the evaluation is carried out by a pairwise comparison. According to the three criteria, the risks are assessed by the pairwise comparison. The essence of the pairwise comparison can be grasped in the form of a prepared table, the output of which is the ranking of risks [6].

The results evaluated by the pairwise comparison can be further examined using the tools of network research. From the results of the pairwise comparison, a criticality network can be created in which the directed edges represent the direction of the preference and the weight of such edges can also be specified as the weight of the preference. Based on the criticality network, PageRank and weighted in-degree values can be used to determine which vertices have the most input edges that are also important or the most high-weight input edges [7]. Using the Pairwise Comparison-based FMEA (PC-FMEA) along with network research, a risk assessment method can be created where risks are evaluated by pairwise comparisons and the most severe risks extracted from the results of networks. The following section introduces this method.

2. Experimental

PC-FMEA is a method based on a pairwise comparison to improve the precision of a risk evaluation. The members of the FMEA team evaluate the risks in pairs based on a defined scale from 0-9, where 0 means equally critical and 9 means extremely critical. The scale was created from the fundamental scale of AHP (Analytic Hierarchy Process), which is a decision-making method
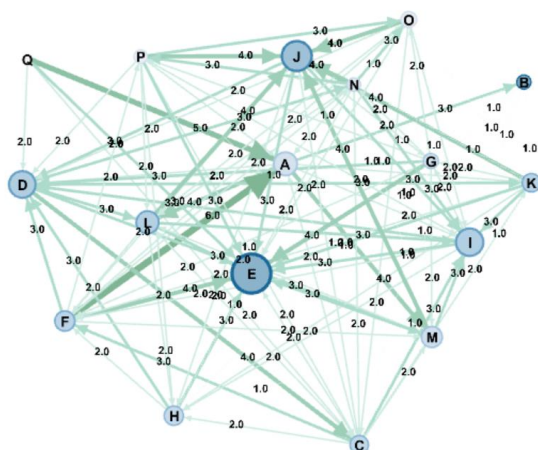
Figure 1. Individual criticality network. The sizes of the nodes show the results based on the weighted in-degree values and the colors of the nodes represent the results of the risk assessment based on the PageRank value

[6]. This scale is based on the three evaluation factors, namely severity, occurrence and detection. The second step of the method is to calculate the importance weights based on a comparison matrix [8]. The presented method offers a new method for enhancing the visual evaluation of the importance weights.

2.1. Modelling risk assessments with networks

Since the network compiled from the results of the pairwise comparison is directed, the direction of criticality is shown. The degree of this criticality can also be specified. The edges are merged with the sum of the weights. A weighted network is C = {V, E, W}, where V denotes the set of vertices, E represents the set of edges and W refers to the weights of the edges. In the network, α_{ij} denotes the connection of node i to node j and each link (i, j) has a weight w_{ij}. The weighted in-degree w_1D_j is calculated as follows [9]:

$$w_1 D_j = \sum_{(v_i,v_j) \in E} w_{ij} \qquad (1)$$

The other indicator from a network that can be easily used for the evaluation of the weights of the risks is the PageRank value. PageRank is an algorithm that defines the importance of a node in a network. The algorithm is calculated from the data to determine how many connections the vertex has and how important they are.

3. Results

The methodology combines the techniques of PC-FMEA and network research. The evaluation is carried out by a pairwise comparison, which is evaluated by network modeling. The following subsections show how the method can be applied to individual and aggregate risk assessments. In both cases, the weighted in-degree and PageRank values are used for ranking. The weighted in-

Table 1. Scale for the occurrence evaluation

Value	Occurrence
0	Equally frequent
1	Slightly more frequent
2	Moderately more frequent
3	More frequent
4	Strongly more frequent
5	Very strongly more frequent
6	Extremely more frequent
7	Extremely more (+) frequent

degree shows how many input edges a given node has and their weights [10]. The PageRank indicator also takes into account the role of these nodes in the network [11]. To demonstrate the method, data were generated randomly.

3.1. Individual criticality network

Risk assessments using the FMEA methodology are in most cases carried out by a team from different professions. Evaluation within the group can be modeled individually and in aggregate with networks. The modeling of an individual evaluation is shown in *Fig.1*, where the vertices indicate the risks and the directed edges between them indicate the preferential relationship. The sizes of the nodes show the weighted in-degree results. The larger the node, the more critical the risk is in that regard. The colors of the nodes illustrate the evaluation according to the PageRank indicator. The darker the node, the more critical the risk. At the edges, weights are visible on a scale of 1 to 7. The sizes of the edges show the extent of the preference. An example scale for the pairwise comparison of the risk according to the occurrence is shown in *Table 1*.

The results of the network model are presented in *Table 2* by the weighted in-degree and PageRank indexes, moreover, are ranked according to the criticality of the risks. It can be seen that the rankings are different based on the two ratings because PageRank also takes into account the role of neighboring nodes in the network.

Each node in the network is visualized in *Fig.2* to show the connected edges with their weights.

3.2. Aggregate criticality network

Aggregate criticality networks can be used to evaluate the risk assessment results produced by an FMEA team. If the evaluation is conducted by everyone individually, the aggregate result can be modeled with networks. Preferences in this case are summarized along with their weights. The results of the aggregate criticality network are shown in *Fig.3*. The visualization of the results is the same as in the individual network.

The results of the network model are presented in *Table 3* in terms of the weighted in-degree and PageRank indexes as well as ranked according to the criticality of the risks. The results of the evaluation are not completely the same in this case either.

Table 2. Results of the individual criticality network model based on the weighted in-degree and PageRank values

ID	Weighted in-degree	ID	PageRank
E	38	B	0.124224
J	27	E	0.113282
I	24	J	0.092585
D	23	D	0.073775
A	19	I	0.072988
L	18	L	0.070678
M	16	K	0.065196
F	15	F	0.063325
H	14	C	0.058084
C	13	H	0.053769
K	13	M	0.044907
O	10	G	0.044183
G	9	A	0.040232
B	8	N	0.029640
N	7	O	0.023272
P	7	P	0.021036
Q	0	Q	0.008824

Figure 3. Aggregate criticality network. The sizes of the nodes represent the results based on the weighted in-degree value and the colors of the nodes show the results of the risk assessment based on the PageRank value

Table 3. Results of the aggregated criticality network model based on the weighted in-degree and PageRank values

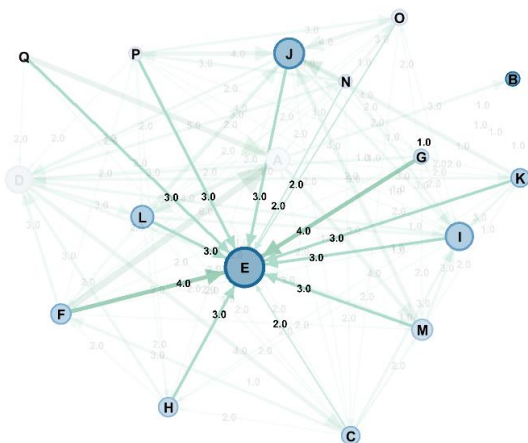| ID	Weighted in-degree	ID	PageRank
I	227	A	0.111017
Q	221	I	0.111016
M	205	Q	0.106530
A	176	M	0.096950
J	141	J	0.070793
H	134	C	0.067337
C	98	H	0.058812
E	97	E	0.055613
B	90	B	0.049083
L	74	L	0.043342
N	69	K	0.040657
P	69	N	0.038440
K	65	D	0.036829
O	48	F	0.032958
F	47	P	0.030556
D	40	G	0.026501
G	36	O	0.023568

Figure 2. Visualization of the connection between a vertex in the network and the weights of the preference

Each node in the network can be visualized to show the connected edges along with their weights as presented in *Fig.4*.

The results of the modeling show that the transformation of the result concerning the pairwise comparison of a risk assessment could yield a new method of evaluation. Severity, Occurrence and Detection values can be evaluated with the weighted in-degree and PageRank values. In a traditional FMEA, the members of the team assess the risks together and try to come to a common understanding. However, the members could have different opinions and comprehend the criticality of the risks in various ways based on their fields of expertise.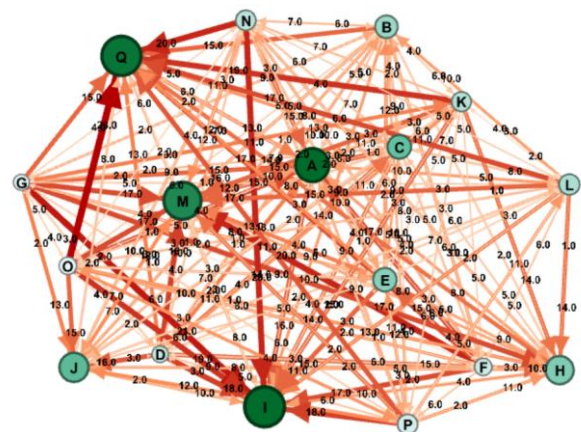 To eliminate subjectivity within the team, individual criticality networks can be used. An aggregated criticality network can evaluate the overall opinion of the team.

4. Conclusions

In this study, how the risks assessed by pairwise comparisons can be modeled by networks was demonstrated. The combination of PC-FMEA and the network research toolkit based on pairwise comparisons provides a new method for implementing risk assessment. Risks can be assessed individually and in aggregate based on two indicators. This modeling can be
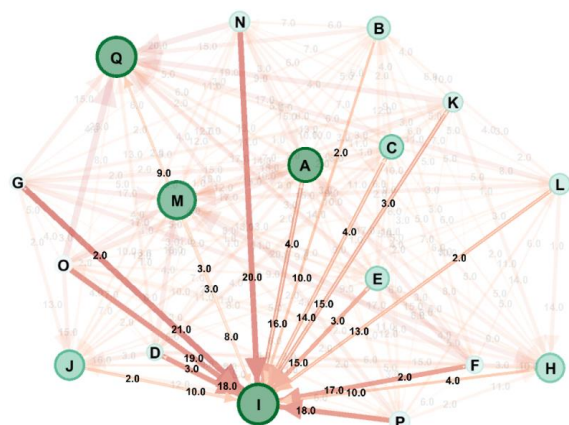
Figure 4. Visualization of the connection between a vertex in the network and the aggregated weights of the preference

applied to all three bases and additional risk factors. Of the two indicators, the FMEA team can choose which one they prefer. Evaluation is not time-consuming and the use of a pairwise comparison and network research reduces the level of subjectivity. The results are less liable to manipulation by participants than in the traditional FMEA, where assessment is added individually to the risks. The results do not match the scales used by the FMEA. Deriving results from scales could be another research direction. Another advantage of this method is that it visualizes the relationship between the risks, which can greatly support their presentation.

REFERENCES

[1] Stamatis, D.H.: Failure mode and effect analysis: FMEA from theory to execution (ASQ Quality Press), 2003, ISBN: 9780873893008

[2] Sharma, K.D.; Srivastava, S.K.: Failure mode and effect analysis (FMEA) implementation: A literature review, *J. Adv. Res. Aeronaut. Space Sci.*, 2018, **5**(1-2), 1–17, ISSN: 2454-8669

[3] Ambekar, S.B.; Edlabadkar, A.; Shrouty, V.: A review: implementation of failure mode and effect analysis, *Int. J. Eng. Innov. Technol.*, 2013, **2**(8), 37–41, ISSN: 2277-3754

[4] Spreafico, C.; Russo, D.; Rizzi, C.: A state-of-the-art review of FMEA/FMECA including patents, *Comput., Sci. Rev.*, 2017, **25**, 19–28, DOI: 10.1016/j.cosrev.2017.05.002

[5] Banghart, M.; Babski-Reeves, K.; Bian, L.; Strawderman, L.: Subjectivity in failure mode effects analysis (FMEA) severity classification within a reliability centered maintenance (RCM) context, *Int. J. Aviat. Aeronaut. Aerosp.*, 2018, **5**(1), 2, DOI: 10.15394/ijaaa.2018.1191

[6] Kulcsár, E.; Csiszér, T.; Abonyi, J.: Pairwise comparison based failure mode and effects analysis (FMEA), *Methodsx*, 2020, **7**, 101007, DOI: 10.1016/j.mex.2020.101007

[7] Kulcsár, E; Gyurika, I.G.; Csiszér, T.: Application of network science to extend the AHP and QFD methods, *Proc. 6th World Congress Mech. Chem. Mat. Eng.*, 2020, DOI: 10.11159/icmie20.137

[8] Sebestyén, V.; Somogyi, V.; Szőke, S.; Utasi, A.: Adapting the SDEWES index to two Hungarian cities, *Hung. J. Ind. Chem.*, 2017, **45**(1), 49–59, DOI: 10.1515/hjic-2017-0008

[9] Kulcsár, E.; Gyurika, I.G.; Csiszér, T.: Network-based – quality function deployment (NB-QFD): The combination of traditional QFD with network science approach and techniques, *Comput. Ind.*, 2022, **136**, 103592, DOI: 10.1016/j.compind.2021.103592

[10] Barabási, A.L.: Network science, (Cambridge University Press), 2016, ISBN: 9781107076266

[11] Abbas, M.; Inayat, I.; Jan, N.; Saadatmand, M.; Enoiu, E.P.; Sundmark, D.: MBRP: Model-based requirements prioritization using PageRank algorithm, *26th Asia-Pacific Software Engineering Conference, Putrajaya, Malaysia*, (IEEE), 2019, pp. 31–38, DOI: 10.1109/APSEC48747.2019.00014